

THE NEW CHRONIC KIDNEY DISEASE MODEL AND ROLE OF CYTOKINE ACCUMULATION
IN THE SEPSIS SUSCEPTIBILITY OF CHRONIC KIDNEY DISEASE

Mr. Asada Leelahavanichkul

A Dissertation Submitted in Partial Fulfillment of the Requirements
for the Degree of Doctor of Philosophy Program in Biomedical Sciences

(Interdisciplinary Program)

Graduate School

Chulalongkorn University

Academic Year 2010

Copyright of Chulalongkorn University

โมเดลใหม่เพื่อการศึกษาโรคไตวายเรื้อรังในหนูและบทบาทของการสะสมไขมันโคโคไลน์
ในภาวะติดเชื้อมีผลต่อของหนูโรคไตวายเรื้อรัง

นาย อัยวุฒิ ลีพหวนิชกุล

วิทยานิพนธ์นี้เป็นส่วนหนึ่งของการศึกษาตามหลักสูตรปริญญาวิทยาศาสตรดุษฎีบัณฑิต
สาขาวิชาชีวเวชศาสตร์ (สหสาขาวิชา)
บัณฑิตวิทยาลัย จุฬาลงกรณ์มหาวิทยาลัย
ปีการศึกษา 2553
ลิขสิทธิ์ของจุฬาลงกรณ์มหาวิทยาลัย

Thesis Title THE NEW CHRONIC KIDNEY DISEASE MODEL AND ROLE
OF CYTOKINE ACCUMULATION IN THE SEPSIS
SUSCEPTIBILITY OF CHRONIC KIDNEY DISEASE.
By Mr. Asada Leelahavanichkul
Field of Study Biomedical science
Thesis Advisor Associate Professor Yingyos Avihingsanon, M.D.

Accepted by the Graduate School, Chulalongkorn University in Partial
Fulfillment of the Requirements for the Doctoral Degree

..... Dean of the Graduate School
(Associate Professor Pornpote Piumsomboon, Ph.D.)

THESIS COMMITTEE

..... Chairman
(Professor Apiwat Mutirangura, M.D., Ph.D.)

..... Thesis advisor
(Associate Professor Yingyos Avihingsanon, M.D.)

..... Examiner
(Associate Professor Nattiya Hirankarn, M.D., Ph.D.)

..... Examiner
(Assistant Professor Kanitha Patarakul M.D., Ph.D.)

..... External Examiner
(Wichai Pornthanakasem, Ph.D.)

อักษุศาสตร์ ลีฬหวนิชกุล: โมเดลใหม่เพื่อการศึกษาโรคไตวายเรื้อรังในหนูและบทบาทของการสะสมไซโตไคน์ในภาวะติดเชื้อในเลือดของหนูโรคไตวายเรื้อรัง (THE NEW CHRONIC KIDNEY DISEASE MODEL AND ROLE OF CYTOKINE ACCUMULATION IN THE SEPSIS SUSCEPTIBILITY OF CHRONIC KIDNEY DISEASE) อ. ที่ปริกษาวิทยานิพนธ์หลัก: รศ.นพ. ยิ่งยศ อวิหิงสานนท์, 112 หน้า.

โรคไตวายเรื้อรังคือการเสื่อมสภาพของหน้าที่ของไตอย่างต่อเนื่อง ซึ่งเป็นผลจากการลดลงของเนฟรอน (nephron) ส่งผลให้เกิดการสะสมของเสียต่างๆ ในเลือดอย่างต่อเนื่อง และเกิดความผิดปกติของภาวะต่างๆ และเสียชีวิตในที่สุด ผู้ป่วยโรคไตวายเรื้อรังมีจำนวนเพิ่มขึ้นเรื่อยๆ เนื่องจากความก้าวหน้าในการรักษาโรคในภาวะฉับพลันต่างๆ ผู้ป่วยโรคไตวายเรื้อรังมีอัตราเสี่ยงต่อการติดเชื้อและมีอัตราตายสูงขึ้น ถ้าเกิดภาวะติดเชื้อในเลือด การศึกษาภาวะติดเชื้อในเลือด (sepsis) ในสัตว์ทดลองที่มีภาวะโรคไตวายเรื้อรังอยู่ก่อนหน้าจะมีความใกล้เคียงกับสภาวะผู้ป่วยโรคไตวายที่มีการติดเชื้อ และอาจนำไปสู่ความสำเร็จในการคิดค้นการรักษาใหม่ๆ อย่างไรก็ตามโมเดลโรคไตวายเรื้อรังในหนูที่มีการเสื่อมของไตอย่างต่อเนื่องนั้น ยังไม่มีการรายงานที่เหมาะสม พบว่าการทำให้หนูมีปริมาณของเนื้อไตลดลงโดยการตัด 5 ใน 6 ส่วนของไต (5/6 nephrectomy: 5/6 Nx) ในหนูพันธุ์ CD-1 หรือ 129 S3 นั้น มีลักษณะต่างๆ ที่ใกล้เคียงกับคนไข้ อาทิเช่น การเพิ่มขึ้นของค่าครีเอตินิน การพบโปรตีนในปัสสาวะ การเกิดความดันโลหิตสูง และลักษณะทางพยาธิวิทยา ซึ่งไม่พบในหนูพันธุ์ C57BL/6 การใช้ยาลดความดันโลหิตในกลุ่มที่เกี่ยวข้องกับแองจิโอเทนซิน (Olmesartan) สามารถลดความรุนแรงของการเกิดเยื่อพังผืดในไต ต่างจากการใช้ยาลดความดัน Hydralazine อันเป็นการเพิ่มความดันโดยใช้แองจิโอเทนซินทู (Angiotensin II) ในหนู C57BL/6 ที่ผ่านการตัดไต 5/6 Nx เกิดภาวะไตวายเช่นเดียวกับหนูพันธุ์ CD-1 แต่การเพิ่มความดันโดย Deoxycorticosterone acetate (DOCA-salt) ไม่เกิดปรากฏการณ์ดังกล่าว การตัดไต 5/6 Nx ในหนู CD-1 หรือ หนู C57BL/6 ร่วมกับการใช้ยาแองจิโอเทนซินทูเป็นโมเดลใหม่ที่เหมาะสมสำหรับโรคไตวายเรื้อรัง การทำให้เกิดภาวะติดเชื้อในเลือดในหนู CD-1 ที่มีภาวะไตวายเรื้อรังอยู่ก่อนหน้ามีความรุนแรงกว่าหนูที่ไตเป็นปกติอยู่ก่อน ซึ่งอาจจะเกิดจากการสะสมไซโตไคน์หลายชนิด ซึ่งปกติมีการขับออกทางไต เราพบว่าไซโตไคน์ที่สำคัญได้แก่ HMGB1 ไม่ใช่ VEGF หรือ inflammatory cytokine อื่นๆ การใช้ Anti-HMGB1 ในการรักษาภาวะติดเชื้อในเลือดในหนูที่มีโรคไตวายเรื้อรังอยู่ก่อนได้ผลดี การรักษาที่มุ่งไปสู่การเปลี่ยนแปลงของ HMGB1 น่าจะมีบทบาทสำคัญในการรักษาภาวะติดเชื้อในเลือดที่มีภาวะไตวายเรื้อรังอยู่ก่อนในมนุษย์

สาขาวิชา ชีวเวชศาสตร์

ลายมือชื่อนิติ.....

ปีการศึกษา 2553

ลายมือชื่อ อ.ที่ปริกษาวิทยานิพนธ์หลัก.....

5187868320 : MAJOR MEDICAL MICROBIOLOGY

KEYWORDS: CHRONIC KIDNEY DISEASE / KIDNEY REMNANT MODEL / CYTOKINES / SEPSIS /
SEVERITY / SUSCEPTIBILITY

ASADA LEELAHAVANICHKUL: THE NEW CHRONIC KIDNEY DISEASE
MODEL AND ROLE OF CYTOKINE ACCUMULATION IN THE SEPSIS
SUSCEPTIBILITY OF CHRONIC KIDNEY DISEASE

THESIS ADVISOR: ASSOC. PROF. YINGYOS AVIHINGSANON, M.D., 112 pp.

Chronic kidney disease (CKD), the progressive worsening of kidney function resulting from the decrease in nephron (functional kidney unit) number, leading to end-stage renal failure and death. The 2 million end stage renal disease patients by 2010 places a substantial burden on global health care delivery systems. CKD was reported as an important prognostic factor in the patient with sepsis, CKD patients have a higher prevalence, severity and mortality of sepsis compared with normal. Knowing the cause of immune compromised in CKD should initiate better patient management. The study on sepsis in predisposing CKD should be more resemble human sepsis condition and results in better opportunity of successful translation. We conducted the series of experiments to initiate proper CKD model and use that model for sepsis studies. Concerning CKD in human definition, we could not find proper CKD model from previous literatures. Then we established new modified kidney remnant model. We found this model in CD-1 or 129 S3 but not C57BL/6 showed progressive worsening in kidney function (serum creatinine, glomerular filtration rate), histology, albuminuria, blood pressure and other comorbidity characters. The hypertension treatment by Olmesartan but not hydralazine reduced kidney fibrosis, in part, reciprocal to human condition. Additionally, the resistance of C57BL/6 overcome by Angiotensin II but not DOCA- salt hypertension. We proposed modified kidney remnant model in CD-1 and in C57BL/6 with Angiotensin II as a proper CKD models. Subsequently, we used this model in CD-1 in sepsis study. We found the accumulation of several cytokines followed kidney injury. However, HMGB1 but not VEGF or other cytokines in CKD causes spleen apoptosis and worsen sepsis condition. The anti HMGB1 treatment in sepsis with pre- existing CKD but not in previously healthy mice was effective. In conclusion, we invented new proper CKD model and reported spontaneous spleen apoptosis after CKD. Then we found that HMGB1 is an important modulator for sepsis severity in CKD. HMGB1 might be an interesting treatment target in sepsis with pre- existing CKD.

Field of study: Biomedical science

Student's signature:

Academic year: 2010

Advisor's signature:

ACKNOWLEDGEMENT

I would like to thank everyone who encouraged and supported me to complete this dissertation. This dissertation could not have been accomplished without the support and funding of Dr. Robert A Star, National Institute of Diabetes and Digestive and Kidney diseases (NIDDK), National Institute of Health (NIH).

CONTENTS

	PAGE
ABSTRACT (THAI).....	IV
ABSTRACT (ENGLISH).....	V
ACKNOWLEDGEMENT.....	VI
CONTENTS.....	VII
LIST OF TABLES.....	X
LIST OF FIGURES.....	XI
LIST OF ABBREVIATIONS.....	XIV
CHAPTER I: INTRODUCTION.....	1
Background and Rationale.....	1
Cause of more severe infection in CKD condition	3
HMGB1, new interesting cytokine CKD, might be important in sepsis.....	4
Hypotheses Mechanism.....	8
Research Methodology.....	8
Research Questions.....	8
Objectives.....	8
Hypotheses.....	9
Key Words.....	9
Expected Benefit.....	9
Conceptual Framework.....	9
CHAPTER II: REVIEW OF RELATED LITERATURE.....	15
Sepsis: a life threatening condition and a worldwide health care problem.....	14
Requirements for animal models of sepsis.....	15
STANDARD ANIMAL MODELS OF SEPSIS	16
LPS-induced inflammation models.....	17
Cecal ligation and puncture (CLP) models of polymicrobial sepsis.....	18
Bacterial infusion or instillation models	21
Large animal sepsis models	21
CLASSIFICATION OF SEPSIS MODELS BY SEPSIS CLINICAL SYNDROME...	22

	PAGE
(a). Model for systemic inflammatory response syndrome (SIRS).....	22
(b) Models for sepsis, severe sepsis or septic shock	23
(c) Models for refractory septic shock	24
(d) Models of sepsis with pre- existing underlying diseases.....	24
THE MODIFICATION OF CLP MODEL IN CURRENT SEPSIS STUDY.....	25
Age, resuscitation, and antibiotics.....	25
Genetic heterogeneity	26
Late stage immunosuppression	26
Additional clinically relevant factors	28
Predisposing co-morbid conditions	28
CHRONIC KIDNEY DISEASE (CKD) AND RENAL FIBROSIS MODEL.....	29
Kidney remnant model	29
Podocyte injury models	30
Tubulointerstitial fibrosis models	31
Other genetic modification models	31
CHAPTER III: MATERIALS AND METHODS.....	34
Animals and animal models.....	34
Chronic kidney disease (CKD) models.....	34
Sepsis models.....	36
Measurement of blood pressure.....	36
Drug administration	36
Blood chemistries, BW and urine measurements.....	37
Blood collection and plasma renin determination.....	38
GFR measurement in conscious mice.....	38
Pharmacokinetics (PK) of cytokines	39
Morphologic evaluation of kidney and heart.....	39
MicroCT imaging.....	40
Statistical analysis.....	40
CHAPTER IV: RESULTS.....	41
THE CHRONIC KIDNEY DISEASE MODEL DEVELOPMENT PART.....	41

	PAGE
The 5/6 nephrectomy (5/6 Nx) model was the appropriate model for chronic kidney disease	41
CD-1 and 129S3 but not C57BL/6 mice develop progressive chronic kidney disease following 5/6 nephrectomy.....	42
Clinically relevant characteristics validation of the 5/6 nephrectomy model of chronic kidney disease.....	46
The progressive hypertension following 5/6 nephrectomy as the validation of CKD characters and strain-selective differences in baseline mean arterial pressure	48
The induction of hypertension by Angiotensin II but not deoxycorticosterone acetate induced CKD in C57BL/6 CKD-resistance.....	50
Global changes in renal architecture visualized <i>ex vivo</i> by contrast-enhanced microCT.....	53
THE SEPSIS EXPERIMENT PART.....	57
Strain-specific severity of sepsis after 5/6 Nx	57
Strain-specific increases in spleen apoptosis, serum HMGB1 and VEGF after 5/6 Nx.....	61
Influence of kidney injury or removal on cytokine production after sepsis	63
Neutralizing HMGB1, but not VEGF, attenuated sepsis severity in mice with pre-existing CKD (5/6 Nx)	66
Spleen apoptosis as an important source of serum HMGB1 in both sepsis and CKD (5/6 Nx)	70
CHAPTER V: DISSCUSSION.....	76
REFERENCES.....	89
APPENDIX.....	108
BIOGRAPHY.....	112

LIST OF TABLES

TABLE		PAGE
1.	Sepsis definition	2
2.	Frequently used sepsis animal models.....	17
3.	The rodent model of podocyte injury.....	31
4.	Characteristics of kidney injury in different renal fibrosis model	57

LIST OF FIGURES

FIGURE	PAGE
1. Chronic kidney disease patient increase infection rate	4
2. Sepsis in pre- existing folic acid injury model.....	5
3. HMGB1 and inflammatory pathway.....	7
4. HMGB1 in sepsis experiments.....	7
5. HMGB1 in chronic kidney disease patient.....	7
6. Simplified clinical course of sepsis.....	16
7. Cecal ligation and puncture procedure.....	19
8. Anatomy of rodent cecum.....	20
9. Histology of AKI in a clinically relevant model of CLP-induced sepsis.....	26
10. Anatomy of renal vascular.....	30
11. FSGS lesion in Six 2 deficient mice	32
12. Schema of 5/6 nephrectomy procedure.....	34
13. Time course of albuminuria after different insults.....	42
14. Strain-specific characters of kidney injury	44

FIGURE	PAGE
15. Changes in glomerular injury following 5/6 nephrectomy.....	45
16. Glomerular injury scoring and tubulointerstitial fibrosis following 5/6 nephrectomy	46
17. Changes in chronic kidney disease characters following 5/6 nephrectomy...	48
18. Changes in mean arterial pressure following 5/6 nephrectomy	50
19. Cardiac fibrosis following 5/6 nephrectomy	51
20. Mean arterial pressure and albuminuria after 5/6 nephrectomy with hypertension induction in C57BL/6 chronic kidney disease resistance.....	52
21. Effect of angiotensin II administration in C56BL/6 and 5/6 nephrectomy.....	53
22. Micro CT pictures in different mouse models.....	56
23. The 5/6 Nephrectomy in different mouse strains before sepsis experiment....	58
24. Severity of sepsis in pre-existing chronic kidney disease in mouse.....	59
25. Tubular vacuolization in chronic kidney disease with and without sepsis.....	60
26. Spleen apoptosis in chronic kidney disease with and without sepsis.....	61
27. Cytokines and spleen apoptosis of chronic kidney disease.....	63

FIGURE	PAGE
28. Time course of cytokines in sepsis with pre-existing chronic kidney disease.	65
29. Clearance and half- life of exogenous cytokines injection.....	66
30. VEGF time course after injury.....	67
31. sFLT-1 treatment in sepsis and sepsis with chronic kidney disease	68
32. Anti- HMGB1 treatment in sepsis and sepsis with chronic kidney disease	69
33. Anti-HMGB1 and cardiovascular effect	70
34. Angiotensin II (Ang II) induced CKD in C57BL/6 5/6 Nx resistant strain and Olmesartan (Olm) improved CKD in CD-1 5/6 Nx	72
35. Spleen apoptosis was the source of serum HMGB1 in sepsis and 5/6 Nx	73
36. Spleen apoptosis in C57BL/6 5/6 Nx with Angiotensin II and CD-1 5/6 Nx with Olmesartan treatment	74
37. Spleen apoptosis of normal or bilateral Nx mice with CLP.....	75

LIST OF ABBREVIATIONS

ACCP	American College of Chest Physician
ACR	Albumin creatinine ratio
AKI	Acute kidney injury
ALT	Alanine transaminase
Ang	Angiotensin
ARB	Angiotensin receptor blocker
ARDS	Acute respiratory distress syndrome
AST	Aspartate transaminase
BP	Blood pressure
BUN	Blood urea nitrogen
BW	Body weight
CASP	Colon ascendens stent peritonitis
CFU	Colony forming unit
CKD	Chronic kidney disease
CLP	Cecal ligation and puncture
COL	Collagen
DC	Dendritic cell
DIS	Disseminated intravascular coagulation
EEG	Electro encephalogram
EPO	Erythropoitin
FA	Folic acid
FITC	Fluorescein isothiocyanate
FLT-1	FMS-like tyrosine kinase 1
FSGS	Focal and segmental glomerulosclerosis
GBM	Glomerular basement membrane

GFR	Glomerular filtration rate
Hct	Hematocrit
HMGB1	High mobility group box 1
HPLC	High performance liquid chromatography
I/R	Ischemic and reperfusion injury
ICU	Intensive care unit
IFN	Interferon
IL	Interleukin
LPS	Lipopolysaccharide
LTA	Lipoteichoic acid
MAP	Mean arterial pressure
MCD	Minimal change disease
MRI	Magnetic resonance imaging
NET	Neutrophil extracellular trap
Nk	Natural killer cell
NO	Nitric oxide
Nx	Nephrectomy
PAF	Platelet activating factor
PAS	Periodic acid–Schiff
PCWP	Pulmonary capillary wedge pressure
PMN	Polymorphonuclear cell
PK	Pharmacokinetic
PRC	Plasma renin concentration
RBF	Renal blood flow
ROS	Reactive oxygen species
SCCM	Society of Critical Care Medicine
SIRS	Systemic inflammatory response syndrome

TLR	Toll like receptor
TNF	Tumor necrosis factor
USRDS	United State renal data system
VEGF	Vascular endothelial growth factor
Veh	Vehicle
UUO	Unilateral ureter obstruction

CHAPTER II

REVIEW OF RELATED LITERATURE

Sepsis: a life threatening condition and a worldwide health care problem

Sepsis is a characteristic set of systemic reactions to overwhelming infection. Sepsis, severe sepsis, and septic shock are defined according to established criteria (see introduction Chapter 1). Discovery of antibiotics has dramatically improved the morbidity and mortality of the infectious diseases for the last decades; indeed antibiotics and volume resuscitation are the first line of sepsis treatment strategy [45]. However, overwhelming inflammatory response accompanied by depression in immunological function causes multiple organ injury and determines clinical outcomes. In addition to inflammation and immunological dysregulation, a number of different mechanisms contribute to sepsis at different phases (Figure 6). For instance, systemic hemodynamics evolves from an early hyperdynamic (“warm shock”) state to a late hypodynamic (“cold shock”) state. A multitude of potential drug targets have been identified in animal models of sepsis; however, translation from animals to humans has been exceedingly difficult. Several reviews have pointed out that the failure to translate results from animals to humans has been attributed to disease characteristics of sepsis (complexity and heterogeneity), inappropriate clinical trials (study of ineffective drugs, inadequate clinical trial designs), and animal models that do not fully mimic human sepsis [11-14].

Requirements for animal models of sepsis

Human sepsis is currently hypothesized to consist of at least two stages: an initial pro-inflammatory burst responsible for hypotension and organ dysfunction, followed by a compensatory anti-inflammatory immune response that leads to an immunosuppressed state often called immune depression or immune dysfunction; however, these stages may overlap temporally (Figure 6) [46]. The latter consists of altered monocyte antigen presentation, decreased lymphocyte proliferation and responsiveness, and lymphocyte apoptosis and anergy, which accounts for nosocomial infections and late deaths in sepsis. Animal models of sepsis need to reproduce the

complexity of human sepsis and its treatment in the ICU. Ideally, animal models should mimic the pace and severity of human sepsis, reproduce key hemodynamic (warm shock followed by cold shock) and immunologic (pro-inflammatory stimulation, anti-inflammatory counter-regulation, i.e., immune depression) stages, mimic histology findings in key organs (lung, liver, spleen, kidney, etc.) that are frequently modest, and perhaps counter-intuitively for animal modelers - exhibit variability among animals.

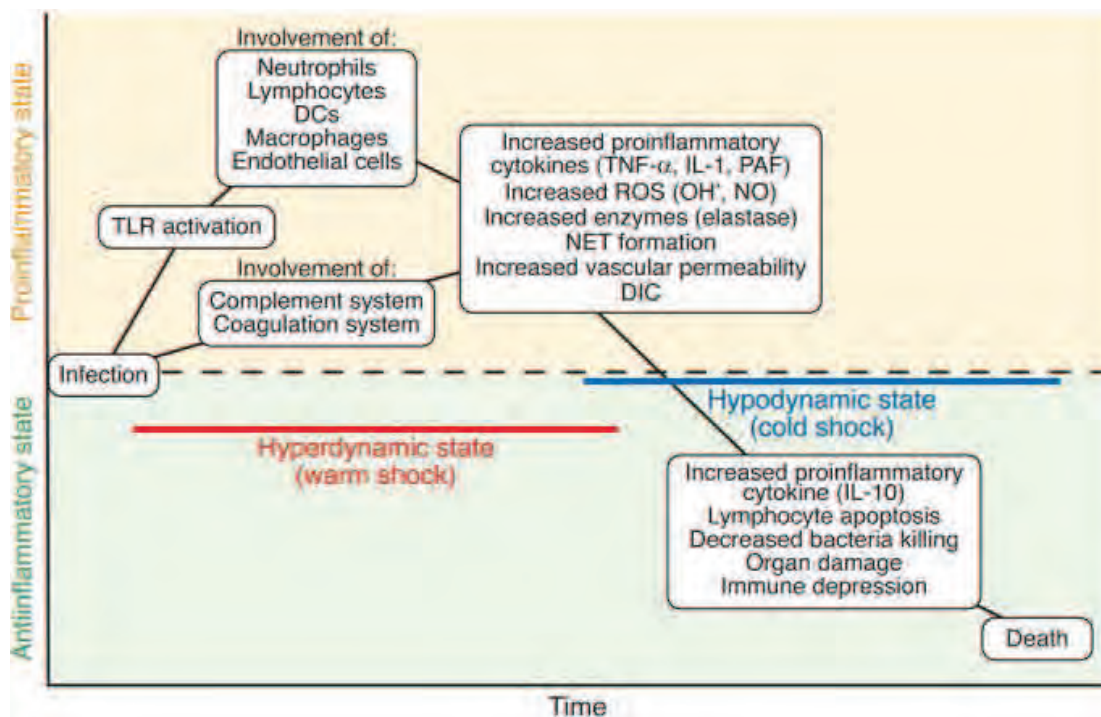


Figure 6. Simplified clinical course of sepsis. Progression of disease is complex, nonlinear, and varies from one patient to another. Shown is an outline of selected landmark events and processes that appear to be common among patients and some animal models. DIC, disseminated intravascular coagulation.

Standard animal models of sepsis

Sepsis animal models can be divided into three categories: (i) exogenous toxin injection (e.g., LPS); (ii) alteration of the animal's endogenous protective barrier, such as intestinal leakage [e.g., cecal ligation and puncture (CLP) or colon ascendens stent peritonitis (CASP)], and (iii) infusion or instillation of exogenous bacteria (Table 2) [46].

Table 2. Frequently used animal model of sepsis

Animal model	Advantage	Disadvantage
LPS injection	Simple, sterile; some similarities with human sepsis pathophysiology	Early and transient increases in inflammatory mediators more intense than in human sepsis
CLP or CASP	Early silent period; moderate and delayed peak of mediators; multiple bacterial flora	Age and strain variability; early hemodynamic period in some models
Clinically relevant CLP	Replication of clinical risk factors	Difficulty in analyzing pathophysiological pathways
Infusion or instillation of exogenous bacteria	Early hyperdynamic state	No change in intrarenal microcirculation; need large animals; labor-intensive

LPS-induced inflammation models. Endotoxin, a component of the outer membrane of Gram-negative bacteria, is involved in the pathogenesis of sepsis, and a LPS infusion/injection model has been widely used for sepsis research. LPS administration induces systemic inflammation that mimics many of the initial clinical features of sepsis, including increases of proinflammatory cytokines such as TNF- α and IL-1, but without bacteremia. Treatment of LPS-injected animals with neutralizing antibody against TNF- α or IL-1 resulted in improved outcomes for this model [47, 48]. A case report describes a patient who self-administered a large dose of LPS and the full clinical manifestations of septic shock developed [49]. LPS infusion also causes renal injury, including decreased GFR, increased blood urea nitrogen (BUN) and increased renal neutrophil infiltration [50-52].

Several clinical trials of anti-TNF- α and anti-IL-1 therapy were performed based on the promising results in LPS animal studies; however, these trials failed to improve survival of septic patients [53, 54]. LPS causes much earlier and higher peak levels of cytokine expression compared with levels observed in human sepsis, with the notable exception of meningococcal sepsis, a rare, pathogen- and site-specific form of sepsis where cytokine levels are comparable to those observed in LPS animal models [55-57]. Also, some features of LPS infusion such as renal hypoperfusion and increased BUN are alleviated by volume replacement, which is routinely performed in clinical management of sepsis [58, 59]. Nevertheless, LPS infusion remains a useful tool to interrogate a simpler subset of the complex trajectory of sepsis. The LPS dose can be titrated to mimic early sepsis without hemodynamic compromise, which has been useful for studying systemic and renal responses during the initial phases of sepsis; doses of LPS typically used induce systemic hypotension and decrease glomerular perfusion,

whereas lower doses of LPS do not cause any systemic hypotension but still decrease glomerular perfusion [60, 61].

Cecal ligation and puncture (CLP) models of polymicrobial sepsis. CLP is currently the most widely used animal model of sepsis [12, 62, 63]. CLP surgery is straightforward: ligation distal to the ileocecal valve and needle puncture of ligated cecum causes leakage of fecal contents into the peritoneum (Figure 7) [64], with subsequent polymicrobial bacteremia and sepsis [64]. This surgical manipulation, while not well standardized, allows the severity to be adjusted by the length of ligated cecum and the size and/or number of the puncture. Supportive treatment with fluids and antibiotics is quite variable across laboratories, and almost always inadequate since typically only a single fluid and/or antibiotic dose is given [65]. Multiple species of bacteria are found in the blood stream and progressive systemic inflammatory response syndrome followed by septic shock and multi-organ injury ensues. Mice subjected to CLP generally became severely hypotensive without an apparent hyperdynamic phase, although more vigorous fluid resuscitation can result in an early hyperdynamic phase detected by echocardiography [66]. CLP-induced sepsis models show a similar cytokine profile to human sepsis [55, 56] and anti-TNF- α treatment fails to alleviate sepsis in CLP models as in human sepsis [56, 67]. As described above, human sepsis is considered to have two immunologically different stages; a pro-inflammatory phase and a compensatory anti-inflammatory phase.

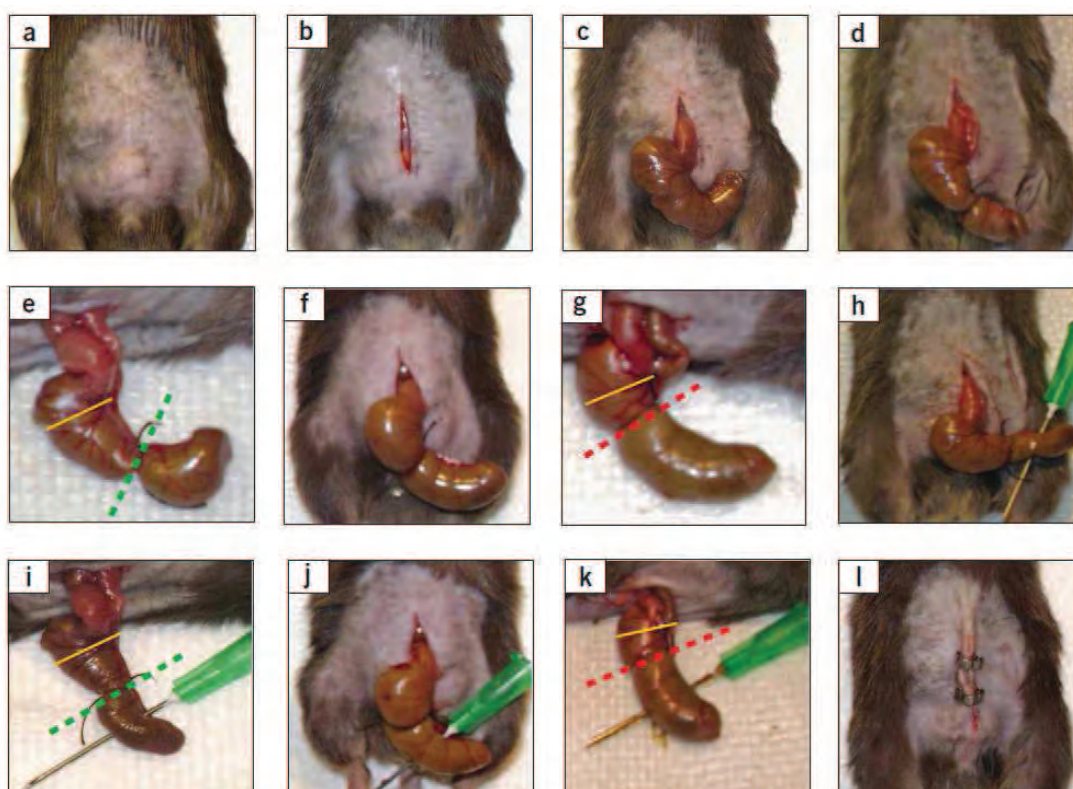


Figure 7. Critical steps in the CLP procedure in mice. (a) Disinfection of the abdominal area after shaving. (b) Skin midline incision. (c) Exposure of the cecum, which can be mostly found in the lower left area of the abdominal cavity. (d,e) Ligation of the cecum at designated positions as the major determinant of sepsis severity. For the induction of mid-grade sepsis resulting in survival rates of 40%, the cecum is ligated (indicated by dotted green line) at half the distance between distal pole and the base of the cecum (black dotted line). (f,g) High-grade sepsis (100% lethality) comprises ligation of 75% of the cecum (dotted red line). The basis of the cecum is indicated by the yellow line. (h,i) Cecal puncture ('through-and-through') from mesenteric toward antimesenteric direction after medium ligation. (j,k) Needle puncture of the cecum under the conditions of high-grade sepsis (large ligation). (l) Wound closure by applying simple running sutures to the abdominal musculature and metallic clips to the skin.

CLP-induced sepsis increased lymphocyte apoptosis, which mimics immunosuppression at the later phase of human sepsis [68-70]. In this respect CLP-induced sepsis is completely different from LPS infusion-induced sepsis and more

closely mimics human sepsis. The standard CLP model encompasses more clinical features and drug responses of human sepsis than the LPS model, but is still missing some key features, especially kidney and lung injury. Additionally, the severity of sepsis can be adjusted by the length of ligated cecum and size of the punctured needle (Figure 8), the larger needle, the more sepsis severity. The difference in anatomy and the tolerance to the surgical procedures between rat and mice will require different surgical techniques (Figure 8)[64].

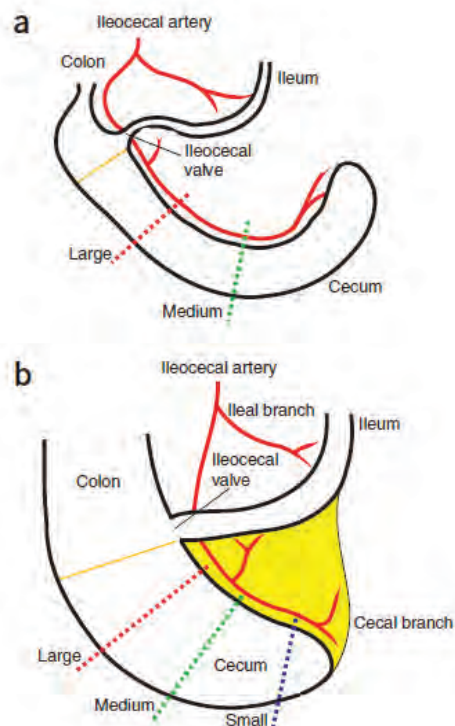


Figure 8. **Anatomy of rodent cecum.** (a,b) Schematic illustration of characterized positions of cecal ligation to induce mid-grade sepsis (medium ligation; dotted green line) or high-grade sepsis (large ligation; dotted red line) in (a) mice and (b) rats. The yellow line represents the basis of the cecum immediately below the ileocecal valve, which should be used as a reference to estimate the length of the cecum to be ligated. A major difference between mice and rats is that in rats a membrane stretches at the mesenteric site of the cecum (yellow area in b), which needs to be dissected before cecal ligation and which is not found in mice. In addition to medium and large ligation, small ligation (dotted blue line) comprising 10% of the cecum is presented for rats in (b).

Bacterial infusion or instillation model. Whereas models such as CLP and CASP are helpful in understanding polymicrobial sepsis, human sepsis may also be caused by a single pathogen. Bacterial infusion models can approximate introduction of a single pathogen in a controlled manner, allowing reproducible infection. These models have been translated to larger animals for the study of systemic and organ-specific hemodynamics (see below). Similarly, instillation can be useful for simulating pneumonia, especially as a nosocomial infection [70]. These models provide complementary information that is likely to be pathogen-specific.

Large animal sepsis models. Large animal sepsis models have been developed using LPS infusion, CLP surgery, and bacterial infusion and inoculation. Since these larger animals can be fully instrumented to measure circulatory parameters and continuously infuse fluids and therapeutic agents, ICU fluid management protocols can be used, and hemodynamic status can be documented. Fink et al. implanted a fibrin clot containing live *Escherichia coli* in the peritoneal cavity of dogs, which increased cardiac output and decreased blood pressure and systemic vascular resistance (SVR) [71]. This canine sepsis model has been used for drug evaluation [66-68]. Recently a new canine sepsis model, induced by intra-bronchial *Staphylococcus aureus* administration, has been developed [72]. In this model, treatment with mechanical ventilation, antibiotics, fluids, vasopressors, sedatives, and analgesics were adjusted based on algorithms similar to the care provided for human sepsis. Renal dysfunction evaluated by serum creatinine and BUN was found in acute non-survivors (<24 h) and decreased urine output in subacute non-survivors (24–96 h). In a baboon model, a hyperdynamic state is pre-activated by injection of killed bacteria, followed by injection with live *Escherichia coli*; renal dysfunction was also demonstrated [73-75]. It is of note that renal histological changes including tubular epithelial cell injury, fibrin deposits, and inflammatory cell infiltration, were found in this model.

Additionally, Failure of the renal circulation is thought to be a crucial factor for developing sepsis-induced AKI; despite lack of demonstrated efficacy, low dose dopamine is often administered to preserve renal blood flow (RBF). However, in recent

reports with a large animal sepsis model, AKI developed even with increased RBF. In sheep infused continuously with live *Escherichia coli*, serum creatinine increased despite a more than doubling of RBF [76]; notably, the expected redistribution of intrarenal circulation between cortex and medulla (measured by implanted Laser Doppler flow probes) was also absent [77]. On the other hand, rodent sepsis models of LPS infusion or CLP developed renal microcirculatory failure, as evaluated by more precise methods, including intravital two-photon video microscopy [78-81]. It should be noted that these rodent sepsis models might have insufficient fluid resuscitation. In septic humans, microcirculatory derangements can be detected by orthogonal polarization spectral imaging [82]. Indeed, mortality was better predicted by microcirculatory failure than systemic hemodynamics [83, 84]. Further investigation is necessary to clarify the relative contribution of global renal blood flow and microcirculation to sepsis and sepsis-induced AKI, and whether defects in one of these vessel beds can be treated without compromising the other.

Classification of sepsis animal models by sepsis clinical syndrome

The limitation in patient histopathology in sepsis leads to extensive animal studies in different models. We should understand the limitation and the representative of each model to properly interpret the study results. The extensive reviews on the detail of sepsis animal models mentioned previously including benefit and limitation [46, 85]. In this part, to match with sepsis definition (varies in the severity) and the adaptation to human conditions, we divided models into 4 categories;

(a). Model for systemic inflammatory response syndrome (SIRS): models in this groups aim to trigger the inflammatory response by endotoxin (lipopolysaccharide: LPS) injection refer to as gram negative bacterial sepsis [86], Lipoteichoic acid (LTA) injection as gram positive bacterial sepsis [87] or killed/ live bolus bacterial injection [88-91]. These models show SIRS as measured by alteration in vital sign and complete blood count but no evidence of infection. The live bacterial injection in lethal [88] or non-lethal dose [77] results in rapid decrease in blood pressure however the 12- 24 h study period might not enough to create actual infection. Additionally, the bolus bacterial injection

does not typically neither colonized, replicated in host nor regularly cause bacteremia as human sepsis [85] except staphylococcal injection [92]. However, the dissemination of microabscess in multiple organs might leads to organ dysfunction independently from SIRS. Then the staphylococcal injection model is the model specific to mimic specific condition such as staphylococcal endocarditis more than sepsis model. Nevertheless, renal dysfunction caused by severe SIRS from high dose bacterial toxic substance (LPS, LTA) might not mediate through SIRS but via direct renal cell receptor activation [93]. Moreover, the rapid exposure of LPS, LTA or bacteria might suddenly overwhelm host defense mechanism which is different from patient sepsis pathophysiology [94]. Despite less sepsis mimicry, the models in this category are more relate to sepsis condition than other SIRS models (eg. smoke inhalation, multiple fracture, burns, acute pancreatitis, etc.) [85, 94-98] and are tremendously useful for understanding SIRS from bacterial components.

(b) Models for sepsis, severe sepsis or septic shock: models in this group mimics real infection in the different organs using several methods eg. cellulitis [99], pneumonia [70], peritonitis [100, 101] or the continuous live bacterial infusion [76]. There are SIRS with documented infection in these models then the local infection will progress into sepsis, severe sepsis and septic shock. In the continuous bacterial infusion, the presence of bacteria in blood mimics sepsis definition with or without real infection. The most widely used model in this category is the peritonitis model using either large animal such as ruptured appendix model [101], fecal peritonitis model or smaller animal such as cecal ligation and puncture (CLP), colon ascendance stent peritonitis (CASP) model [85]. The investigator can choose the proper time point in these models to explore sepsis (without organ failure) or severe sepsis (with organ failure) or septic shock (with low blood pressure). However, if the insults are less severe then there will be no shock in model with lower mortality. Thus, it might be more practical to determine these different severity syndromes by the survival which more commonly presented in most studies than cardiovascular parameters. We purposed as sepsis, mortality less than 5- 10%; severe sepsis, mortality less than 50% and septic shock, mortality more than 50%. We used 50% as the cutting point due to human sepsis

mortality is around 50%. The main mechanisms of sepsis injury in these 3 clinical syndromes might be different with some overlaps. Hence, the translation from animal models to the matched reciprocal patient categories might lead to more success patient studies [102].

(c) Models for refractory septic shock: models in this category are the same as previous category but need to administer vasopressor and fluid to maintain blood pressure. The “refractory” will be determined by the high dose of vasopressor to maintain BP. Some of the animals in specific experimental groups in several studies are in this category which might be the most resembles human sepsis conditions. Most of the large animal studies use vasopressors and fluid resuscitation in the experiments [103]. However, the study that selectively studies only “refractory shock” is lacking. The high cost of large animal maintenance, manipulation and monitoring limits number of studies in this group.

(d) Models of sepsis with pre-existing underlying diseases: the investigators recently try to mimic patient sepsis which mostly complicated with pre-existed underlying disease such as pneumonia, burn or fracture [15, 70, 104, 105]. We introduced sepsis with pre-existed chronic kidney disease by folic acid injection and 5/6 nephrectomy [15] which showed different result with sepsis in healthy animal.

The stratification of the sepsis studies might be easier for interpretation and translation from the current extensive and increasing number of sepsis studies. However, the current definition of sepsis might still not perfect despite has been used for decade [106]. The interpretation of animal model studies should always develops along with the clinical definition to mimic specific human clinical syndrome.

Considering the mimicry to sepsis patient, the CLP model should be the most appropriate model for our sepsis in CKD study.

The modification of CLP model in current sepsis study

Animal models of sepsis differ from human sepsis because of age, comorbidity, and use of supportive therapy [13]. Starting from a clinical perspective, we reasoned that within practical limitations animals should receive treatment comparable to the

supportive therapy that is standard for ICU patients. This is essential to enable us to test if a therapy has additional benefit beyond that supplied by conventional fluid and antibiotic therapy. We also hypothesized that the CLP model could be improved by simulating one or more underlying baseline conditions typically present in septic patients, such as advanced age or chronic disease.

Age, resuscitation, and antibiotics. Since the incidence of sepsis dramatically increases with age, and elderly patients are especially prone to sepsis and sepsis-induced AKI [107], our first modification of standard CLP models was to employ older mice, i.e., retired breeders. We and others found that aged mice (16 to 50 weeks old) were more susceptible to CLP and LPS than young mice around 8 to 16 week old [59, 108, 109]. In standard mouse CLP models, animals are typically given a small amount of fluid resuscitation and perhaps a dose of antibiotics immediately after surgery, but fluid and antibiotic treatment are not continued. Because volume resuscitation can reverse LPS-induced renal injury in aged mice [59], we added volume resuscitation and antibiotic treatment to the standard CLP model. Animals became clinically ill at 5–6 hours after surgery, at which time they had evidence of liver damage; kidney damage was evident by MRI early [110], but serum creatinine and BUN did not significantly increase until 12 hours after surgery [111]. With these additions, consistent histological renal damage with significant increase of serum creatinine were observed, not because fluids and antibiotics were harmful to the kidney, but because the animals could survive long enough to develop AKI [59, 112]. Acute tubular necrosis is found in ischemic and toxic AKI, but is not present in any of our mouse CLP models; in contrast, we observed areas of proximal tubular cells that contain prominent intracellular vacuoles of unknown composition (Figure 9) [111]. Although a similar tubular vacuolization is found in cyclosporine nephropathy [113], its significance and relevance in sepsis still needs to be clarified[114].

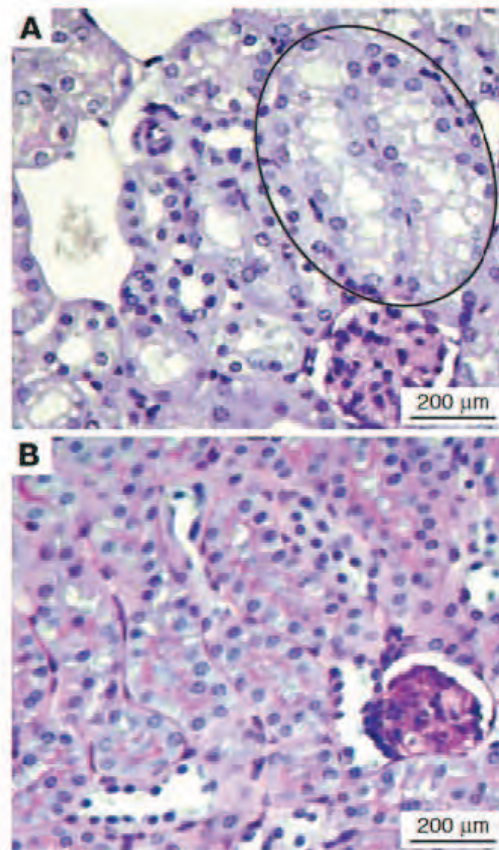


Figure 9. Histology of AKI in a clinically relevant model of CLP-induced sepsis.

Periodic acid-Schiff (PAS) staining of mouse kidney cortex 24 hours after CLP surgery (A) or sham surgery (B). Pink staining of brush border is visible in sham cortical tubules, and loss of brush border is evident, as is mild dilation, after CLP. Vacuolization is seen after CLP in almost all tubules, most prominently in two tubules in the upper-right corner (circled). Original magnification, $\times 400$. Scale bar: 200 μm .

Genetic heterogeneity. We next developed a CLP model in aged outbred rats (Sprague Dawley strain). We originally switched to rats because serum and urine are difficult to collect from mice [115]. In contrast to the mouse CLP model, which consistently develops multi-organ injury, the rat CLP model showed heterogeneous responses, with a wide spectrum of degrees of organ injuries. This model demonstrated early but not late increases in IL-6 levels that corresponded with development of kidney injury, similar to those seen in septic patients [116].

Could the variability and sensitivity to AKI be attributed to the outbred Sprague Dawley strain? We shifted our CLP mouse model to the outbred CD-1 strain, and found that CD-1 mice developed sepsis AKI at a young age [112]; whereas the inbred C57BL6 strain developed AKI only at an advanced age [59]. The reason for this difference in susceptibility is unknown, but the genetically heterogeneous human population should be more accurately represented by outbred mice, reducing the bias found in inbred strains that might contain or lack recessive disease susceptibility loci, depending on selective pressures [102, 117].

Late stage immunosuppression. Despite a focus on the proinflammatory aspects of sepsis, most deaths in sepsis occur from nosocomial infections during a late prolonged immunosuppressed state, even in the face of successful early, supportive therapies. Septic patients have defects in innate and adaptive immunity, including altered monocyte antigen presentation, decreased lymphocyte proliferation and responsiveness, and lymphocyte apoptosis and anergy [11, 70]. Prevention and/or treatment of this immune deficiency should be a focal point for novel treatments; immunostimulatory therapies such as IFN- γ and GM-CSF are being tested in early phase clinical trials [118]. However, this dimension of sepsis has been underrepresented in animal models; simple CLP models have splenic apoptosis, but generally die too early before later immunosuppression fully develops. More complex models have been developed recently. A 'two-hit' model of CLP followed by instillation of bacteria (*Pseudomonas aeruginosa* or *Streptococcus pneumoniae*) mimics nosocomial infections that result from immune depression [70, 119]. In these animals, pro-inflammatory cytokines (e.g., IL-6) were decreased, anti-inflammatory (e.g., IL-10) cytokines were increased, bacteria clearance was reduced, and profound lymphocyte apoptosis was observed. An alternative model for late hypoimmune events involves CLP in mice and subsequent removal of the necrotic cecum, which can lead to a complete recovery. Peritoneal macrophages isolated from CLP mice that had cecectomy four days after sepsis induction had lower IL-6 production, indicating a hypoimmune state [120]. IFN- γ production by splenocytes was suppressed in CLP mice but was reversed by cecectomy and IL-10 injection [121]. Recently, serum cytokine analysis in a

community-acquired pneumonia cohort showed that mortality was not predicted by either pro-inflammatory IL-6 or anti-inflammatory IL-10, but high levels of both cytokines were more predictive. Thus, by the time of hospital admission, high levels of IL-6 and IL-10 portend the worst mortality; either the early pro-inflammatory phase had passed, or the early and late phase are coincident [7], which requires further investigation.

Additional clinically relevant factors. We must be cautious about species differences in terms of susceptibility to pathogenic factors. For instance, rodents are much less sensitive to LPS than humans [113]. We also need to consider that microbial toxins can accelerate sepsis. Alverdy and colleagues [122] performed a 30% hepatectomy, which allowed exotoxin A to be disseminated systematically after direct injection of *P. aeruginosa* into the cecum. The mortality rate of this sepsis model could be increased to 100% by modifying the virulence of bacteria.

Predisposing co-morbid conditions. Animal studies typically examine sepsis and related organ failure in otherwise healthy animals, despite numerous epidemiological studies of human sepsis that show the importance of pre-existing co-morbid conditions [1, 123]. Severe sepsis occurs frequently in patients with underlying chronic diseases (co-morbidities) including chronic kidney disease (CKD), liver disease, and diabetes, and has an extremely high mortality rate [1, 123]. CKD is found in approximately 30% of AKI patients in the ICU [7, 124]. Patients with CKD also have an increased risk of morbidity and mortality from sepsis [21, 125-127]. These findings suggest that clinical sepsis and sepsis-induced AKI are dramatically influenced by underlying diseases, which may help explain why simple animal models of sepsis do not mimic human sepsis, and do not predict human response to therapeutics. We recently established a two-stage mouse model of pre-existing renal disease with subsequent sepsis (CKD-sepsis) to mimic the complexity of human sepsis; mice were given folic acid to induce renal fibrotic injury, then subjected two weeks later to CLP surgery [15]. This CKD-sepsis model showed increased vascular permeability and decreased bacteria clearance compared with sepsis animals without the comorbidity of CKD. Combination therapy with soluble FMS-like tyrosine kinase 1 (FLT1; also known as VEGF receptor 1) and chloroquine, which block vascular and immunological dysfunction, respectively,

showed the best survival rate. Both drugs were effective individually in simple CLP models, but neither drug alone was effective in the more complex CKD/CLP model, suggesting that multiple therapeutic interventions (“combination chemotherapy”) may be required for the treatment of sepsis complicated with co-morbidity. The complex models including several underlying conditions of age, fluid, antibiotics, and chronic co-morbidity may be an improvement for testing therapeutics because the models may ultimately predict human drug responsiveness more accurately. However, they appear to alter and complicate the underlying pathophysiological mechanisms. Therefore it is important to compare the complex models with the simpler models systematically to distinguish between core vs amplifying factors in sepsis, in hopes of discovering new methods to better classify septic patients into informative subgroups with a more uniform set of pathophysiological mechanisms.

CKD model and renal fibrosis model

In order to study sepsis in pre-existing chronic kidney disease (CKD), the review of CKD and/or renal fibrosis is necessary. The animal models of CKD initially aim to have renal fibrosis and/or albuminuria which mostly lack the progression of disease. There are 4 large categories of CKD model in the literature (i) kidney remnant model (eg. 5/6 nephrectomy model) (ii) podocyte injury model (eg. puromycin, nephrotoxic serum nephritis model) (iii) tubulointerstitial fibrosis model (eg. folic acid injection model) (iv) other genetic modification mice (eg. six2 deficiency [128], COL4A3 deficiency [129]). The unilateral ureter obstruction (UUO) also caused renal fibrosis in obstructed kidney but did not show kidney injury because of contralateral normal kidney. The UUO model does not count as CKD model category.

Kidney remnant model. The principle of this model followed the observation of CKD progression in patient which occurred after nephron loss more than 50%. The histopathology of this model mimics focal and segmental glomerulosclerosis (FSGS). The different insults were used for reduce nephron number and subsequently cut one kidney. The model can be done as 1 stage operation (kidney injury along with unilateral nephrectomy) or 2 stage operation (kidney injury then unilateral nephrectomy later).

Most of the model in this category followed 2 stage operations because of higher mortality rate after 1 stage operation. The insults for initiate kidney injury are including renal artery ligation, upper and lower pole kidney resection, physical injury to renal cortex (using electro cautery, thermal, cold). The anterior division of renal artery responsible for 5/6 of kidney mass (Figure 10). The ligation of this branch is the standard protocol for kidney remnant in rat but not in mouse. The anatomical variation and the small size of artery lead to the technical difficulty [130, 131]. The physical injury has the reproducible problem because of the difficulty in controlling the depth of injury [132-134].

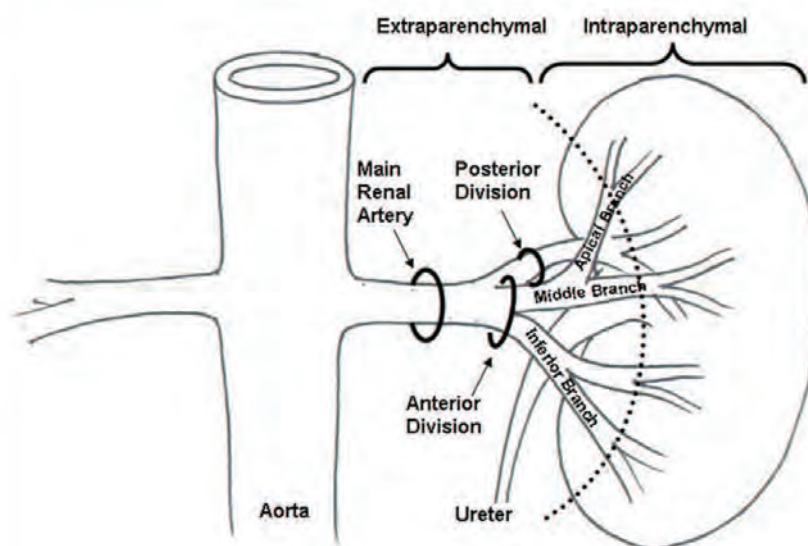


Figure 10. **Anatomy of renal vascular.** The anterior division of renal artery nourishes 5/6 of kidney and posterior division responsible for 1/6 of kidney mass

The kidney pole resection seems to be the appropriate approach for this model. However, there are no standard of the amount of resected kidney mass and mostly no progression showed in several literatures [135].

Podocyte injury models. Several models are included in this category such as the nephrotoxic serum nephritis model mimics anti- glomerular basement membrane [136] disease, chronic puromycin injection mimics FSGS progress from minimal change disease (MCD) and chronic LPS model [137] (table 3). Most of the models in this group are a result follow podocyte injury. Podocytes are vulnerable to many forms of injury.

Immune-mediated processes include immune complex deposition with subsequent complement activation, as seen in membranous nephropathy, as well as cellular mechanisms characteristic of MCD or FSGS. Nonimmune injury includes hemodynamic insults (systemic hypertension, states of reduced nephron mass) and metabolic (diabetes mellitus), infectious (human immunodeficiency virus), toxin-mediated (puromycin, adriamycin), and genetic mutations essential to slit diaphragm assembly (nephrin, CD2AP, PLC-1, podocin).

Table 3. The rodent models of podocyte injury

Human Disease	Rat Models	Mouse Models
FSGS: Classic variant	Puromycin aminonucleoside nephrosis (high or repeated doses) Adriamycin nephrosis Remnant kidney	Adriamycin nephrosis
FSGS: Collapsing variant Membranous nephropathy	Not available Passive Heymann nephritis Active Heymann nephritis	HIV-associated nephropathy Cationic BSA
Minimal change disease Crescentic glomerulonephritis	Puromycin aminonucleoside nephrosis (low dose) Not available	Not available Anti-GBM nephritis
No specific human disease, but rather a generalized response of podocytes to injury in clinical disease: Foot process effacement Slit diaphragm protein abnormalities	LPS Protein overload Protamine sulfate	LPS Protamine sulfate

FSGS, focal segmental glomerulosclerosis; HIV, human immunodeficiency virus.

However, the study of sepsis on these models might be too specific to the representative patients.

Tubulointerstitial fibrosis models. There is less study on this group due to lower incident of pure tubulointerstitial fibrosis in CKD patient. We are the pioneer in this study using cecal ligation and puncture (CLP) sepsis model on top of the folic acid injection [15]. The result of the study mentioned previously. The folic acid activates folate receptors in endothelial cell within several organs. Kidney has more injury due to the tubular reabsorption and secretion lead to rapid tubulointerstitial fibrosis. However, the kidney injury in this model is no or very slow progression which differ from CKD characters. Then we seek for better models.

Other genetic modification models. Models in this group do not have the abnormality in podocyte but involve in other mechanisms. The example of models in this group is including six 2 deficiency and COL4A3 deficiency. The six 2 deficiency mice show the abnormality in oropharyngeal area with less embryogenic nephron numbers.

These mice develop FSGS (Figure 11) in various periods from several months to year due to the variation of nephron number [128].

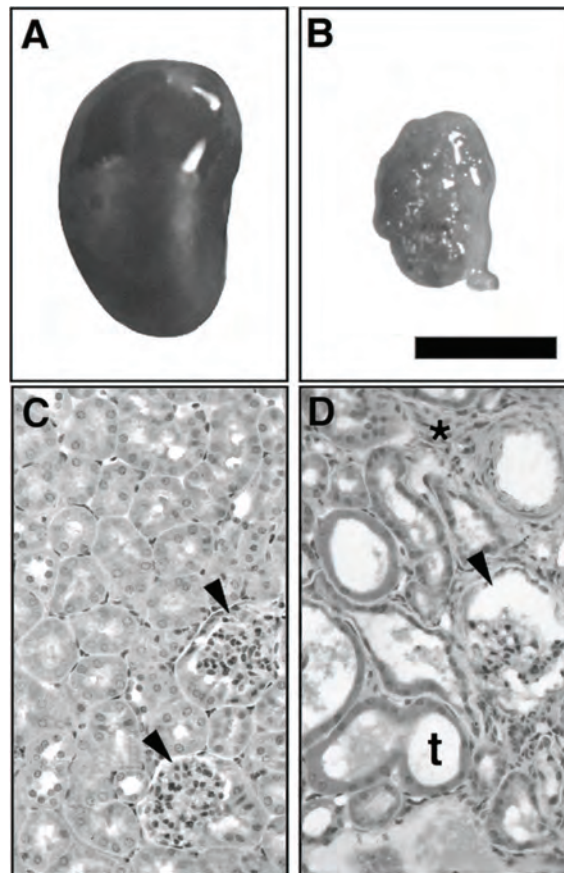


Figure 11. FSGS lesion in Six 2 deficient mice. Six 2 deficient mice showed small irregular kidney (B) with enlarge glomeruli (D arrow head) and tubule (t) compare with normal kidney (A, C).

The COL4A3 gene encodes for the $\alpha 3$ chain of type IV collagen, the gene deficient mice was mimic Alport syndrome [129]. These mice lack normal composition of $\alpha 3$ (IV), $\alpha 4$ (V), and $\alpha 5$ (IV) type IV collagen chains in glomerular basement membrane (GBM). The renal disease is initially as splitting GBM then crescentic glomerulonephritis and severe renal fibrosis. The end stage renal disease developed around 14 wk in 129 Sv background and 32 wk in C57BL/6 back ground. The sepsis study in these mice are interesting but the genetic deficiency might affect other unknown immune function and difficult to use as translation.

In conclusion, considering the representative to patient condition in each model, we interested in using kidney remnant model as a CKD model then use cecal ligation and puncture model (CLP) as the sepsis insults.

CHAPTER III

MATERIALS AND METHODS

Animals and animal models

Animal care followed the National Institutes of Health (NIH) criteria for the use and treatment of laboratory animals. Male mice, 6-8 weeks CD-1 (Charles River Laboratories, MA); C57BL/6 and 129S3 (also known as 129S1/SvImJ/Cr; NCI-DCT, Frederick, MD) had free access to water and chow. Morbidly ill animals were euthanized per animal protocol.

Chronic kidney disease (CKD) models

There are 3 insults for nephron reduction part of chronic kidney injury (CKD) models then unilateral nephrectomy at 5-14 days later;

1. The 5/6 nephrectomy (5/6 Nx) was performed in two stages under isoflurane anesthesia (Figure 12). At the first stage (wk-1), the left kidney was decapsulated to avoid ureter and adrenal damage, then the upper and lower poles were partially resected via a left flank incision. Bleeding was controlled by microfibrillar collagen hemostasis (Avitene, Davol, Cranston, RI). The upper and lower poles were weighed. One week later (week 0), the entire right kidney was removed via a right flank incision and weighed. Animals with insufficient kidney resection [as determined by the ratio of removed left kidney weight (at week -1) to the removed right kidney weight (at week 0) < 0.55] were euthanized.

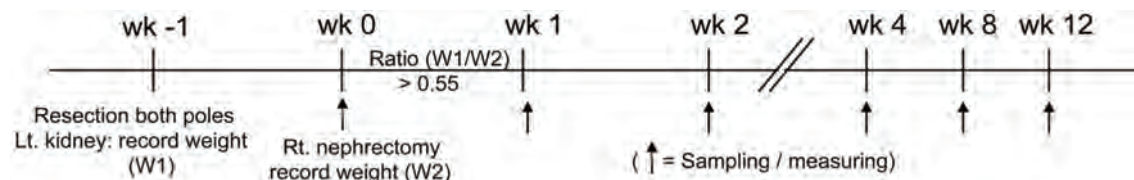


Figure 12. Schema of the 5/6 nephrectomy procedures. The upper and lower poles of left kidney were resected and weighed. Then right nephrectomy was done 1 week later. Mice with ratio of resected left kidney/ right kidney ($W1/W2$) more than 0.55 were selected.

The mortality rate in the first week after right nephrectomy was 10% in CD-1, 6% in 129 S3 and 9% in C57BL/6. In preliminary studies, we found that adequate resection of the left kidney (weight ratio between 0.55-0.72) in CD-1 caused significant albuminuria at 4 weeks [trace dipstick proteinuria or albumin creatinine ratio (ACR) > 700 µg/mg] in most of the mice (data not shown). In the sham surgery control mice, a left flank incision was performed at week 1, both poles of kidney were identified, then the flank incision was closed; a subsequent right flank incision was performed at week 0; the right renal artery was identified, then the flank incision was closed. In the partial nephrectomy (2/6 Nx) control mice, the upper and lower poles of left kidney were cut in week -1 and the right renal artery was identified at week 0. The bilateral nephrectomy surgery in C57BL/6 for testing angiotensin II effectiveness was done under isoflurane anesthesia via bilateral flank approach.

2. Folic acid-induced tubulointerstitial fibrosis (FA) was performed as previously described [15]. Briefly, mice were administered FA (Sigma-Aldrich, St. Louis, MO, USA) 250 mg/kg in vehicle (0.2 ml of 0.3mM NaHCO₃) or given vehicle alone intraperitoneally at week -1. Two days later, 60–70% of the mice developed AKI (defined as BUN ≥ 100 mg per 100 ml) as previously described. In all experiments, we used animals only with sufficient acute renal damage (BUN ≥ 100 mg per 100 ml) at 48 h after FA injection. Then right nephrectomy was operated via right flank incision at week 0 as schema of 5/6 Nx above. The control mice were injected by vehicle (NaHCO₃) and follow as experimental group.

3. Chronic post-ischemic reperfusion injury with contralateral nephrectomy (chronic post-I/R) was performed in two stages, a modification of previously reported methods [138-140]. In the first stage (week -1), the left renal artery was clamped for 35 min via a left flank incision under ketamine anesthesia on a 37°C heated operation table. One week later (week 0), the right nephrectomy was performed under isoflurane anesthesia via a right flank incision. The clamping time more than 35 min or clamping both renal artery for 35 min cause more than 70% mortality rate which is too high to use as a model (data not showed). On the other hand, the clamping less than 35 min was not enough to cause kidney fibrosis even after 3 months of observation (data not

shown). FA mice were euthanized after 2 weeks; 5/6 Nx mice were euthanized after 4-16 weeks, and chronic post-I/R mice were euthanized 12-16 weeks after surgery.

Additionally, the unilateral ureter obstruction was performed as the control model for kidney fibrosis. The left ureter was ligated via left flank incision at week 0 then follow-up along with other models

Sepsis models

Cecal ligation and puncture model (CLP) was performed as previously described [111]. In short, we ligated the cecum at 12 mm in length and punctured twice with a 21-gauge needle then gently squeezed to express a small amount of fecal material and returned to the central abdominal cavity. In sham-operated animals, the cecum was isolated, but neither ligated nor punctured. Pre-warmed normal saline (30 ml/kg) was immediately given intraperitoneally after surgery and antibiotic was given subcutaneously (imipenem/cilastatin; 14 mg/kg in 1 mL of normal saline) 6h later. Eighteen hours after surgery, blood was collected by cardiac puncture for measurement of serum markers of organ injury and cytokine response. Kidneys, liver and spleen were fixed in 10% neutral buffered formalin for histology

Measurement of blood pressure

Mean arterial pressure (MAP) was measured by radiotelemetry as previously described [141]. A telemeter transmitter (model TA11PA-C10, Data Sciences International, St Paul, MN) was implanted in a subcutaneous pocket on the left flank and the tip of the catheter was inserted into the aortic arch via the carotid artery one week before subsequent operations (e.g., week -2 of the 5/6 Nx model).

Drug administration

Val5- Angiotensin II (Ang II) 0.75 µg/kg/min (Sigma- Aldrich, St. Louis, MO) in normal saline (NSS) or vehicle (NSS alone) was infused by subcutaneous osmotic minipump (Alzet model 1004, Cupertino, CA). The osmotic minipump was inserted under isoflurane anesthesia at 3 days after right Nx or sham surgery of right Nx in 5/6 Nx experiment, and immediately after bilateral Nx. Alternatively, a deoxycorticosterone acetate (DOCA)

pellet (Innovative Research of America, Sarasota, FL) (50 mg per pellet for 21 day release) or placebo was implanted subcutaneously 3 days into C57BL/6 mice after right Nx and at the beginning of wk4 to increase blood pressure [142]; all mice were given 0.9% NSS as drinking water upon drug pellet implantation. In sepsis experiments, recombinant human soluble Flt-1 domain D1-3 (sFLT-1: Cell Sciences, Canton, MA, USA) 1 mg per 30 g mouse (or an equal volume of NSS for sham treatment) was injected intravenously every 3 h (four doses), started immediately after CLP [15]. A single dose of anti-HMGB1 neutralizing antibody or neutralizing purified mouse IgG (Sigma- Aldrich, St. Louis MO) for sham treatment, was injected intraperitoneally (3.6 mg/kg) [143] 6 h after CLP in CD-1 mice either untreated (“normal”) or 4 weeks after 5/6 Nx . To reduce the CKD severity and spleen apoptosis, animals were treated with the selective angiotensin receptor blocker (ARB) Olmesartan (100 mg/kg) or placebo mixed with mouse chow (Bio-Serv, Frenchtown, NJ) starting 3 days after kidney surgery [144].

Blood chemistries, BW and urine measurements

At week 0, 1, 2, 4, 8, 12 after surgery, 60 μ l of blood was collected by retro-orbital approach under isoflurane anesthesia and the body weight (BW) was recorded. The following measurements were obtained: hematocrit (Hct) by the microhematocrit method with micro capillary reader, serum creatinine (Scr) by high-performance liquid chromatography (HPLC) [59], blood urea nitrogen (BUN) by colorimetric assay (QuantiChrom Urea assay kit DIUR-500, Hayward, CA) and erythropoitin (EPO) by enzyme-linked immunosorbent assay (ELISA: R&D Systems, Minneapolis, MN). Spot urine at 9:00- 10:00 AM was collected for albumin creatinine ratio (ACR) measured by ELISA (Albuwell M, Exocell, Philadelphia, PA). ACR measurement was confirmed by 24h urine albumin using mouse metabolic cages (Hatteras Instrument, Cary, NC). In sepsis experiments,

at week 0 (immediately before 2nd stage operation: 1 week after both pole resection), 1, 2, 4, 8, 12 after CLP surgery, 60 μ l of capillary tube blood was collected by retro-orbital approach under isoflurane anesthesia then centrifuged at 1,000 x g for 8 min to remove cells. VEGF, TNF- α , IL-6, IL-10 (R&D Systems, Minneapolis, MN) and HMGB1 (Shino-

Test Corporation, Kanagawa, Japan [145] were measured by ELISA. Aspartate transaminase (AST), alanine transaminase (ALT), was measured by an autoanalyzer (Hitachi 917, Boehringer Mannheim, Indianapolis, IN).

Blood collection and plasma renin determination

Mice were kept in separate cages overnight before starting the experiment. Blood was collected from conscious mice by puncturing the submandibular vessels with a Goldenrod animal lancet and collecting about 20-40 μ l of the emerging blood into an EDTA-containing microhematocrit tube. Red cells and plasma were separated by centrifugation for 3 minutes at 12000 rpm; the plasma was ejected into an Eppendorf tube and frozen until used for renin determinations. Plasma renin concentration (PRC) was measured in a 20-fold dilution as generation of Ang I following addition of excess rat substrate, with final plasma dilutions around 1:120. Ang I generation was determined for a 1-hour incubation period at 37°C and expressed as ng AngI/ml/hr. Substrate without plasma was incubated for the same time, and any background Ang I formation was subtracted from the plasma-containing samples by taking an aliquot from the same sample before it was incubated at 37°. A radioimmunoassay kit (DiaSorin CA1553, Stillwater MN) was used to determine the amount of angiotensin I in each sample.

GFR measurement in conscious mice

The fluorescein isothiocyanate (FITC)-labeled inulin clearance was used for GFR measurement as previously described (see appendices)[15, 146], Briefly, a single dose of FITC-inulin (3.7 ml/g bodyweight) was injected intravenously then blood samples were collected 10, 15, 35, 55, and 75 min later from the tail vein. Serum fluorescence was measured by a Nanodrop-ND-3300 fluorescence spectrometer (Nanodrop Technologies, Wilmington, DE). GFR was calculated using a two compartment model (SigmaStat 3.1, Systat Software, Inc., Point Richmond, CA) as previously described [15, 146].

Pharmacokinetics (PK) of cytokines

Cytokine clearance was studied in CD-1 mice. A single dose of recombinant cytokine was injected intravenously immediately after sham surgery in normal, 5/6 Nx at 4 weeks and immediately after bilateral Nx: mouse TNF- α , IL-6, IL-10, VEGF (eBioscience, San Diego, CA) and recombinant human HMGB1 (R&D Systems, Minneapolis, MN) at the dose 0.03 μ g; 3 μ g; 0.3 μ g; 0.03 μ g and 6 mg/kg respectively. Each dose of cytokine was validated to have no effect on mice (symptoms and endogenous cytokine production: data not shown). Sixty μ l of capillary blood collected via retro-orbital sinus > 1 day before injection as a baseline and at 5 min, 0.5, 1, 3, 5, 8, or 24 h after injection were used to measure an individual cytokine. Area under the concentration time curve from 0-24 hours ($AUC_{0-24\text{ hr}}$) was calculated by trapezoidal rule [147]. Elevated levels of HMGB1 and VEGF after 5/6 Nx were assumed to be in steady state, and PK parameters were calculated after subtraction of the baseline level. Previously described equations [148, 149]; were used for pharmacokinetic parameters 1) K_e = maximal concentration/ $AUC_{0-24\text{ hr}}$; 2) half-life ($t_{1/2}$) = $0.693/K_e$ 3); volume of distribution (V_d) = known injected dose/maximal concentration; 4) Clearance (CL) = $0.693*V_d/t_{1/2}$. The cytokine level 5 min after injection was used as maximal concentration.

Morphologic evaluation of kidney and heart

Kidney and heart specimens (4 mm) fixed in 10% formalin, paraffin-embedded, and stained with Masson's trichrome and Periodic acid-Schiff (PAS) reagent (Sigma-Aldrich) (see appendices). Semi-qualitative histologic changes were assessed by a masked observer. The total numbers of kidney glomeruli were counted, and the degree of glomerular damage was estimated at 400X magnification from the degree of mesangial expansion in PAS stained tissue as follow: <25%, 25-50%, 50-80%, >80% [150]. Kidney interstitial fibrosis was estimated at 200X magnification on Masson's trichrome-stained sections using 10 randomly selected fields for each animal by the following semiquantitative criteria: 0, area of damage <5%; 1, areas of damage 5-10%; 2, damage involving 10-25%; 3, damage involving 25-50%; 4, >50% of the area being

affected [151]. The cardiac fibrosis area was determined at 200X magnification in Masson's trichrome stained sections using ImageJ 1.36b (National Institutes of Health, USA).

MicroCT imaging

The formalin fixed kidney specimens were stained using Numira Biosciences protocol (Salt Lake City, UT) for microCT based Virtual Histology™ (microCT), submicron resolution imaging which can be differentially stained using heavy metal elements and explore several aspect of tissue without actually destroying tissue specimens to achieve physiological distinction in a 3D data of structures in different directions [152].

In brief, kidneys were stained to saturation overnight in a solution of 0.1 M sodium cacodylate (pH 7.2), 1% glutaraldehyde, and 1% osmium tetroxide rocking at room temperature, then transitioned viaby a series of gradients to 100% ethanol, then stained with a proprietary cocktail (Numira Biosciences). prior to scanning. High-resolution volumetric CT imaging of kidneys was performed at 6 μm³ isometric voxel resolution using an SCANCO uCT 40 (SCANCO Medical, Zurich, Switzerland). eXplore Locus SP MicroCT specimen scanner (GE Healthcare, London, Ontario, Canada): 6 μm isometric voxel resolution at 200 ms exposure time, 2000 views and 10 frames per view. The platform-independent parameters of current, voltage, and exposure time were kept constant at 100 IA, 80 kVP, and 4,000 ms, respectively. Images were reconstructed with the SCIRun software (University of Utah Scientific Computing and Imaging Institute) for false color image processing to generate a 3-dimensional reconstruction of volume rendering (VR: red color) and spinning sagittal sections (DS: blue- green color) picture.

Statistical analysis

Differences between the groups were examined for statistical significance by student t-test or analysis of variance (ANOVA) with an appropriate multiple comparison correction (SigmaStat 3.1, Systat Software, Inc., Point Richmond, CA); longitudinal blood pressure measurements were analyzed by Repeated Measures ANOVA to test time- and strain-

dependent interactions (SAS, Cary, NC). A P value < 0.05 was accepted as statistically significant

CHAPTER IV

RESULTS

The study on sepsis in pre-existing chronic kidney disease (CKD) needs to develop CKD model with progressive kidney dysfunction. Then we will use that model for sepsis experiments. The results will separate into the CKD development part and sepsis in CKD part.

The CKD model development part

The 5/6 nephrectomy (5/6 Nx) model was the appropriate model for chronic kidney disease

The loss of nephron more than 50% causes progressive kidney injury and CKD. We used 3 different insults to reduce nephron mass then cut one kidney out to allow less than 50% functional nephron in CD-1 mice as the pilot experiments. We found that only our modified method 5/6 Nx model showed highly progressive albuminuria as measured by urine albumin creatinine ratio (Figure 13).

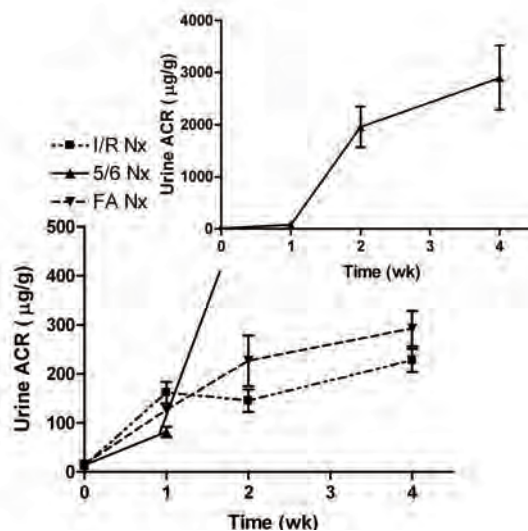


Figure 13. Time course of albuminuria after different insults. Time course of albuminuria after different insults with nephrectomy. Urine albumin creatinine ratio (urine ACR) of ischemic reperfusion injury with nephrectomy (I/R Nx) and folic acid injection

with nephrectomy (FA Nx) were in microscopic level (large graph). Urine ACR of 5/6 Nx model reached macroscopic level after 1 week. (n = 4-6/ group)

All of the mice in different models showed albuminuria but the severity of albuminuria reach macroscopic level only by 5/6 Nx model. Urine ACR increase more than 1000 $\mu\text{g/g}$ as early as 1 week after surgery and increasing. The 5/6 Nx model should be the appropriate model for further experiments.

CD-1 and 129S3 but not C57BL/6 mice develop progressive chronic kidney disease following 5/6 nephrectomy.

We then compared the development of renal and extra-renal manifestations of chronic kidney disease in three mouse strains (Fig 2). The other inbred strain might be important for sepsis experiments. We select C57BL/6 and 129 S3 as selected inbred strains due to the commonly used as wild type. One week after 5/6 Nx, kidney function was appropriately low in all three mouse strains (C57BL/6, 129S3, and CD-1 mice) as determined by increases in BUN and serum creatinine (SCr), but did not change in normal, sham surgery, nor 2/6 Nx control mice (Figure 14A, B). The kidney injury progressed fastest in CD-1 mice, more gradually in 129S3, and remained stable after the initial jump in C57BL/6 mice, consistent with previously reports [131, 153]. The glomerular filtration rate (GFR) determined in conscious mice showed parallel changes (Figure 14C). Urine albumin excretion, as spot urine albumin/creatinine ratio (ACR), dramatically increased more rapidly in CD-1 mice than 129S3 (Figure 14D). In contrast, the ACR remained stable in C57BL/6 mice after 5/6 Nx. Thus, CD-1 and 129S3 showed strain-dependent susceptibility to progressive CKD; whereas C57BL/6 mice were resistant. Induction of 5/6 nephrectomy in susceptible mouse strains caused mesangial expansion and glomerular fibrosis detected with Periodic acid-Schiff (PAS) stain and interstitial fibrosis detected with Masson's trichrome stain (Fig 15, 16). In contrast, glomerular damage was much less severe, without progression, in C57BL/6, even after 16 weeks. Tubulointerstitial fibrosis also appeared more rapidly after 5/6 Nx in CD-1 mice (Fig 16).

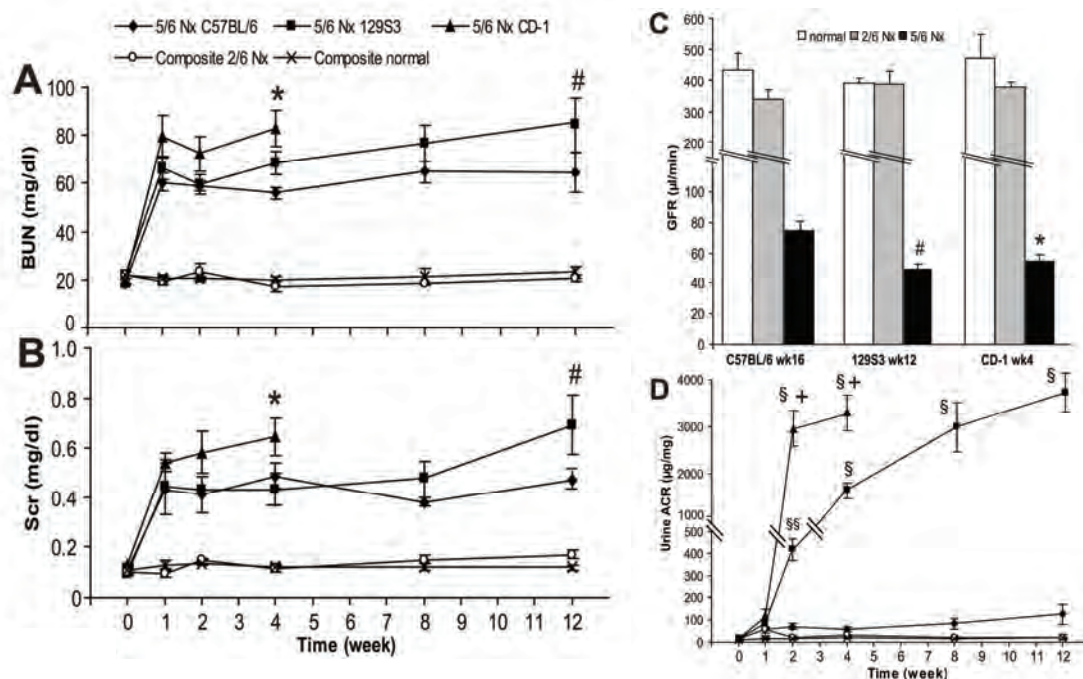


Figure 14: Strain-specific characters of kidney injury. Strain-specific temporal changes in kidney function and albuminuria following reduction of renal mass. Time course of renal function as determined by BUN (A) or serum creatinine (B) and albuminuria as determined by spot urine albumin/creatinine ratio (ACR) (D) in composite normal control (n=6), composite 2/6 Nx control (n=6), 5/6 Nx in C57BL/6 (n=5-9), 129S3 (n=5-11) and CD-1 (n=5-12) strains. The GFR (C) of C57BL/6, 129S3 at wk10 and CD-1 at wk4 with normal sham surgery control, 2/6 Nx control and 5/6 Nx (n=4/group). *, P<0.05 5/6 Nx in CD-1 vs C57BL/6; #, P<0.05 5/6 Nx in 129S3 vs C57BL/6; +, P<0.005 5/6 Nx in CD-1 vs 129S3 in the same time point; §, P<0.001 urine ACR at specific time point vs wk0; §§, P<0.05 urine ACR at specific time point vs wk0

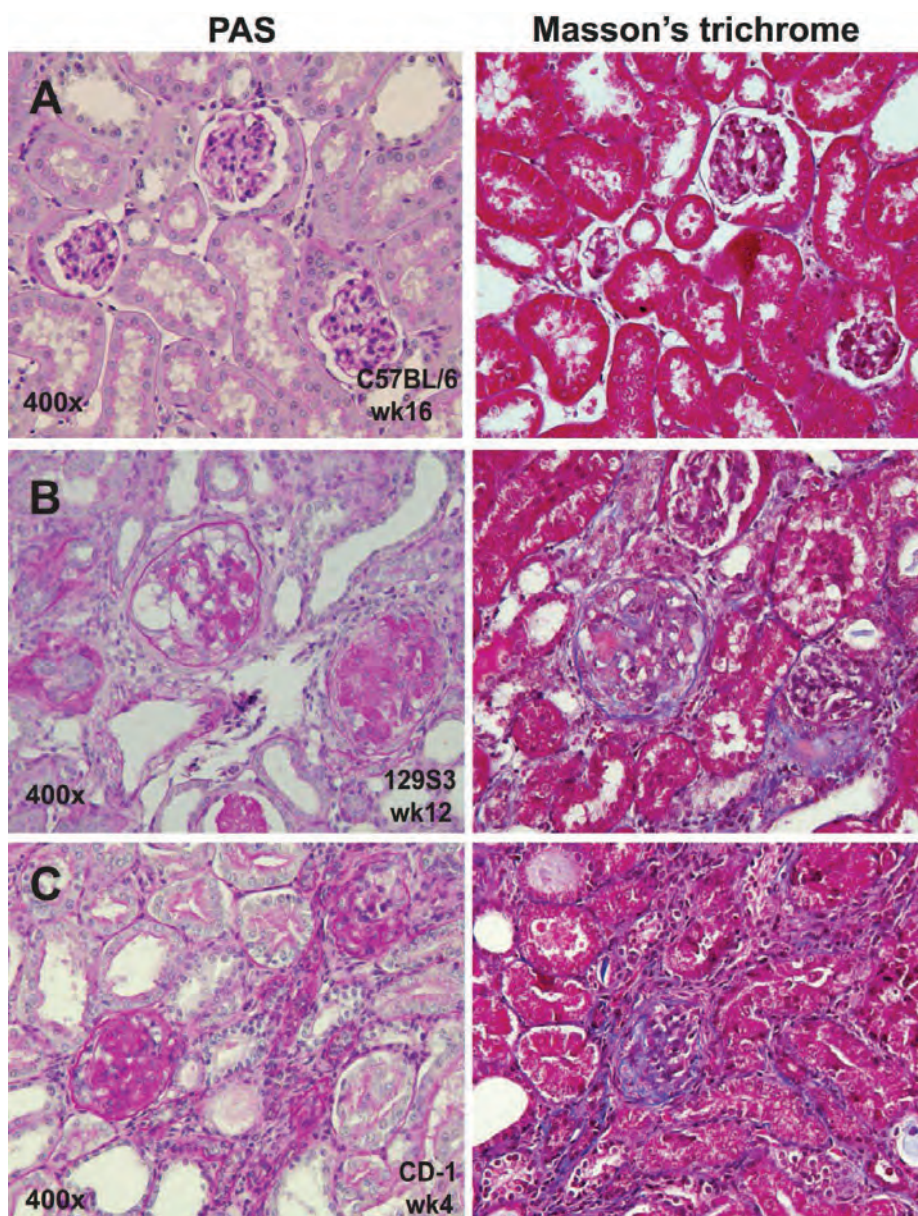


Figure 15: Changes in glomerular injury following 5/6 nephrectomy. Representative images of sections stained by periodic acid-Schiff (left panels) and Masson's trichrome (right panels) after 5/6 Nx in C57BL/6 at wk16 (A), 129S3 at wk12 (B) and CD-1 at wk4 (C) (original magnification 400x).

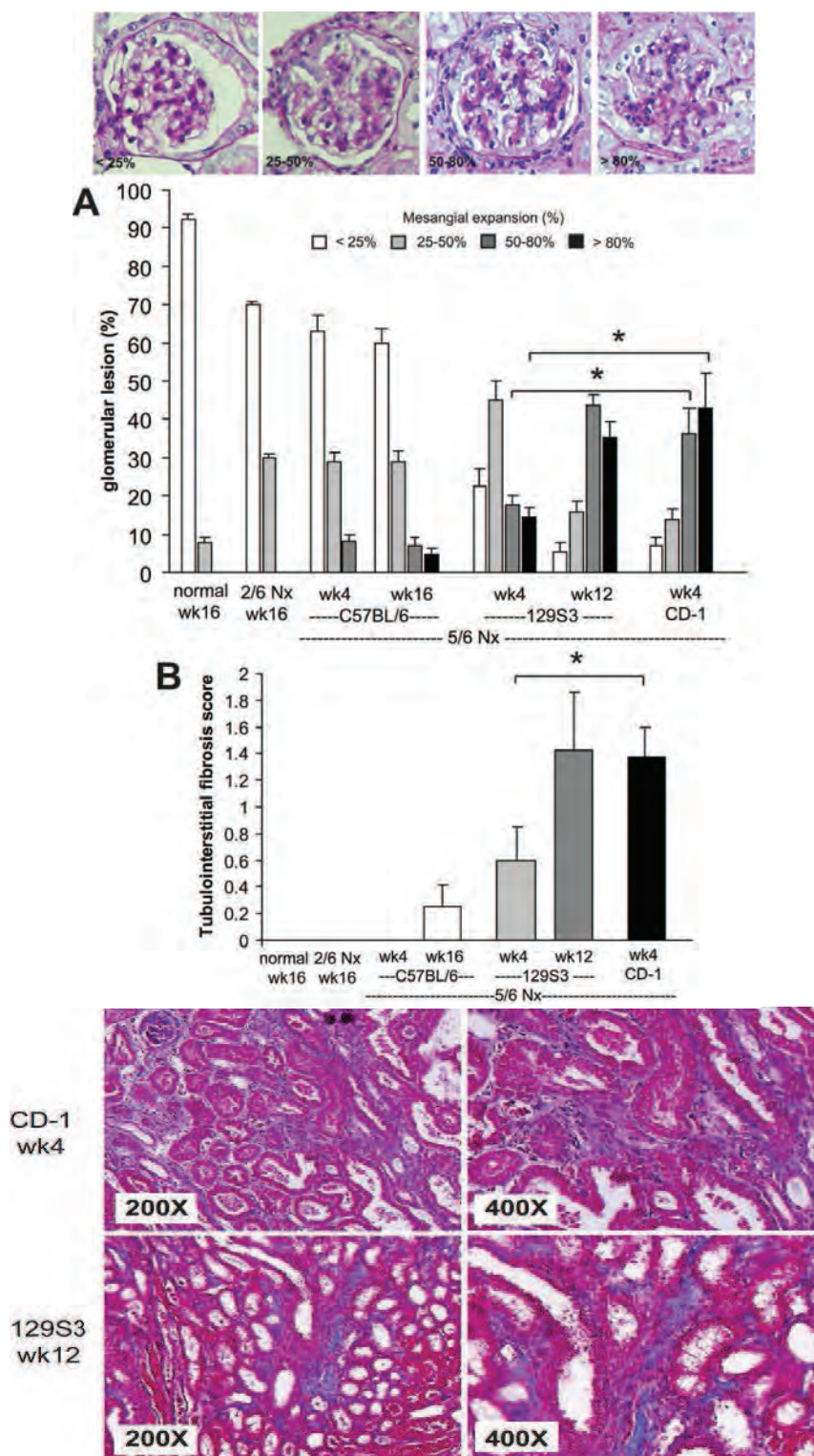


Figure 16: Glomerular injury scoring and tubulointerstitial fibrosis following 5/6 nephrectomy. Semi-quantitative measures of glomerular injury assessed by mesangial expansion in periodic acid-Schiff stain (upper panel 400x original magnification) and tubulointerstitial fibrosis score from Masson's trichrome stain of composite normal

control at wk16 (n=5), composite 2/6 Nx at wk16 (n=5), 5/6 Nx in C57BL/6 at wk4 (n=4), wk16 (n=8), 5/6 Nx in 129S3 at wk4 (n=5), wk12 (n=7) and 5/6 Nx in CD-1 at wk4 (n=10 (middle panel). The representative Masson's trichrome stain of tubulointerstitial fibrosis pictures were showed (lower panel). See Methods section for details. *, P<0.05 5/6 Nx in CD-1 wk4 vs 129S3 wk4

Clinically relevant characteristics validation of the 5/6 nephrectomy model of chronic kidney disease

Weight loss, hyperphosphatemia anemia with low erythropoietin are common clinical consequences of chronic kidney disease[16, 17]. Normal 7-9 week old mice gain weight as they grow; in contrast, 129S3 and C57BL/6 mice did not gain weight, whereas CD-1 mice lost weight after 5/6 nephrectomy (Figure 17A). Control 2/6 nephrectomy mice had a non-significant, transient decrease in body weight after surgery but then resumed normal growth within 2 weeks. Within one week of the 2/6 Nx surgery (both 2/6 Nx and 5/6 Nx groups, 0 weeks) mice were anemic with corresponding high (>10,000-fold increase) erythropoietin (EPO) levels, reflecting a compensatory increase that occurs clinically within 1 week after acute anemia [154, 155]. Mice subjected to only 2/6 Nx were able to recover from their anemia, with a corresponding return to baseline EPO levels (Figure 17B, C). All mouse strains subjected to 5/6 Nx had a further decline in hematocrit after the right kidney was removed at 0 weeks, and EPO levels declined precipitously within 1 week, with only a modest increase at two weeks, relative to the progressing anemia. The rate of development of anemia and hyporesponsiveness of EPO level paralleled the serum creatinine increase. Mice subjected to 2/6 Nx rapidly resolved their surgical anemia eventually returning their transiently elevated EPO levels to normal (Figure 17C). All 3 mouse strains developed hyperphosphatemia after 5/6 nephrectomy, although the degree of hyperphosphatemia was worse in CD-1 and 129S3 strains; amyloasemia was elevated in all three mouse strains, with 129S3 and CD-1 slightly higher than C57BL/6 (Figure 17D). Therefore, several non-renal manifestations of CKD observed in patients are replicated in this 5/6 nephrectomy mouse model.

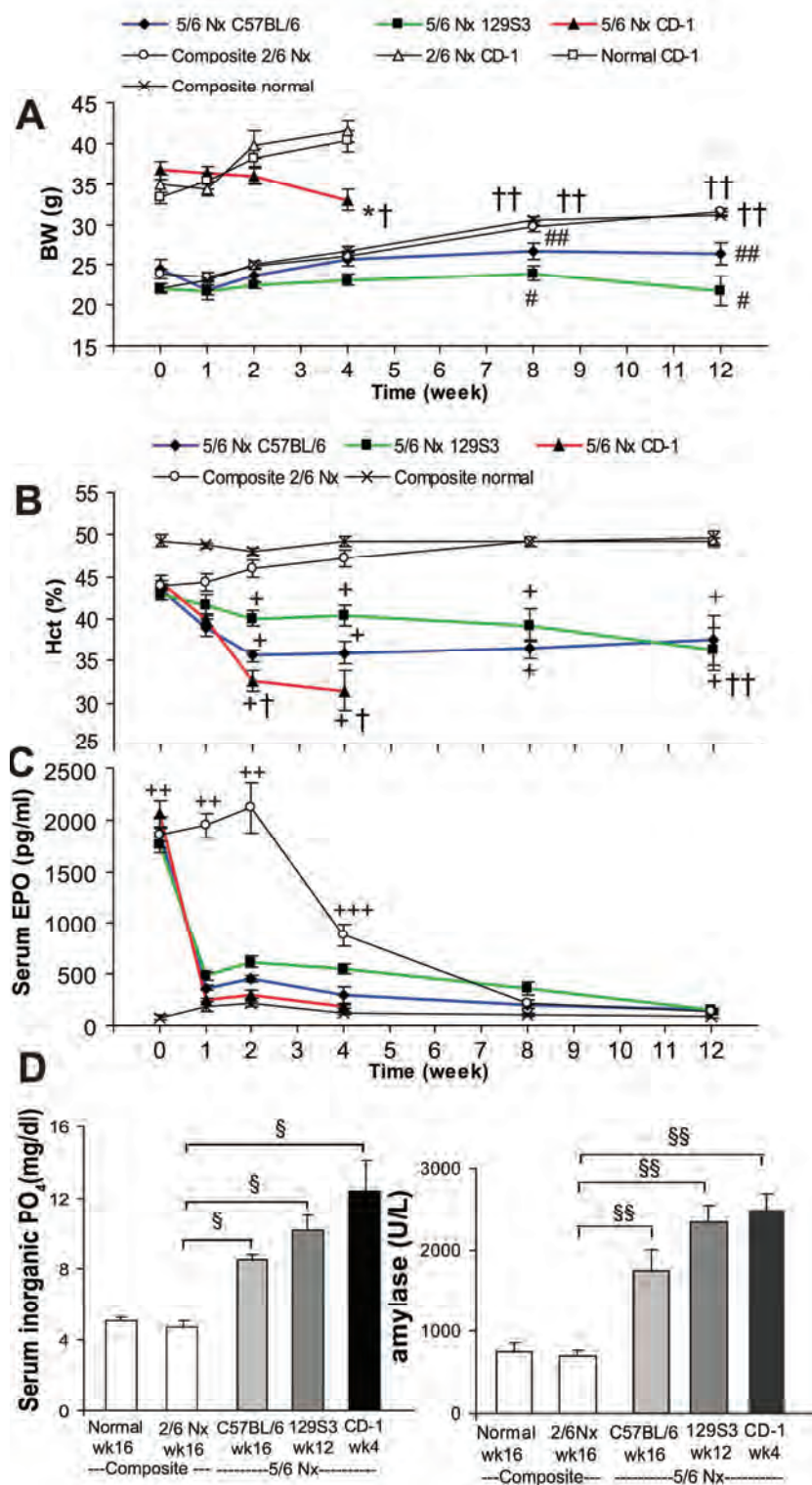


Figure 17. Changes in chronic kidney disease characters following 5/6 nephrectomy. Strain-specific temporal changes in body weight (BW), anemia, erythropoietin (EPO), and serum phosphate following reduction in renal mass. Temporal changes in (a) BW, (b) hematocrit (Hct), and (c) serum erythropoietin (EPO). Number of animals for body

weight ((CD-1 with normal sham surgery control (n=7), 2/6 Nx control (n=4), and 5/6 Nx (n=12)), (129S3 and C57BL/6 with normal sham surgery control (n=5), 2/6 Nx control (n=8), 129S3 5/6 Nx (n=12), and C57BL/6 5/6 Nx (n=9)), Hct and serum EPO (composite normal sham surgery control (n=6), 2/6 Nx control (n=6), CD-1 5/6Nx (n=12), 129 Sv 5/6 Nx (n=12), and C57BL/6 5/6 Nx (n=9)), (d) serum phosphate and (e) amylase (composite normal sham surgery control at week 16 (n=6), composite 2/6 Nx control at week 16 (n=6), C57BL/6 5/6 Nx at week 16 (n=4), 129S3 5/6 Nx at week 12 (n=4) and CD-1 5/6 Nx at week 4 (n=4)). *P<0.001 CD-1 5/6 Nx vs 2/6Nx; † P<0.005 5/6 Nx at specific time point vs week 0; †† P<0.05 5/6 Nx at specific time point vs week 0; #Po0.001 5/6 Nx in 129S3 vs composite 2/6 Nx; ##Po0.005 5/6 Nx in C57BL/6 vs composite 2/6 Nx; +P<0.001 5/6 Nx vs composite 2/6 Nx; ++ P<0.001 composite 2/6 Nx vs normal; +++P<0.05 composite 2/6 Nx vs normal; §P<0.05 5/6 Nx vs composite 2/6 Nx; §§P<0.001 5/6 Nx vs composite 2/6 Nx.

The progressive hypertension following 5/6 nephrectomy as the validation of CKD characters and strain-selective differences in baseline mean arterial pressure

Elevated mean arterial pressure (MAP) is one of the important CKD clinical characters. We then inserted radiotelemetry catheter in the carotid artery for measured conscious mouse MAP which more accurate than tail cuff measurement. After 5/6 nephrectomy, MAP in CD-1 and 129S3 mice increased progressively as early as 2 weeks after surgery, and the differences in MAP between all three strains expanded over time, $p < 0.0001$ (Fig 6B-D). In contrast, the MAP in C57BL/6 was only moderately elevated 1 week after 5/6 nephrectomy, and then stabilized (Figure 18B, E). As a result, the MAP in CD-1 and 129S3 strains, even baseline values, were higher than C57BL/6 at every time point. The circadian variation (daytime dipping during sleep) was not altered by 5/6 nephrectomy (Figure 18A, C-E), differs from CKD patients. Additionally, the baseline MAP in CD-1 and 129S3 were significantly higher than C57BL/6 mice (Figure 18A, B) which might responsible for the rapid progression of CKD in CD-1 5/6 Nx. In any

case, the progressive increase MAP is very promising in this model. Interestingly, the cardiac fibrosis also paralleled with the severity of MAP (Figure 19).

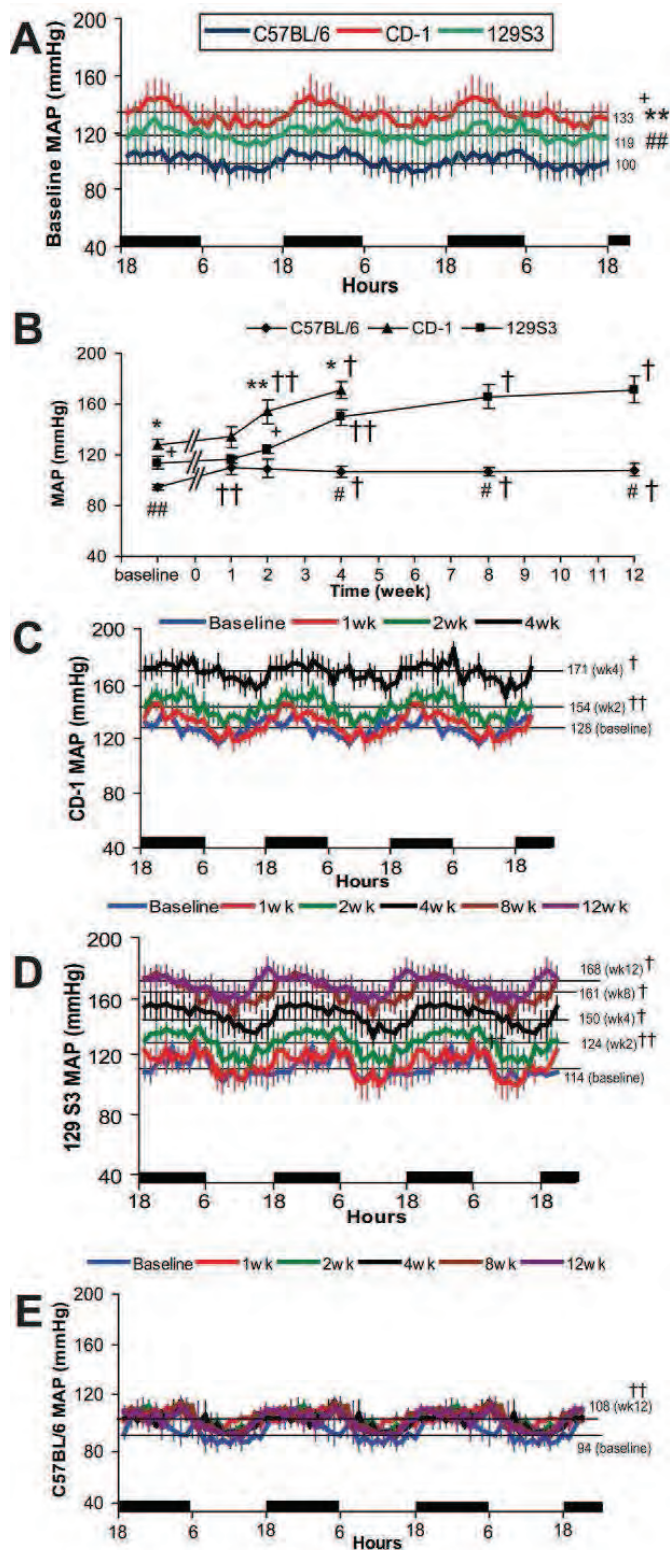


Figure 18: Changes in mean arterial pressure following 5/6 nephrectomy. Systemic blood pressure measured by telemetry. Diurnal changes in baseline (A) mean arterial pressure (MAP; n = 11-13/group), temporal changes in MAP following 5/6 Nx (B; n = 4-5/group), and diurnal changes in MAP following 5/6 Nx in C57BL/6, 129S3, and CD-1 mice (n = 4-5/group) (C-E). Black bars = night time. ; * P<0.001 CD-1 vs C57BL/6**, P<0.05 CD-1 vs C57BL/6; # P<0.005 129S3 vs C57BL/6; ##, P<0.05 129S3 vs C57BL/6; +, P<0.05 CD-1 vs 129S3; †, P< 0.001 MAP at specific time point vs baseline; ††, P<0.05

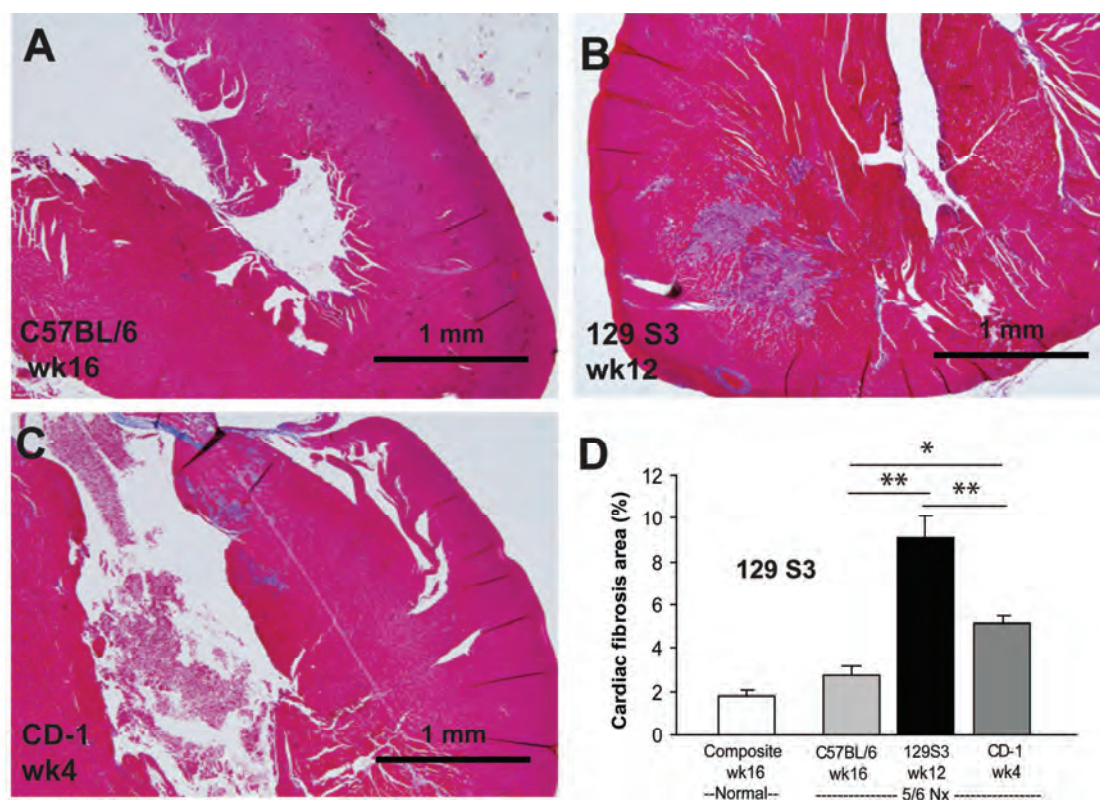


Figure 19: Cardiac fibrosis following 5/6 nephrectomy. Typical images of Masson's trichrome stained cardiac sections after 5/6 Nx in C57BL/6 at wk16 (A), 129S3 at wk12 (B), and CD-1 at wk4 (C) (original magnification 20x). *, P<0.05, **, P<0.001.

The induction of hypertension by Angiotensin II but not deoxycorticosterone acetate induced CKD in C57BL/6 CKD- resistance

We proposed that C57BL/6 resisted to CKD progression after kidney remnant injury from lower blood pressure. Then we induced hypertension in C57BL/6 5/6 Nx mice by several drugs; norepinephrine, midodrine, angiotensin II by osmotic minipump or deoxycorticosterone acetate with salt water (DOCA- salt). Unfortunately, the epinephrine and midodrine increase blood pressure very slightly but mainly elevated heart rate (data not shown). However, angiotensin II and DOCA increase blood pressure significantly (Figure 20).

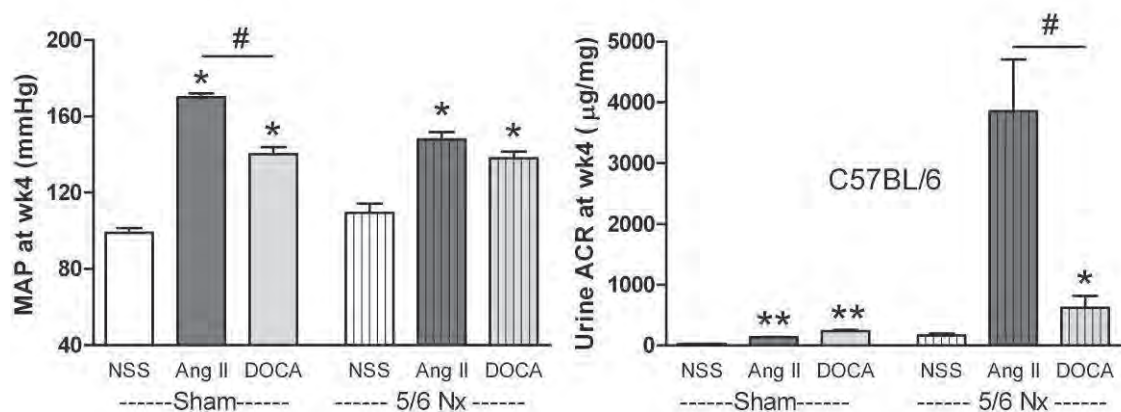


Figure 20. Mean arterial pressure and albuminuria after 5/6 nephrectomy with hypertension induction in C57BL/6 chronic kidney disease resistance. MAP (left) and albuminuria (right) 4wk after 5/6 Nx or sham surgery controls (sham) in C57BL/6 mice followed by angiotensin II (Ang II) or DOCA-salt (normal saline substituted for drinking water) administration or normal saline (NSS) control. *, $P < 0.005$ drug administration vs control in each group; **, $P < 0.05$ drug administration vs control in each group; #, $P < 0.005$

Angiotensin II (Ang II) infusion induces hypertension in experimental animals [156, 157], and increases CKD progression in the rat 5/6 nephrectomy model [158], although it not been studied in mice after 5/6 nephrectomy. Infusion of Ang II by osmotic minipump (0.75 µg/kg/min) increased blood pressure in both normal and 5/6 Nx C57BL/6 mice within 1 week (Figure 20); by 4 weeks the blood pressure had risen. Ang II infusion rapidly induced albuminuria within 1 week in both 5/6 Nx and sham surgery control

mice, although the ACR was 15-fold higher in 5/6 Nx group throughout the 4 weeks of administration. Daily (24 hr) albumin excretion was similarly increased by 9-fold. Ang II further reduced kidney function as measured by elevated BUN and serum creatinine and decreased GFR (Figure 18F,G) and caused glomerular and tubular injury (Figure 19A-D) in mice subjected to 5/6 nephrectomy but not in sham controls. Ang II infusion also caused other signs of chronic kidney disease including polyuria (Figure 21).

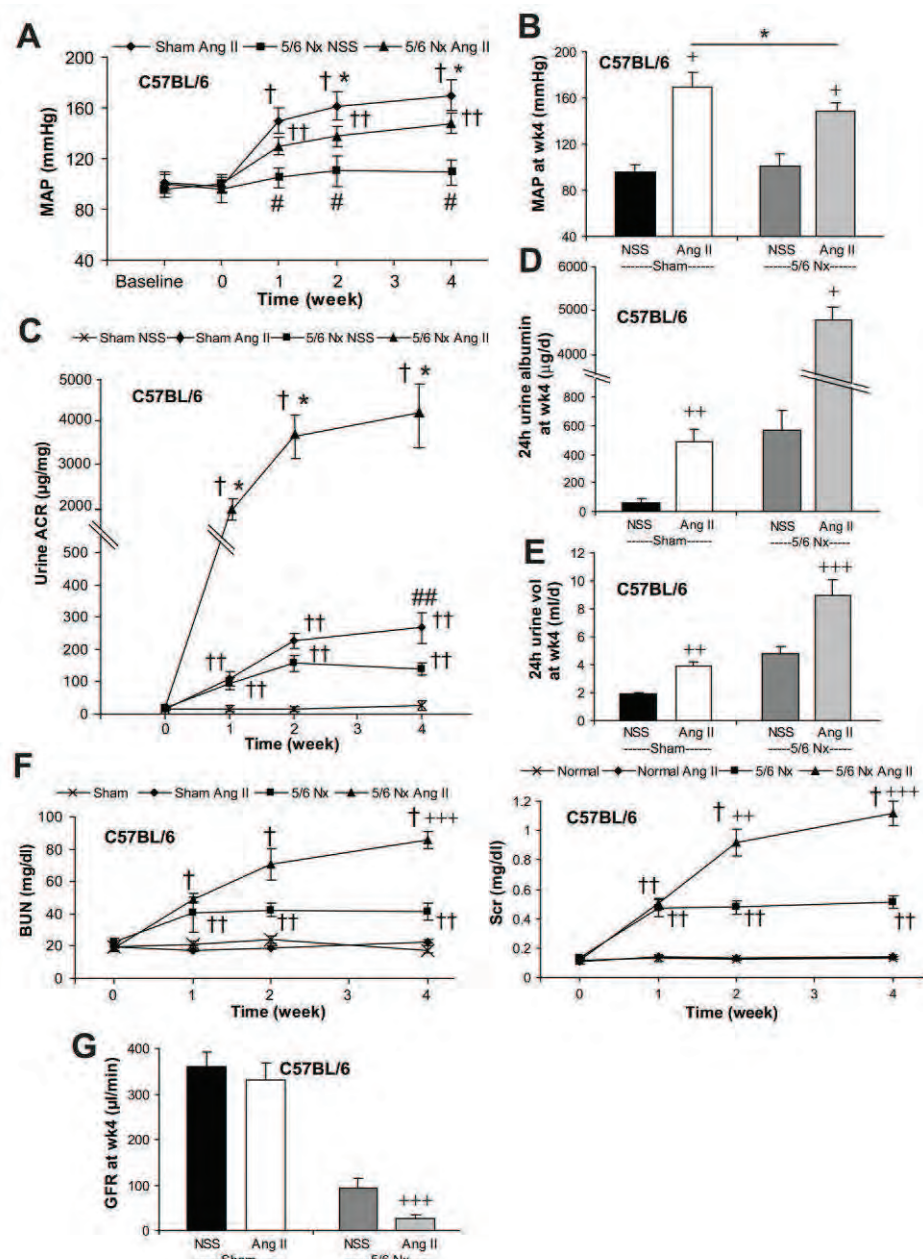


Figure 21: Effect of angiotensin II administration in C56BL/6 and 5/6 nephrectomy. MAP change of C57BL/6 mice following 5/6 Nx (5/6 Nx) or sham surgery controls (sham) with

Angiotensin II (Ang II) administration or normal saline (NSS) control (A). Effect of Angiotensin II or NSS control on MAP at wk4 (B), increase in spot urine albumin/creatinine ratio (ACR) (C), 24h urine albumin at wk4 (D), 24h urine volume at wk4 (E), progression in BUN, Scr (F), GFR at wk4 (G) in C57BL/6 mice subjected to 5/6 Nx vs. sham surgery control treated with NSS or Angiotensin II; (n=4-6/group).

*, P<0.005 5/6 Nx + Ang II vs sham + Ang II; **, P<0.05 5/6 Nx + Ang II vs sham + Ang II, #, P<0.001 5/6 Nx + NSS vs sham + Ang II, ##, P<0.05 5/6 Nx + NSS vs sham + Ang II; +, P<0.001 Ang II vs NSS; ++, P<0.005 Ang II vs NSS; +++, P<0.05 Ang II vs NSS; †, P< 0.001 value at specific time point vs baseline; ††, P< 0.05 value at specific time point vs baseline

After short term (2 weeks) administration of Ang II albuminuria and histological damage was still present even 2 weeks after discontinuation of Ang II (data not shown), consistent with a durable, irreversible effect. In summary, the C57BL/6 resistance to CKD could be only overcome by the combination of reduced kidney mass and Ang II-induced hypertension. On the other hand, DOCA-salt which elevated MAP to the same extent as angiotensin II (Figure 8), but caused only modest albuminuria (Figure 20) relative to angiotensin II, consistent with a largely blood pressure-independent effect of angiotensin II to convert C57BL/6 mice from CKD resistant to CKD susceptible after 5/6 Nx. This further supports a primarily blood pressure-independent role for angiotensin II in our 5/6 Nx CKD model. Subsequently, we created the model of CKD in C57BL/6 with pre-existing 5/6 Nx which originally resisted to CKD progression by Ang II administration. This model can be used in sepsis experiments in case the inbred mouse background is needed.

Global changes in renal architecture visualized *ex vivo* by contrast-enhanced microCT

The regional differences in kidney injury were implied upon histological staining of sections at low magnification, but serial sections are impractical. To complement the detailed, cellular level view provided by histology, we used MicroCT imaging to gain a more global view of kidney damage in moderate detail to compare some of our models (Figure 22). Changes in renal structures are difficult to discern in the original microCT

images, but digital rendering with false coloring of subtle differences in staining revealed gross changes in morphology. In normal kidneys the surface is clearly smooth, in contrast to irregular surface of the fibrotic kidney after folic acid treatment (Figure 22 A, B 3th column). The bumpy surface was more subtle in the chronic post-I/R kidney (Figure 22 A, B 4th column) and bumpy contours were not evident on the non-resected surfaces of the 5/6 nephrectomized kidney (Figure 22A, B 2nd column), consistent with a lower severity in fibrosis. The interior of the kidney also revealed some striking differences. The difference of the density in organ was digitally transformed into 3-dimensional digital soft tissue images with the volume rendering (VR) and the spinning sagittal sections (DS) technique. There were more clump of hazy red color in VR picture (Figure 22A) and more dense yellow/ orange in DS picture (Figure 22B) in 5/6 Nx and Chr I/R than in normal and 2/6 Nx (Figure 22) which reciprocal to albuminuria in the model (table 4). In the normal kidney large branched structures could be traced to the renal pelvis, indicating a predominant staining of renal collecting ducts (Figure 22 A, B 1st column); a stellate structure in the renal medulla is also visible, only in normal kidney. Kidneys from the folic acid model (Figure 22 A, B 3th column) and 2/6 nephrectomy controls (Figure 22 C, D left panel) were similar in their largely transparent appearance, lack of fine structure, and prominence of apparent large branches of collecting ducts, which were fewer in number, relative to normal (Figure 22 A, B 1st column). The most severely injured kidneys from the 5/6 Nx (Figure 22C, D right panel) and chronic post-I/R (Figure 22 A, B 4th column) models had very dense staining that corresponds roughly with the level of albuminuria (Table 4). The density of staining and the non-contiguous nature of the branched structures made it impossible to distinguish between vasculature and tubules; notably absent were clearly visible glomeruli, which would be useful landmarks to define nephrons. Some spherical staining can be spotted, especially in kidneys from the chronic post-I/R model, but staining of a truncated vessel or tubule could not be ruled out. Although regional differences in fibrosis, especially seen in the folic acid model, were not directly reflected in staining of affected areas, these differences appeared to coincide with the drop-out of staining of major collecting duct structures.

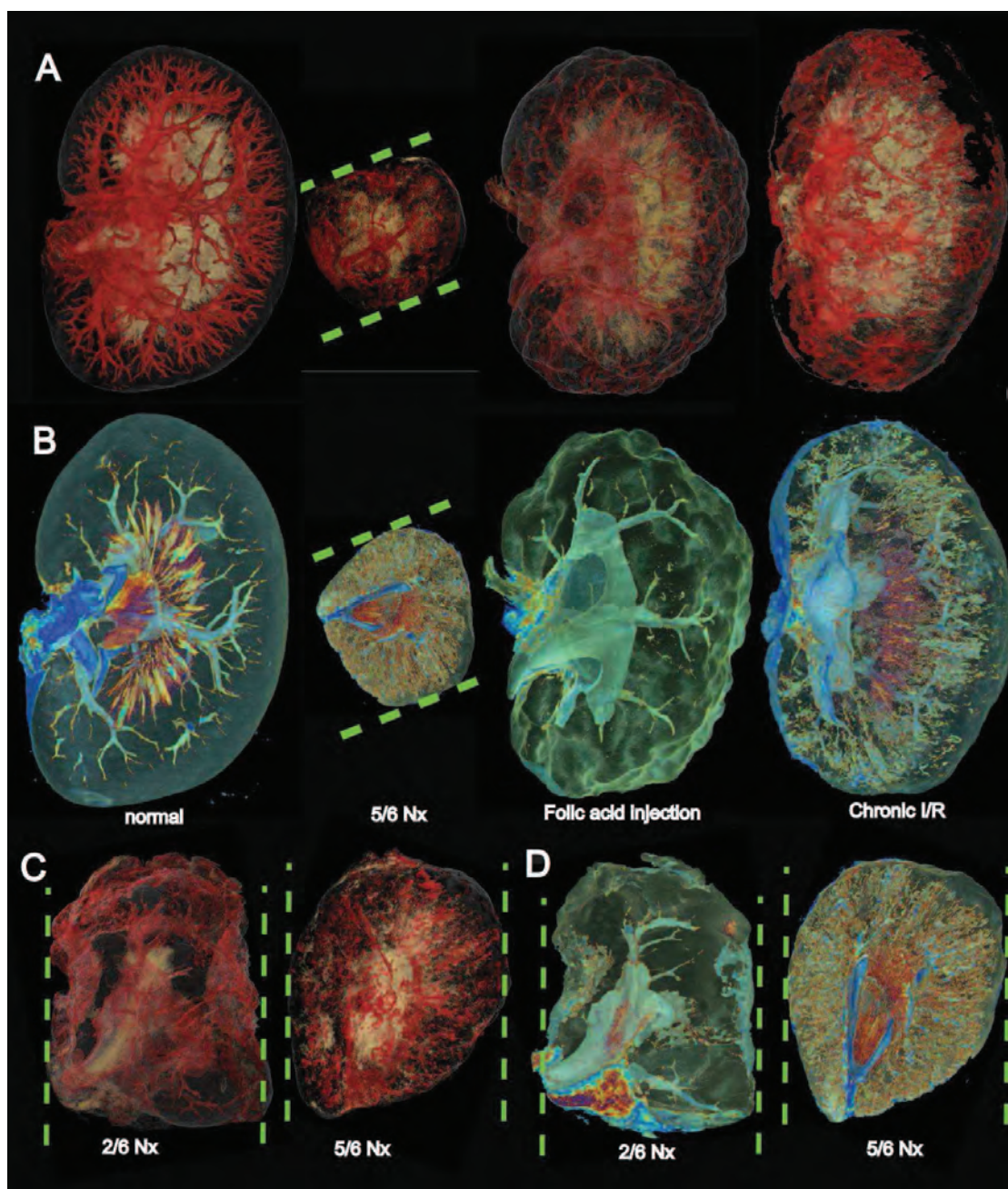


Figure 22. Micro CT pictures in different mouse models. Three-dimensional rendering of mouse kidney acquired through microCT based Virtual HistologyTM from normal, 5/6 Nx, folic acid injection and chronic post-I/R. Renderings from serial microCT sections from CD-1 mice in volume rendering technique (VR) (A) and spinning sagittal sections (DS) technique (B) in different model and 5/6 Nx with 2/6 Nx control picture in VR (C) and DS (D) technique were demonstrated. The digital sagittal sections of the 3-dimensional image from sham normal kidney showed smooth surface and clear cortical area (A, B 1st

column), 2/6 Nx control demonstrated mild irregular surface but clear cortical area (C, D left panel), in contrast, dense opaque yellow color was found in 5/6 Nx model (A, B 2nd column) reciprocal with very high proteinuria. The severe irregular surface with clear cortical area in folic acid model (A, B 3rd column) correlated with severe interstitial fibrosis without albuminuria in this model. Moderately dense yellow color in cortical area of chronic post I/R (A, B 4th column) corresponded with moderate albuminuria.

It was possible that this clumping hazy red color in VR picture was the results from hyperfiltration in nephron and patchy yellow/ orange in DS picture represented albuminuria or secondary change. In any case, the difference in 5/6 Nx and 2/6 Nx control were easily distinguished (Figure 22) which demonstrated the potential of this technique as the new study tool.

Table 4: Characteristics of kidney injury in different renal fibrosis model. (use UUO as a control group).

		BUN (mg/dl)	Scr (mg/dl)	ACR (μ g/mg)	Hct (%)	EPO (pg/ml)	BW (g)	Sham BW (g)	Δ BW (g)
UUO (2wk)	C57BL/6	20 \pm 3	0.16 \pm 0.02	26 \pm 3	50 \pm 2	102 \pm 13	24 \pm 1	26 \pm 1	2 \pm 1
	129S3	15 \pm 2	0.15 \pm 0.01	25 \pm 3	50 \pm 1	91 \pm 11	24 \pm 1	25 \pm 1	1 \pm 0.5
	CD-1	20 \pm 2	0.13 \pm 0.01	17 \pm 3	50 \pm 1	85 \pm 12	35 \pm 1	38 \pm 1	3 \pm 1
5/6Nx (2wk)	C57BL/6	58 \pm 3*	0.38 \pm 0.09 [†]	69 \pm 16	36 \pm 1 [†]	421 \pm 89 [†]	22 \pm 1	26 \pm 1	4 \pm 1 [#]
	129S3	73 \pm 3*	0.41 \pm 0.08*	559 \pm 110*	37 \pm 1*	386 \pm 64 [†]	22 \pm 1	25 \pm 1	4 \pm 1 [#]
	CD-1	79 \pm 9*	0.49 \pm 0.1*	1,176 \pm 277*	35 \pm 2*	91 \pm 24	34 \pm 2	38 \pm 1	4 \pm 2 [#]
5/6Nx (12wk) (4wk in CD-1)	C57BL/6	58 \pm 9*	0.54 \pm 0.04*	78 \pm 75*	37 \pm 1*	98 \pm 34	28 \pm 1	32 \pm 1	4 \pm 1 [#]
	129S3	83 \pm 16*	0.73 \pm 0.19*	2,545 \pm 596 [†]	37 \pm 1 [†]	85 \pm 36	23 \pm 2	31 \pm 1	8 \pm 1 [#]
	CD-1 [§]	79 \pm 19*	0.48 \pm 0.06*	2,640 \pm 502*	34 \pm 3*	50 \pm 24	39 \pm 2	41 \pm 2	7 \pm 4 [#]
FA (2wk)	C57BL/6	57 \pm 4*	0.61 \pm 0.01*	98 \pm 10*	39 \pm 1*	160 \pm 70	24 \pm 1	26 \pm 1	2 \pm 1
	129S3	58 \pm 5*	0.47 \pm 0.04*	80 \pm 9*	39 \pm 1*	124 \pm 45	23 \pm 1	26 \pm 1	3 \pm 1
	CD-1	59 \pm 9*	0.59 \pm 0.06*	89 \pm 13*	40 \pm 1*	109 \pm 65	33 \pm 1	36 \pm 1	5 \pm 1 [#]
FA (12wk)	C57BL/6	50 \pm 5*	0.59 \pm 0.03*	110 \pm 24*	45 \pm 2 [†]	490 \pm 85 [†]	32 \pm 1	33 \pm 1	1 \pm 1
	129S3	50 \pm 5*	0.49 \pm 0.08*	220 \pm 36*	39 \pm 2*	340 \pm 40 [†]	31 \pm 1	32 \pm 1	1 \pm 1
	CD-1	50 \pm 5*	0.46 \pm 0.08*	158 \pm 12*	41 \pm 2*	290 \pm 98 [†]	53 \pm 1	56 \pm 2	4 \pm 1 [#]
Chr I/R (2wk)	C57BL/6	64 \pm 9*	0.54 \pm 0.02*	232 \pm 29*	25 \pm 1	114 \pm 6	24 \pm 1	26 \pm 1	2 \pm 1
	129S3	73 \pm 10*	0.57 \pm 0.04*	112 \pm 15*	27 \pm 2*	194 \pm 9 [†]	23 \pm 1	26 \pm 1	3 \pm 1
	CD-1	64 \pm 9*	0.54 \pm 0.02*	92 \pm 12*	25 \pm 1*	214 \pm 6 [†]	32 \pm 1	38 \pm 1	5 \pm 1 [#]
Chr I/R (12wk)	C57BL/6	43 \pm 5*	0.66 \pm 0.05*	434 \pm 118 [†]	34 \pm 2	268 \pm 28 [†]	30 \pm 1	33 \pm 1	3 \pm 1
	129S3	58 \pm 9*	0.46 \pm 0.04*	644 \pm 191 [†]	34 \pm 1	272 \pm 30 [†]	26 \pm 1	31 \pm 1	4 \pm 1 [#]
	CD-1	40 \pm 5*	0.62 \pm 0.06*	776 \pm 91*	35 \pm 2*	328 \pm 39 [†]	47 \pm 2	56 \pm 2	8 \pm 1 [#]

UUO, unilateral ureter obstruction; 5/6 Nx, 5/6 nephrectomy; FA, folic acid injection; Chr I/R, chronic ischemic reperfusion injury with unilateral nephrectomy; BUN, blood urea nitrogen; Scr, serum creatinine; ACR, urine albumin creatinine ratio; Hct, hematocrit; EPO, erythropoitin; Δ BW = Sham BW-model BW at reciprocal age; Data are mean \pm SE; n = 4/gr; §, data from CD-1 5/6 Nx wk4; #, P < 0.05 vs sham; †, P < 0.05 vs UUO; *, P < 0.005 vs UUO

The sepsis experiment part

Then we used new developed CKD model in sepsis experiment. The severity of CKD in different mouse strains was confirmed before used in sepsis experiment (Figure 23).

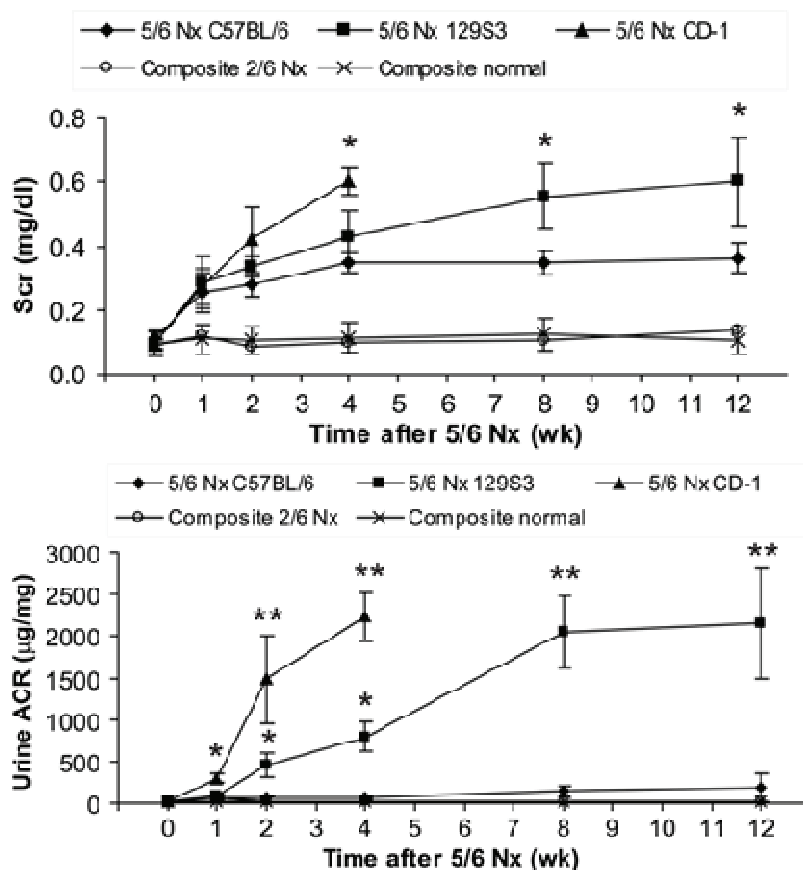


Figure 23. The 5/6 Nephrectomy in different mouse strains before sepsis experiment. The 5/6 Nx in different mouse strain before sepsis experiment confirmed the result in previous model development section

Strain-specific severity of sepsis after 5/6 Nx

Because the severity of sepsis was comparable among different control groups (sham surgery or 2/6 nephrectomy in each mouse strain) the data was combined into a composite control group. We performed CLP at the time of advanced CKD: 4 weeks after 5/6 Nx in CD-1 mice, 12 weeks after 5/6 Nx in 129S3 mice and compared the severity of sepsis with C57BL/6 mice subjected to 5/6 Nx, which do not develop CKD even at 16 weeks [144].

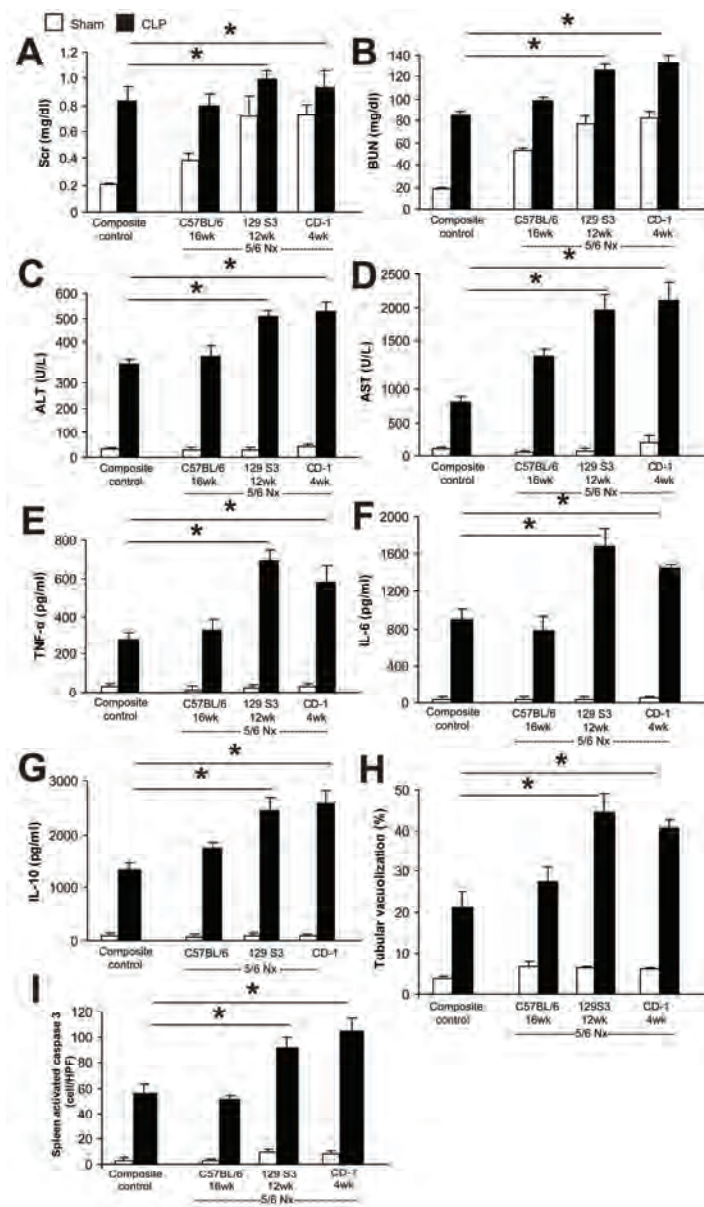


Figure 24. Severity of sepsis in pre-existing chronic kidney disease in mouse. Severity of mouse CKD-sepsis-induced organs injury corresponds with strain-specific severity of CKD (5/6 Nx). Outcomes in CLP were not strain-dependent in normal (non-CKD) mice, so these data were combined (composite control). CKD was induced by 5/6Nx in CD-1, 129S3, or C57/BL6 mice and CLP surgery was performed in 4, 12, or 16 weeks later, respectively. Organ injury was measured at 18 h after sham (white bar) or CLP (black bar) surgery. Renal function was determined by serum Cr (A) and BUN (B), liver function was determined by ALT (C), AST (D), inflammation was determined by serum cytokine levels (TNF- α , IL-6, IL-10) (E-G), renal injury was determined by semi-quantitative measurement of renal vacuolized tubules (H), and splenic apoptosis was measured by

activated caspase 3 (I) in composite normal mice with sham 5/6 Nx at 16 weeks (n= 7-9 in sham and CLP), C57BL/6 5/6 Nx at 16 weeks (n= 5-6 in sham and CLP), 129S3 5/6 Nx at 12 weeks (n=6-7 in sham and CLP) and CD-1 5/6 Nx at 4 weeks (n=6-7 in sham and CLP). *, P<0.05 CLP after 129S3 5/6 Nx or CD-1 5/6 Nx vs. CLP after C57BL/6 5/6 Nx

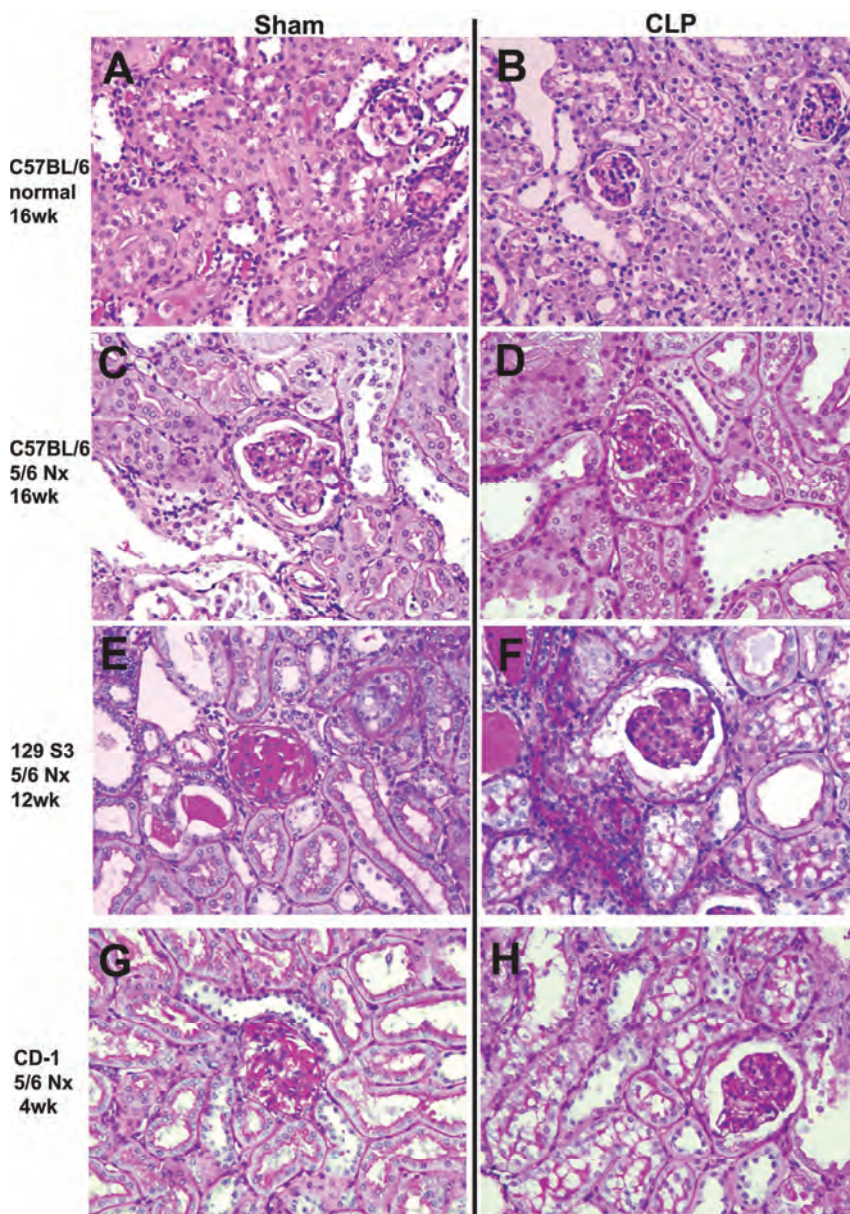


Figure 25. Tubular vacuolization in chronic kidney disease with and without sepsis.

Strain-specific severity of 5/6 Nx and sepsis on renal tubular vacuolization.

Representative images of periodic acid- Schiff-stained renal cortex image of renal cortex in normal (C57BL/6 sham 5/6 Nx at 16 weeks as a typical example in of the composite normal control group) (A, B), C57BL/6 5/6 Nx at 16 weeks (C, D), 129S3 5/6 Nx at 12

weeks (E, F) and CD-1 5/6 Nx at 4 weeks (G, H) in sham (left panel) and CLP (right panel). (400X original magnification 400x)

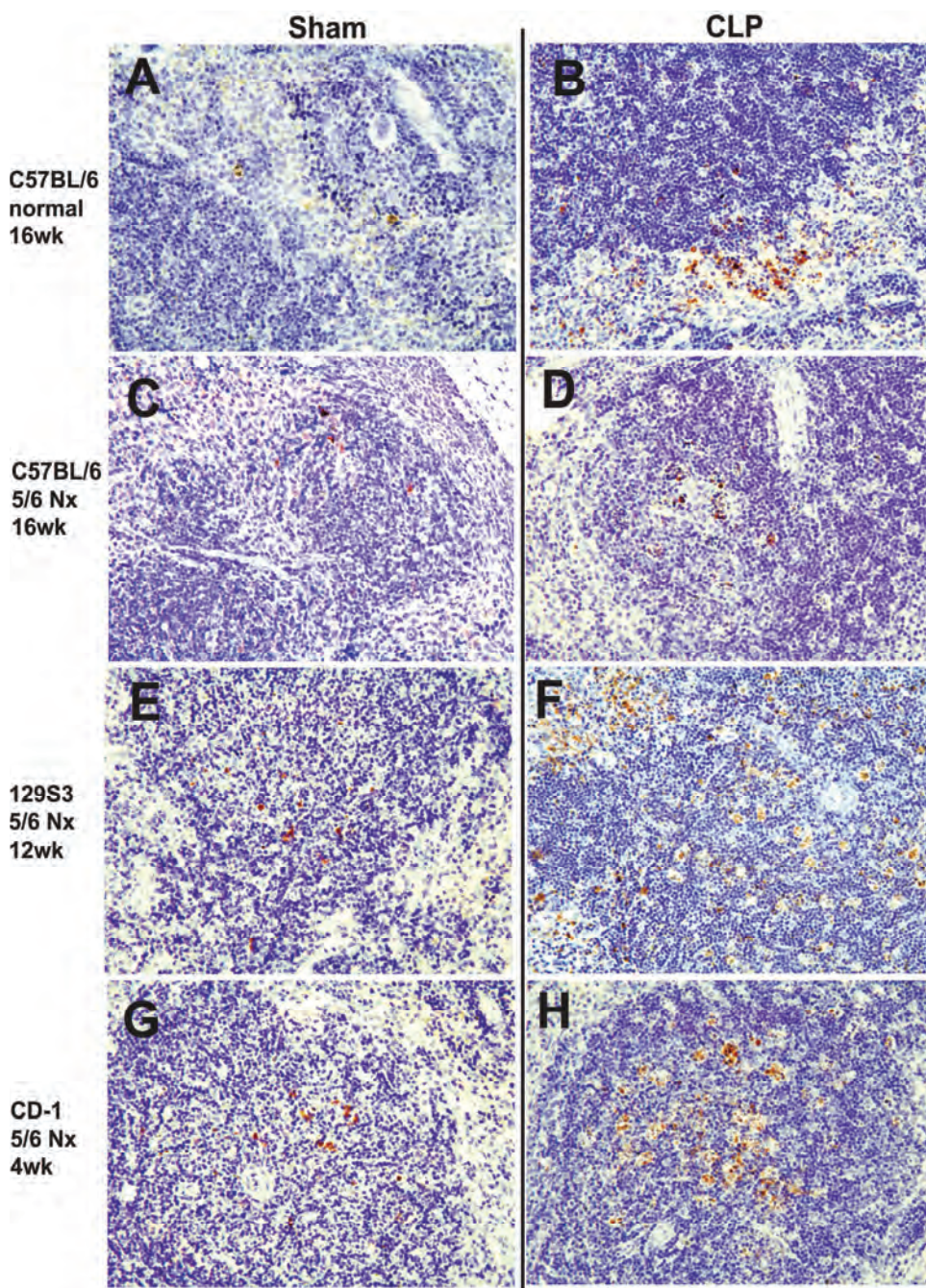


Figure 26: Spleen apoptosis in chronic kidney disease with and without sepsis.

Representative images of spleen stained for activated caspase3 in normal (C57BL/6 sham at 16 weeks as a typical example of the composite control group) (A, B), C57BL/6 5/6 Nx at 16 weeks (C, D), 129S3 5/6 Nx at 12 weeks (E, F) and CD-1 5/6 Nx at 4 weeks (G, H) in sham (left panel) and CLP (right panel). (400X magnification)

CD-1 mice and 129S3 mice showed more severe sepsis at 18 h after CLP compared with C57BL/6 mice as measured by kidney injury (Scr, BUN, and renal tubular vacuolization), liver injury (ALT, AST), serum inflammatory cytokine levels (TNF- α , IL-6, IL-10), and spleen apoptosis (Figure 24-26). Surprisingly, 5/6 Nx almost uniformly increased this broad set of organ-specific and systemic manifestations of sepsis: the extent of which correlated with the degree of kidney injury after 5/6 Nx, prior to the CLP insult (Figure 23).

Strain-specific increases in spleen apoptosis, serum HMGB1 and VEGF after 5/6 Nx

Spleen apoptosis is a well documented characteristic of sepsis that is associated with increased mortality in mouse models, and also in humans [159]. The greater degree of spleen apoptosis in 5/6 Nx + CLP in the CKD-susceptible strains, (CD-1 and 129S3) vs. normal/CLP (Figure 24, 26) or the CKD-resistant C57BL6 strain (Figure 24, 26) could be due to underlying, CKD-dependent spleen apoptosis, but there were no reports in the literature. Therefore, we measured spleen apoptosis (by activated caspase 3 staining) at different times during the course of CKD. The amount of spleen apoptosis progressively increased in 129S3 and CD-1 (without sepsis) and corresponded to the severity of CKD (Figure 27A). The composite 2/6 Nx control did not demonstrate spleen apoptosis, the healing process from the resected kidney wounds was not enough to increase serum HMGB1 (Figure 27A). Because VEGF and HMGB1 increase in human CKD [44, 160, 161], and splenic apoptosis is associated with systemic accumulation of HMGB1 [114, 162], we measured both VEGF and HMGB1. Serum HMGB1 and VEGF progressively increased after 5/6 Nx with a faster time course (CD-1 > 129S3 > C57BL/6) that paralleled the strain-specific progressive renal function decline and albuminuria seen previously [144]. VEGF was elevated more rapidly than HMGB1 (as early as 1 week) after 5/6 Nx, consistent with a faster response of VEGF to injury. In contrast, other inflammatory cytokines (TNF- α , IL-6, IL-10) were not elevated at early time points (data not shown) nor showed strain specificity, however, they were elevated only at the last time point in each strain (Figure 27D-F). Thus, Spleen apoptosis, HMGB1

and/or VEGF, but not other inflammatory cytokines (TNF- α , IL-6, IL-10), paralleled the strain specific differences in CKD and could be important factors of sepsis severity after 5/6 Nx.

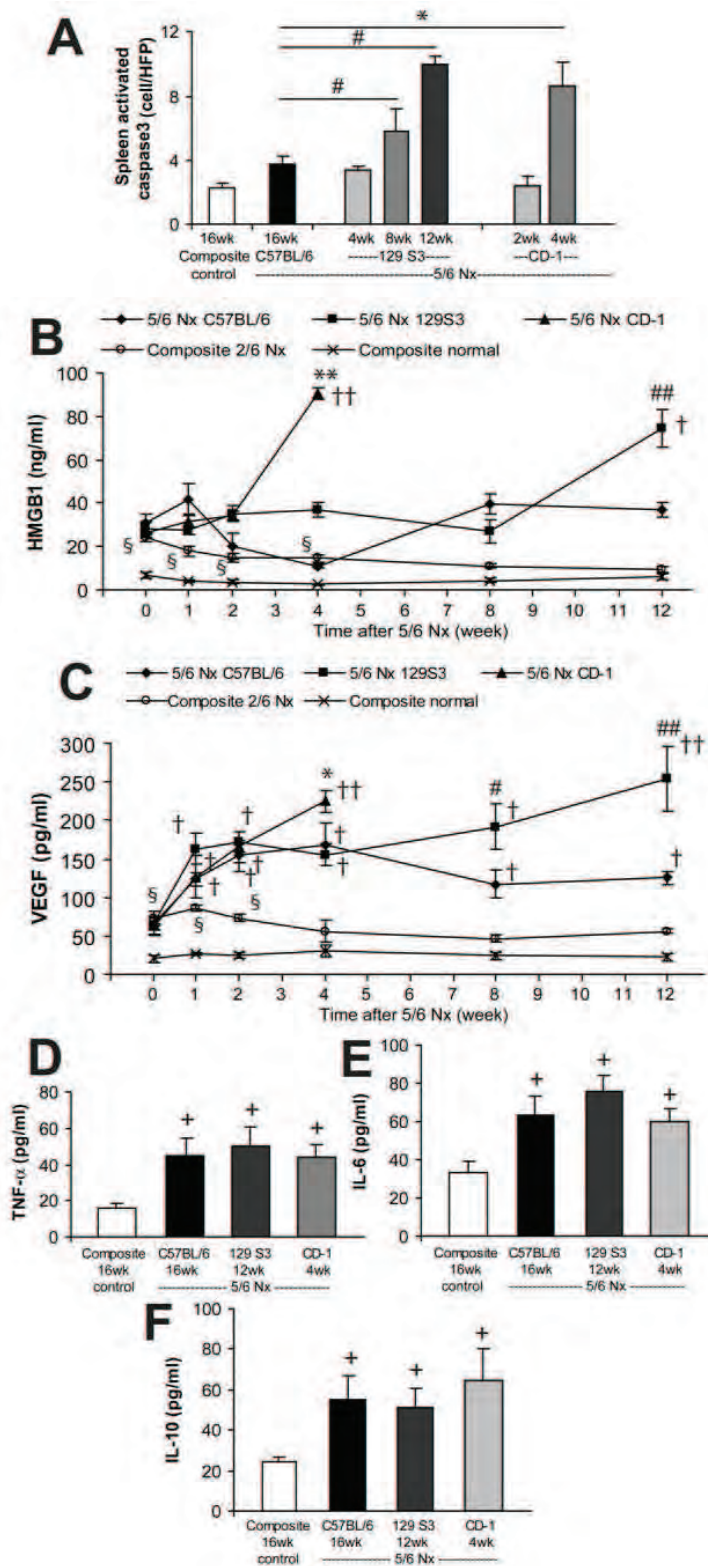


Figure 27. **Cytokines and spleen apoptosis of chronic kidney disease.** Data from the three strains were not different (splenic apoptosis, A, TNF- α , D, IL-6, E, IL-10, F), and normal and 2/6 Nx groups were also not different, so data were combined in a single composite control group. Data from the three strains were not different, but normal and 2/6 Nx groups were different (HMGB1, B, VEGF, C) then data were combined into composite normal and composite 2/6 Nx groups. Semi-quantitative measurement of activated caspase3 positive cell in spleen of composite control at 16 weeks (n=9); C57BL/6 5/6 Nx at 16 weeks (n=4); 129S3 5/6 Nx at 4, 8, 12 weeks (n= 4/group); CD-1 5/6 Nx at 2, 4 weeks (n=4/group) (A); time course of serum HMGB1 (B) and VEGF (C) comparing composite normal, composite 2/6 Nx, C57BL/6 5/6 Nx, 129S3 5/6 Nx and CD-1 5/6 Nx (n=4-6/group); accumulation of serum TNF- α (D), IL-6 (E), IL-10 (F) comparing composite control at 16 weeks, C57BL/6 5/6 Nx at 16 weeks, 129S3 5/6 Nx at 12 weeks and CD-1 at 4 weeks (n= 4-6/group). * P<0.05 CD-1 5/6 Nx vs C57BL/6 5/6 Nx, ** P<0.005 CD-1 5/6 Nx vs C57BL/6 5/6 Nx, # P<0.05 129S3 5/6 Nx vs C57BL/6 5/6 Nx, ## P<0.005 129S3 5/6 Nx vs C57BL/6 5/6 Nx, § P<0.05 composite 2/6 Nx vs composite normal, † P<0.05 value at specific time point vs baseline, †† P<0.005 value at specific time point vs 0 week, + P<0.05 5/6 Nx vs composite 2/6 Nx

Influence of kidney injury or removal on cytokine production after sepsis

Inflammatory cytokines, including VEGF and HMGB1, have been implicated as markers and/or pathogenic mediators responsible for the severity of sepsis [62, 114, 162-164]. To determine the dynamic changes of these cytokines in chronic kidney injury and sepsis, CD-1 mice were used because of the rapid nature of CKD progression. Additionally, bilateral nephrectomy was employed to determine the renal-specific contribution. Serum HMGB1 increased late after CLP alone or after bilateral Nx plus CLP (Figure 28A). In contrast, in 5/6 Nx mice, HMGB1 was elevated at baseline, and progressively increased early after CLP (Figure 28A). Other cytokines (VEGF, TNF- α , IL-6, IL-10) were increased at 6h in CLP alone, 5/6 Nx plus CLP and bilateral Nx plus CLP (Figure 28B-E). The cytokines were often higher in bilateral Nx because of increased cytokine production and/or less renal elimination, as described by others [165, 166].

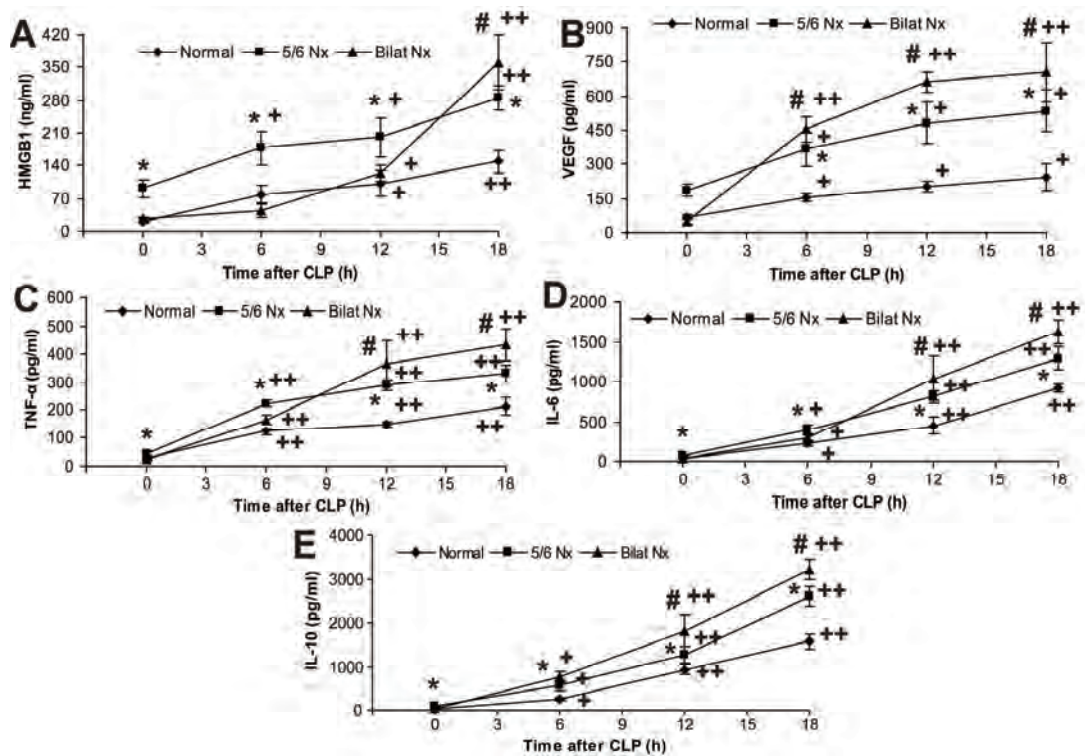


Figure 28. Time course of cytokines in sepsis with pre-existing chronic kidney disease. Serum HMGB1 (A), VEGF (B), TNF- α (C), IL-6 (D) and IL-10 (E) at indicated time points in CD-1 mice with normal/CLP, 5/6 Nx/CLP and bilateral Nx/CLP. (n=4-5/time point) * P<0.05 5/6 Nx vs normal, # P<0.05 bilateral Nx vs normal, + P<0.05 value at specific time points vs at 0 h, ++ P<0.005 value at specific time points vs at 0 h

To determine if kidney function was important for cytokine elimination, bilateral Nx or 5/6 Nx was performed, then exogenous cytokines were intravenously injected and measured frequently to calculate cytokine clearance and half-life values. The half-life of HMGB1 increased by 60% and the half-life of TNF- α , IL-6, IL-10 increased by 2-3 fold in 5/6 Nx compared to normal (Figure 29). The pharmacokinetics of VEGF in bilateral Nx could not be calculated because endogenous VEGF increased as early as 30 min after bilateral Nx (Figure 30). The rapid accumulation of VEGF after bilateral Nx implies that the kidney is the dominant organ of VEGF elimination. Cytokine accumulation in sepsis with pre-existing impaired kidney function, was a result, in part, of impaired renal cytokine elimination which can contribute to the higher sepsis severity after 5/6 Nx.

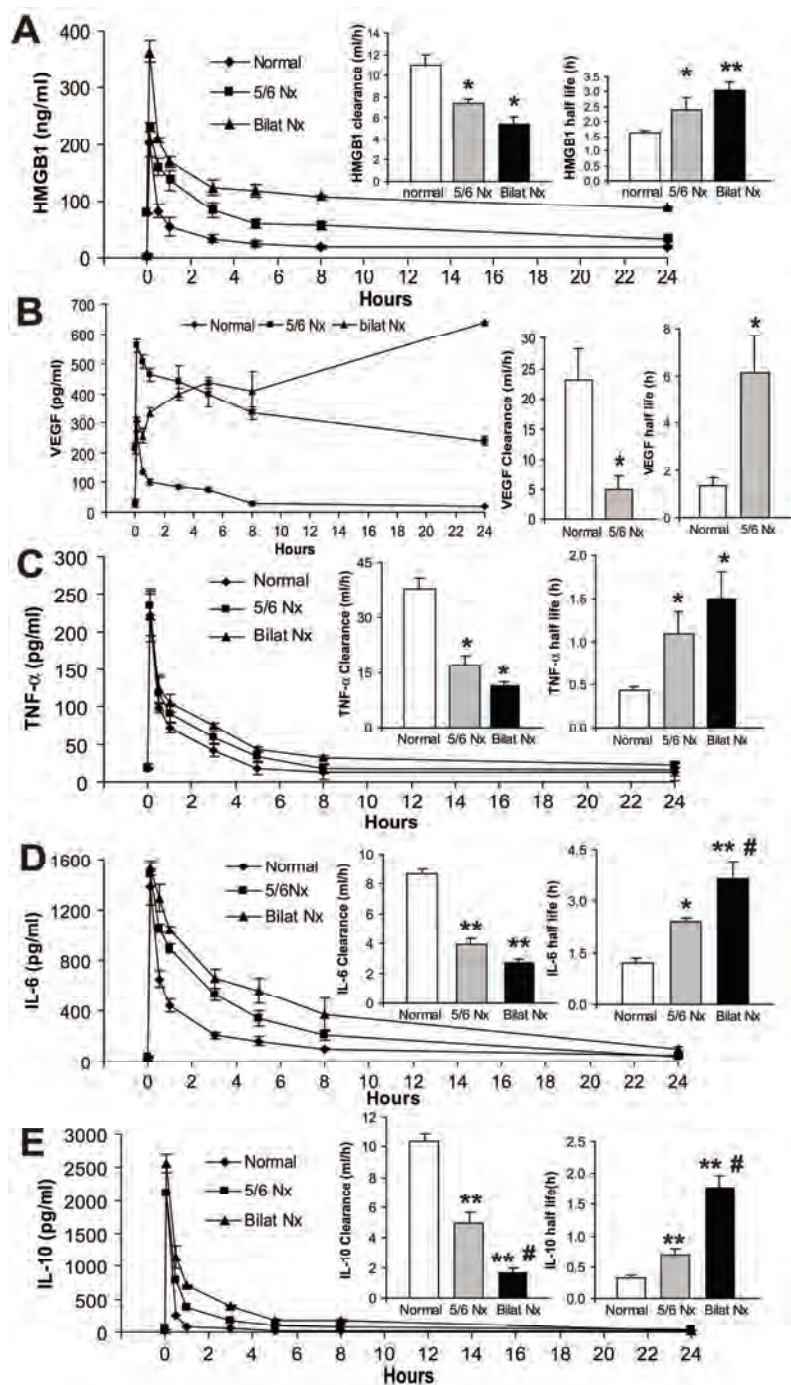


Figure 29. Clearance and half- life of exogenous cytokines injection. The clearance/ half-life of cytokines after injection of exogenous recombinant HMGB1 (A), VEGF (B), TNF- α (C), IL-6 (D) or IL-10 (E) serum cytokine concentration were measured at different times for area under the curve (AUC), clearance, and half-life calculations. (n=4-5/group) * P<0.05 5/6 Nx or bilateral Nx vs. normal, ** P<0.03 5/6 Nx or bilateral Nx vs. normal , # P <0.05 5/6 Nx vs bilateral Nx

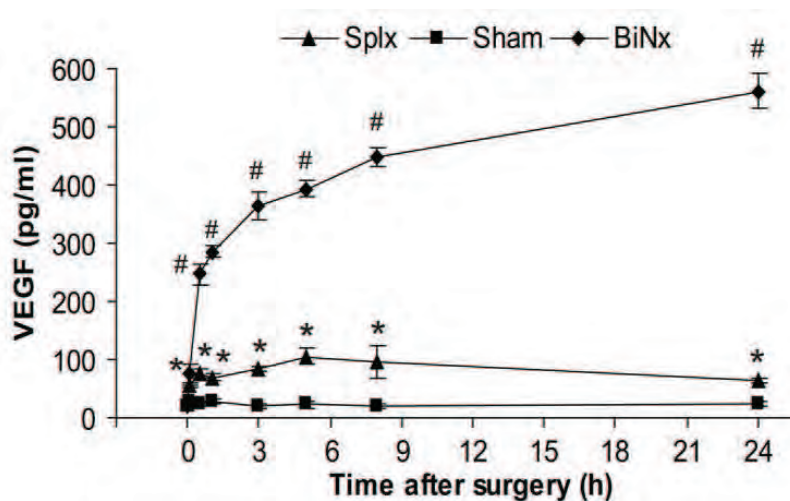


Figure 30. VEGF time course after injury. The VEGF increase after splenectomy (splx), bilateral nephrectomy (BiNx) or sham surgery (bilateral frank incision). Serum VEGF increase tremendously after BiNx and mildly after Splx but not sham surgery. The intensive operation cause VEGF elevation might be due to wound injury- repair process. However, in case of BiNx the production- excretion mismatch caused very high level of VEGF.* P<0.05 vs sham, # P < 0.001 vs sham

Neutralizing HMGB1, but not VEGF, attenuated sepsis severity in mice with pre-existing CKD (5/6 Nx)

To compare the early VEGF or late HMGB1 contributions to the severity of sepsis after 5/6 Nx, we administered neutralizing antibodies in normal and 5/6 Nx CD-1 mice. Soluble FLT-1 (sFLT-1), an endogenous, circulating VEGF receptor splice variant [167], was used to counteract the decreased clearance of VEGF. sFLT-1 administered immediately after CLP, then every 4h, attenuated sepsis severity in normal mice as described previously [15, 62, 163] but was not effective after 5/6 Nx-CLP (Figure 31), similar to our previous report using a folate kidney fibrosis model combined with CLP [15]. In contrast, a single dose of anti-HMGB1 at 6h after CLP attenuated sepsis severity in 5/6 Nx mice but not in normal mice, as measured by kidney injury (Scr, BUN), liver injury (ALT, AST), and inflammatory cytokines (TNF- α , IL-6, IL-10), but not splenic apoptosis (Figure 32). Furthermore, a single dose of anti-HMGB1 also improved

systemic hemodynamics and delayed sepsis mortality in pre-existing 5/6 Nx with CLP (Figure 33).

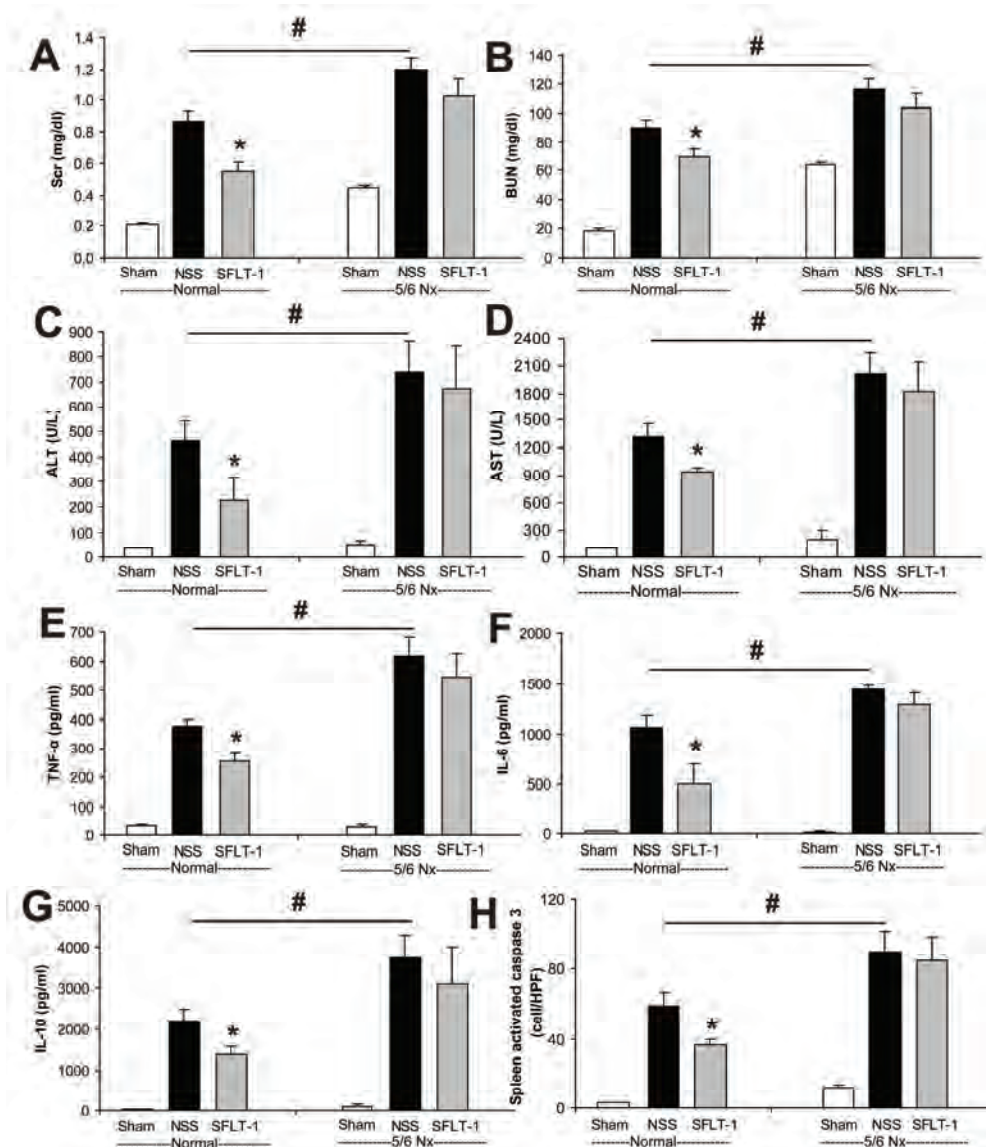


Figure 31. Anti-VEGF (sFLT-1) treatment in sepsis and sepsis with chronic kidney disease. sFLT-1 attenuated sepsis severity in normal/CLP but not in 5/6 Nx/CLP mice. Anti VEGF (sFLT-1) intravenously injection every 4 h started immediately after CLP attenuated sepsis severity in CD-1 normal but not 5/6 Nx as measured by renal injury (Scr, BUN) (A, B), liver injury (ALT, AST) (C, D), inflammatory cytokines (TNF- α , IL-6, IL-10) (E-G), and splenic apoptosis (H) compared with control normal saline treatment. (n=4-6/ group) * P<0.05 anti VEGF vs. control normal saline, # P<0.05 control normal saline in normal vs. control normal saline in 5/6 Nx

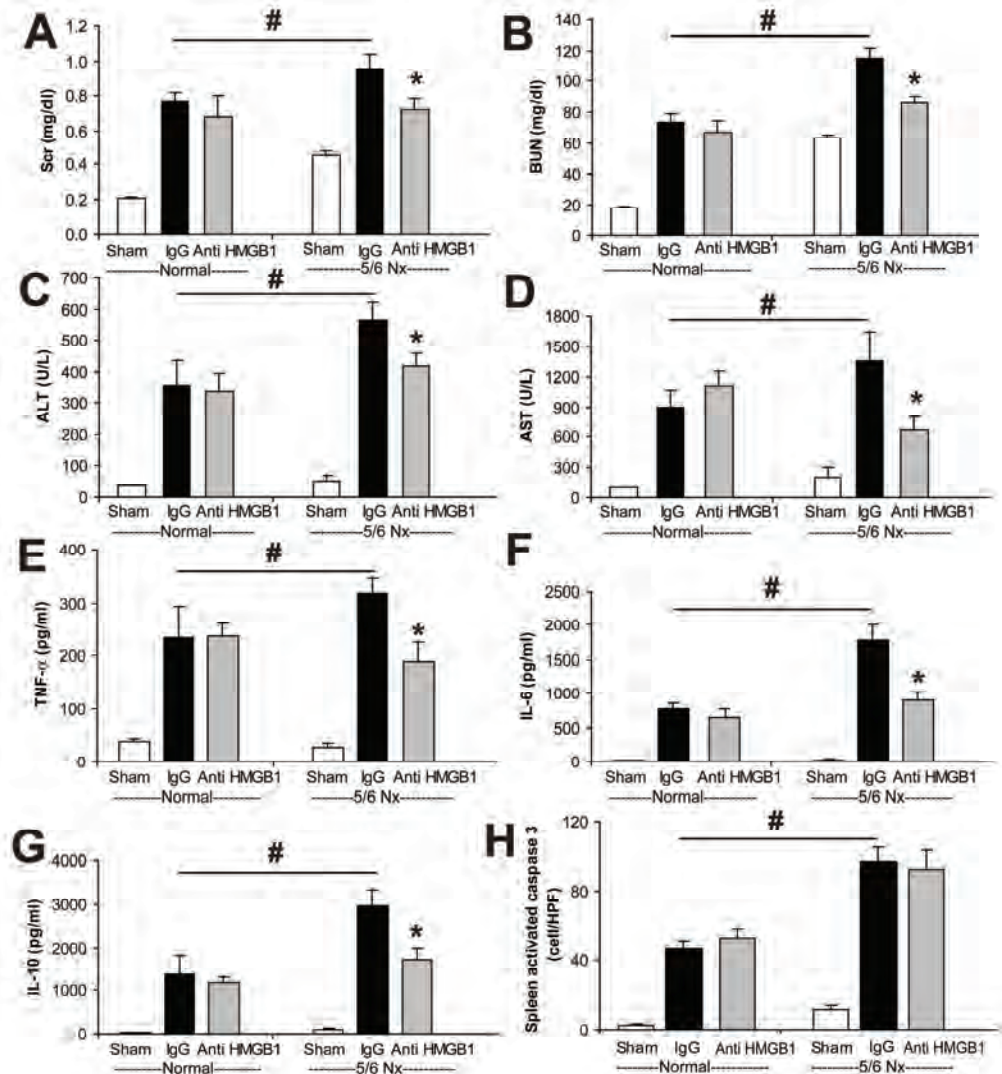


Figure 32. Anti-HMGB1 attenuated sepsis in 5/6 Nx but not normal mice.

Anti-HMGB1 single dose intraperitoneally injection at 6 h after CLP (n = 4-6/ group) attenuated sepsis severity in CD-1 5/6 Nx but not in normal mice as measured by renal injury (Scr, BUN) (A, B), liver injury (ALT, AST) (C, D) and inflammatory cytokine (TNF- α , IL-6, IL-10) (E-G) compared with control rabbit IgG injection; however, anti-HMGB1 did not decrease splenic apoptosis in either group * P<0.05 anti-HMGB1 vs. control rabbit IgG, # P<0.05 control mouse IgG in normal vs. control mouse IgG in 5/6 Nx

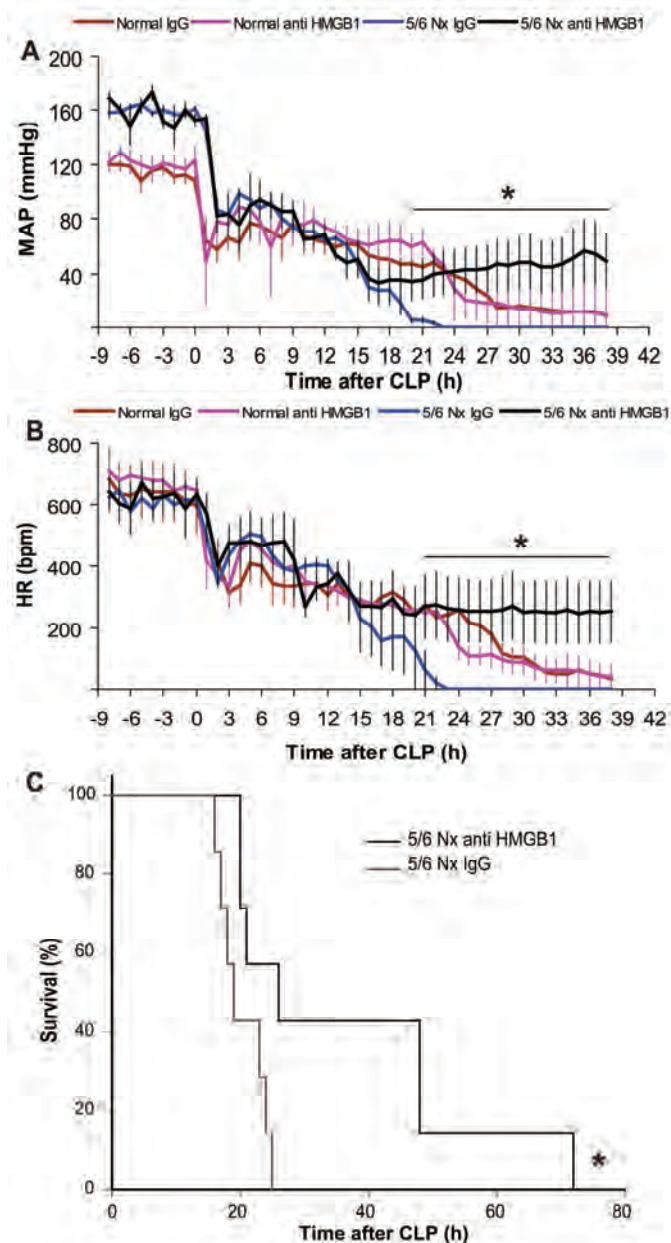


Figure 33. Anti-HMGB1 and cardiovascular effect. Anti-HMGB1 improved sepsis-induced hypotension, bradycardia and survival after 5/6 Nx and sepsis. Telemetric recording of conscious mean arterial pressure (MAP) (A) and heart rate (HR) (B) of normal (red, pink) or 5/6 Nx mice (blue, black) subjected to CLP, and after 6 hours injected with rabbit IgG control (red, blue) or anti-HMGB1 (pink, black) (n=4/group). Survival curve (C) of 5/6 Nx mice subjected to CLP, then 6 hours later treatment with rabbit IgG control (gray) or anti-HMGB1 (black) (n = 7/group). * P<0.05 anti-HMGB1 vs. mouse IgG control

Spleen apoptosis as an important source of serum HMGB1 in both sepsis and CKD (5/6 Nx)

Spleen apoptosis has been shown to be the source of serum HMGB1 both in vitro and in vivo following sepsis [114, 162]. Splenectomy performed during CLP surgery reduced serum HMGB1 acutely by 42% in normal mice as previously described [114, 143]. To determine if spleen apoptosis correlated with serum HMGB1 in the chronic setting of 5/6 Nx, we treated a CKD-resistant strain (C57BL/6) with angiotensin II (Ang II) and treated a CKD-susceptible strain (CD-1) with olmesartan for 4 weeks then measured serum HMGB1. Ang II (0.75 µg/kg/min by osmotic minipump for 4 weeks) induced progressive kidney injury, proteinuria and splenic apoptosis in C57BL/6 (CKD-resistant strain) after 5/6 Nx but not in normal mice (Figure 34, 35). When CD-1 (CKD susceptible strain) mice were subjected to 5/6 Nx, olmesartan treatment for 4 weeks reduced kidney injury, proteinuria and splenic apoptosis (Figure 35 upper panel, 36). Serum HMGB1 increased in proportion to splenic apoptosis in C57BL/6 5/6 Nx treated with Ang II and decreased in parallel to splenic apoptosis in CD-1 5/6 Nx treated with olmesartan (Figure 22B). We also studied 5/6 Nx in the 129S3 strain, which has a slower rate of CKD progression, allowing temporal study of splenic apoptosis and HMGB1. In 129S3 an increase in splenic apoptosis was observed at 8 weeks after 5/6 Nx, which preceded the increase in serum HMGB1 at 12 weeks (Figure 16A, B). Recombinant HMGB1 administration (6 mg/kg) did not induce splenic apoptosis even after bilateral Nx (data not shown). Moreover, the splenectomy reduced serum HMGB1 in CLP both in previously healthy mice and pre-existing bilateral nephrectomy (Figure 35 lower panel, 37). Therefore, our data supports a model whereby increases in serum HMGB1 occur downstream of splenic apoptosis in both sepsis and 5/6 Nx, and spleen is a dominant source of systemic HMGB1 in both conditions.

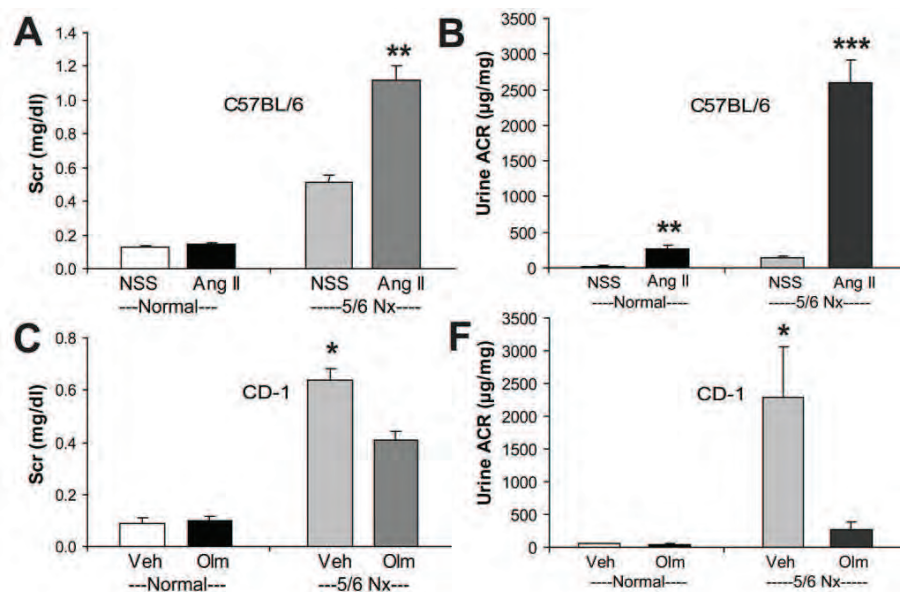


Figure 34. Angiotensin II (Ang II) induced CKD in C57BL/6 5/6 Nx resistant strain and Olmesartan (Olm) improved CKD in CD-1 5/6 Nx. Angiotensin II (Ang II) induced CKD progression in C57BL/6 (CKD resistance strain) after 5/6 Nx as demonstrated by increased Scr (A) and albuminuria (B). Olmesartan (Olm) reduced CKD progression in CD-1 (CKD susceptible strain) after 5/6 Nx as shown by Scr (C) and albuminuria (D). * P < 0.05, ** P < 0.03, *** P < 0.001

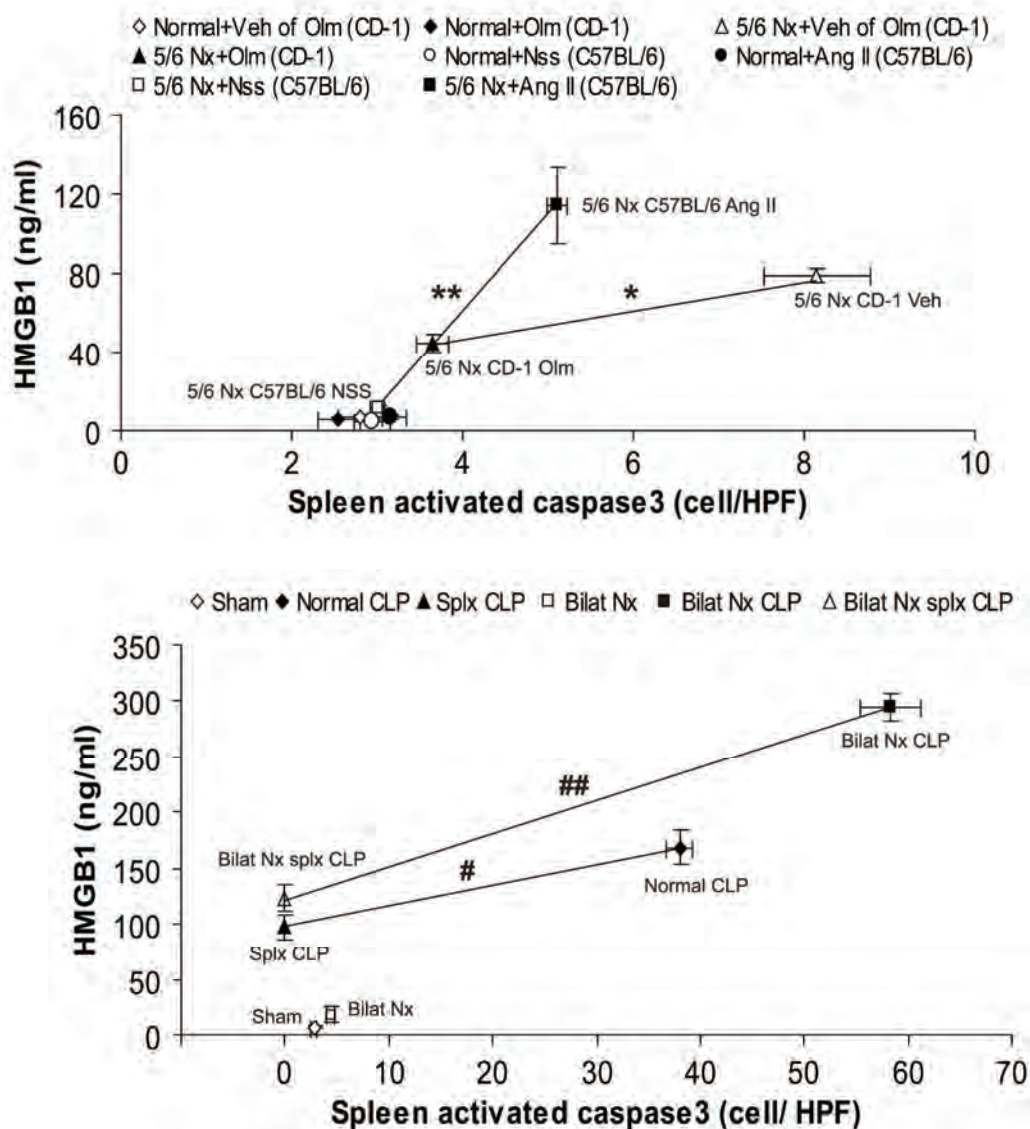


Figure 35. Spleen apoptosis was the source of serum HMGB1 in sepsis and 5/6 Nx. Spleen apoptosis and corresponding serum HMGB1 of C57BL/6 (CKD resistant strain) normal mice with Angiotensin II or normal saline (n=4/gr), C57BL/6 5/6 Nx mice with Angiotensin II or normal saline (n=4/gr), CD-1 (CKD susceptible strain) normal mice with Olmesartan or vehicle (n=4/gr) and CD-1 5/6 Nx with Olmesartan or vehicle (n=4/gr) was demonstrated (upper). Spleen apoptosis and corresponding serum HMGB1 of CLP mice in normal sham (n=4), normal CLP (n=5), splenectomy CLP (n=5), bilateral Nx sham (n=4), bilateral Nx CLP (n=6), and bilateral nephrectomy with splenectomy CLP (n=6) was showed (lower). # P<0.05 non splenectomy vs splenectomy

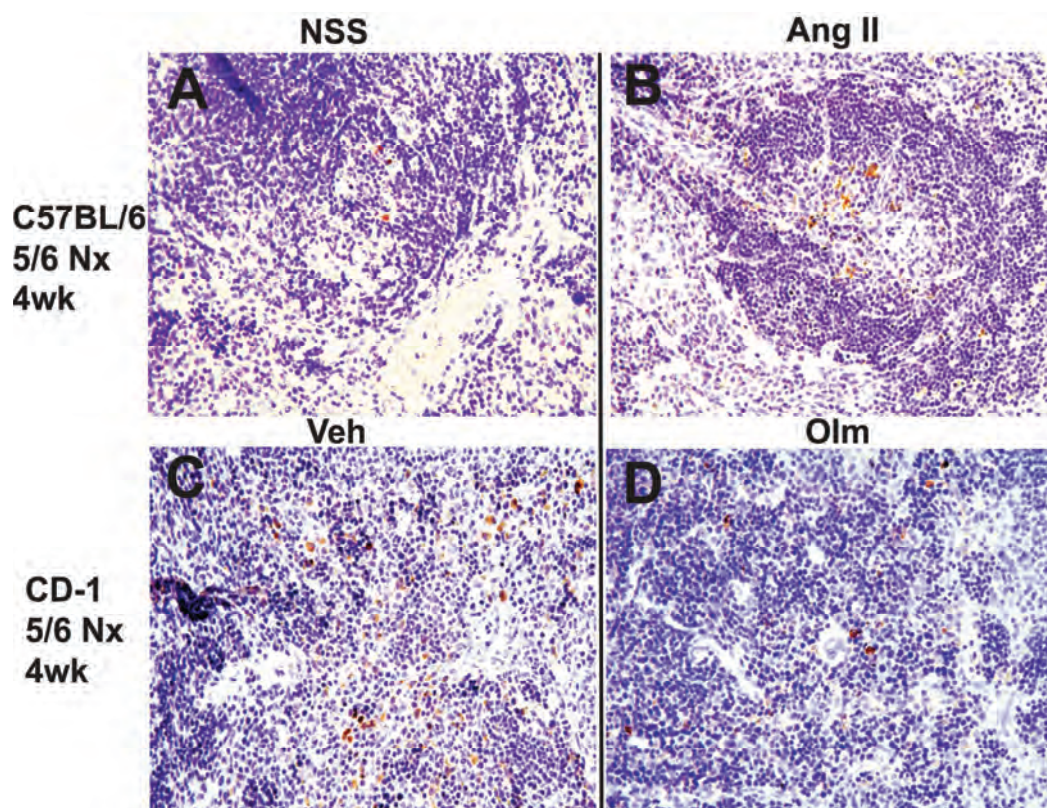


Figure 36. Spleen apoptosis in C57BL/6 5/6 Nx with Angiotensin II and CD-1 5/6 Nx with Olmesartan treatment. Representative picture of spleen activated caspase3 in C57BL/6 5/6 Nx with normal saline (Angiotensin II control) (A) or Angiotensin II injection (B) and CD-1 5/6 Nx with vehicle (C) or Olmesartan (D) for 4 week. (original magnification 400x)

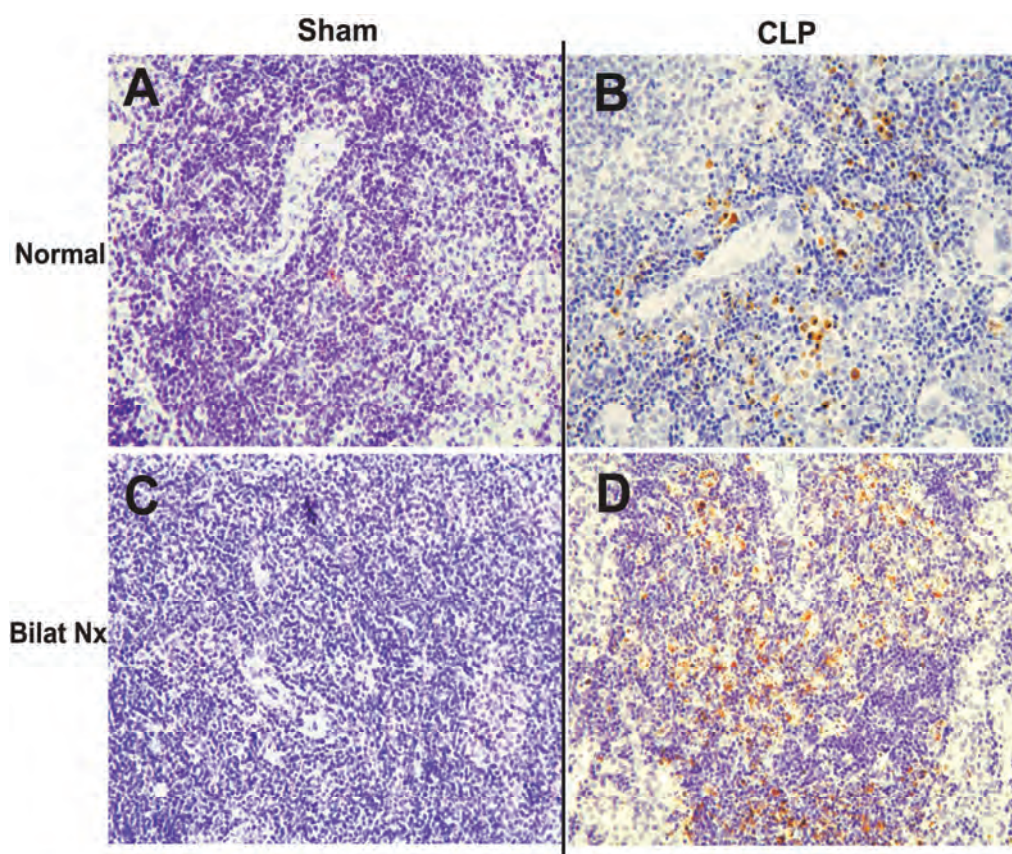


Figure 37. Spleen apoptosis of normal or bilateral Nx mice with CLP.

Representative picture of spleen activated caspase3 in normal (upper panel) and bilateral Nx (lower panel) with sham surgery (left panel) or CLP (right panel). (original magnification 400x)

CHAPTER V

DISCUSSION

We aimed to study sepsis in pre-existing chronic kidney disease (CKD) because the sepsis in pre-existing folic acid kidney fibrosis (FA) showed different natural history of sepsis in previously healthy mice [15]. Unfortunately, FA model is non-appropriate chronic kidney disease (CKD) model due to no progression of kidney injury. Then we need more appropriate CKD model. Chronic kidney disease (CKD) is the results of different pathophysiologic processes associate with progressive decline in glomerular filtration rate (GFR) which leading to uremic syndrome (weight loss, anemia, cachexia, cardiomyopathy, etc) [16, 17]. The renal injury can be demonstrated grossly by radiology (small size, irregular surface) and by histology (glomerulosclerosis, interstitial fibrosis) [168]. Although a mouse CKD model would allow dissection of pathophysiological mechanisms using knock-out/ transgenic approaches and require smaller amount of therapeutic agents with lower cost of maintainance, the number of publications using mouse models of CKD is limited, in part, because of a concern that mice do not develop renal fibrosis in response to reduction in kidney mass[153], and because of difficulties in surgical nephrectomy due to inter-species differences in arterial supply to the kidney. The proper mouse CKD model will be a tremendously benefit to the scientific progression in this topic including our sepsis study. Then we seek the proper method for CKD model. Most of the literatures report 5/6 nephrecctomy using an anterior renal artery branch ligation with contra-lateral nephrectomy as a standard method in rat but not mouse, in part, because of arterial vascular supply is quite different than in the rat [130]. The reports on mouse kidney remnant model consist of contralateral nephrectomy with the initial nephron removal by different methods including anterior or posterior renal arterial branch ligation, electro cautery or heat of cold injury on kidney surface and upper- lower pole resection [132-134]. We selected an alternative approach employing removal of the left upper/ lower pole with adequate hemostatis [169] follow with right nephrectomy at 1 wk later. It is interesting that using this procedure in C57BL/6 did not showed progressive kidney injury and no weight loss

leading to the conclusion that C57BL/6 resisted to CKD progression [153]. However, we postulated that the resistance might be due to inadequate kidney removal then the remained nephron still higher than 50% after insults. To the best of our knowledge, there is no control method to demonstrate the adequacy of kidney mass removal in mouse kidney remnant model. Then we measured the “removed kidney ratio” (see **Methods**) to determine the adequacy of surgical resection and use as reference value among different mouse strains. Additionally, there are other easier, non-complex operative methods to initiate kidney injury which never been used as a part of CKD models such as ischemic reperfusion injury (I/R), toxic substances injection (folic acid, cisplatin, contrast media, mercuric chloride, etc.). Subsequently, we selected other 2 easier methods (I/R and folic acid injection (FA)) to initiate nephron loss then remove one kidney to see if we can get easier, less complex operative CKD model. Then we test these 3 candidate CKD model in CD-1 mice which is bigger and easier for the operation as a pilot study. Unfortunately, the insults by I/R or FA injection then nephrectomy were not severe enough to use as CKD model (Figure 1). However, the 5/6 Nx in CD-1 showed very rapid CKD progression as screening by urine albumin creatinine ratio.

The rapid kidney function deterioration in CD-1 glomerulosclerosis

We demonstrate the adequacy of kidney mass removal, by high BUN/Scr in 5/6 Nx mice at wk1, resulted in rapid deterioration of kidney function (Figure 2A-B) in 129S3 and CD-1 but not in C57BL/6. The level of BUN and Scr of CD-1 5/6 Nx at wk4 was higher than 129S3 at wk8 but comparable with 129S3 at wk12. The progression of renal failure was closely parallel to high tubulointerstitial fibrosis histology (Figure 3B) consistent with patient data [170]. The correspondence between Scr and conscious GFR was demonstrated by using some representative mice in each group (Figure 2C). The difference between control and 5/6 Nx was higher with GFR measurement (300-400 $\mu\text{l}/\text{min}$) compare with Scr (0.5-0.6 mg/dl). Scr had the limitation to demonstrate the severity of kidney injury consistent with previous study [171]. The kidney damage progression measure by urine protein excretion was very rapid in CD-1 and 129S3 with 5/6 Nx which increased as early as wk2 in both strains but more rapid in CD-1 (Figure

2D). Urine ACR of C57BL/6 with 5/6 Nx at wk12 was also slightly higher than control at wk12 (127 ± 97 vs 22 ± 10 $\mu\text{g}/\text{mg}$) but non-statistically significant. The numbers of moderate and severe mesangial expansion glomeruli, parallel to urine protein excretion, were higher in CD-1 5/6 Nx at wk4 which comparative to 129S3 5/6 Nx at wk12 (Figure 3A, 4). Interestingly, C57BL/6 with adequate kidney resection as measured by rapid higher of BUN/ Scr at wk1 and confirmed by very low GFR showed no progression of kidney function, albuminuria and histology (Figure 2-4). We confirmed the resistance to kidney function worsening of C57BL/6 after 5/6 Nx which might be the results of less proteinuria or lower blood pressure [172].

The validation of CKD model to CKD patient in weight loss, anemia with relatively low erythropoietin (EPO) and hyperphosphatemia

In this present study, there were several clinical manifestations that mimic CKD patient.

1). Weight loss: The accumulation of uremic toxin results in nausea, vomiting and weight loss in CKD patient [16, 173]. Body weight (BW) loss was more prominent, rapid in CD-1 than 129Sv after 5/6 Nx (Figure 5A). C57BL/6 with 5/6 Nx, with no kidney injury progression, also showed relatively low BW with tendency of weight loss compare with control mice. The cachexia in C57BL/6 5/6Nx indicated the adequacy of kidney mass removal in our model. 2). Anemia with relatively low EPO level: EPO, erythropoiesis glycoprotein hormone mainly from peritubular kidney cell [174, 175], response rapidly up to more than 10,000 times after acute anemia within 1 week in normal patient [174, 175]. In our present model, 1st stage surgery (Figure1) produced mild anemia in 5/6 and 2/6 Nx at wk0 but the 2/6 Nx mice EPO level rapidly raised up to compensate low Hct level and Hct return to normal at wk2-4 with constantly high EPO level (Figure 5B, C). 3). Hyperphosphatemia and hyperamylasemia: The excretion failure in CKD results in hyperphosphatemia is common metabolic complications of CKD. Serum phosphate and amylase in every mouse strains with 5/6 Nx were higher than control (Figure 5D, E). In C57BL/6, glomerulosclerosis resistant strain after 5/6 Nx, there were relatively weight loss, anemia, low EPO and hyperphosphatemia which demonstrated the adequate kidney mass removal of this model but not parallel to kidney function progression.

Hence, these parameters alone without kidney function measurement were not appropriate to follow up CKD patient. The adequate kidney mass reduction in CD-1 showed several mimic CKD manifestations in very short period of time might be the useful CKD animal model.

The validation of CKD model in blood pressure (BP) progression and cardiovascular damage

The systemic hypertension initiate CKD is controversial opinion but it is accepted that high BP can exacerbate all form of CKD [176]. 129S3 mouse (susceptible 5/6 Nx induced glomerulosclerosis) shows tendency of high baseline BP in some literatures [131, 169]. However, blood pressure measurement in all mouse 5/6 Nx literature, so far, uses intermittent tail- cuff method which maneuver trained mice are needed. In this present study, the radiotelemetry, an alternative method of obtaining the continuous stress- free physiological measurements from awake and freely moving mice, was used [15, 112, 177]. Surprisingly, the around- the- clock telemetric records of baseline mean arterial pressure (MAP) in CD-1 were distinguished higher than 129S3 and MAP in CD-1 and 129Sv were significantly higher than C57BL/6 (Figure 6A). However, elderly normal CD-1 mice (8 months) did not show spontaneous albuminuria and glomerulosclerosis (data not shown) but the rapid high BP progression could be found after 5/6 Nx. MAP of CD-1 and 129S3 5/6 Nx continuous increased from baseline as early as wk2 in both strains which consistent with previous study with tail- cuff measurement [131, 178] (Figure 6B). MAP of C57BL/6 5/6 Nx was slightly increased after wk1 but non- significant difference. Mice are nocturnal creature so BP normally dipping in daytime as circadian variation. The non- dipping of blood pressure in patient which has been recognized as the risk factor of more cardiovascular organs damage can be found in CKD[179]. In our model with severe kidney impairment, there were normal blood pressure dipping in all of the 5/6 Nx mice (Figure 6C-E). The abnormal in autonomic function might be more important cause of non- dipping phenomenon than kidney impairment. The exploration in autonomic function of CKD patients with non- dipping blood pressure is interesting to study. Although there is normal dipping of BP, the cardiovascular organ damage

measured by cardiac fibrosis can be demonstrated in this model (Figure 7). The cardiac fibrosis is one of the uremic cardiomyopathy reported in both patient [180, 181] and CKD animal model [178, 182, 183] which might cause by rennin angiotensin aldosterone system (RAS) activation, hyper phosphatemia, parathyroid hormone or oxidative stress in CKD condition [184]. In our present 5/6 Nx, massive cardiac fibrosis was also found in both CD-1 at wk4 or 129S3 at wk12 but not in C57BL/6 even after wk16 (Figure 7) despite there was hyperphosphatemia (Figure 5D). The severity of cardiac fibrosis seems to parallel to the duration of hypertensive state (Figure 6B, 7) more than phosphate level. High BP might be one of the critical factors for cardiac fibrosis in CKD. CD-1 5/6 Nx in our model showed rapid BP progression with cardiovascular organ damage as measured by cardiac fibrosis. The higher baseline BP in CD-1 and 129S3 compare with C57BL/6 might be the important exacerbation factor for more rapid glomerulosclerosis and albuminuria after 5/6 Nx which leading to more kidney injury progression.

The new CKD model in inbred mouse strain by angiotensin II administration but not deoxycorticosteroid (DOCA)- salt

We postulated that the different in baseline blood pressure in different strains might be responsible for CKD progression and the inbred mouse experiment might be needed for further sepsis experiments. Then we increased BP in C57BL/6 5/6 Nx which resistance to the progression. Angiotensin II (Ang II) induce hypertension is widely use hypertensive model [156, 157]. Ang II increase BP via 2 main mechanisms; direct vasoconstriction and renal salt reabsorption from renin activation then higher aldosterone [185, 186]. Renin is normally excreted from juxtaglomerular area in hypoxic or volume depletion condition. In 5/6 Nx mice, renin activity is slightly high despite less renal mass (data not shown) might due to hypoxia from surgical scar. In any case, the effect of Ang II in kidney remnant rat model is demonstrated [158] but in mouse is never published. Ang II 0.75 µg/kg/min rapidly increased BP in both normal and 5/6 Nx C57BL/6 mice within 1 week (Figure. 9A, B). Ang II slightly increased higher BP in normal than 5/6 Nx (Figure 8 left panel) might due to more salt reabsorption in normal

kidney. Additionally, Ang II increased BP in early phase of bilateral nephrectomy mice up to 18 h before BP drop from severe uremic condition (data not shown). We hypothesized that Ang II have direct vasopressive effect which transiently increase MAP after bilateral Nx which correspondance to the study in rat [187, 188], however, these effect might, in part, correlate with less Na reabsorption in kidney remnant function as mentioned in other studies [156, 186, 189]. There might be the threshold of remnant kidney function which 2/6 Nx and unilateral Nx can be compensated to reach normal kidney reabsorption function. Further study on effect of Ang II in kidney remnant is needed to answer this question. In any case, we surprisingly found very rapid, high albuminuria as early as 1 wk after Ang II administration then constantly high in 5/6 Nx and significant microalbuminuria (dipstick negative) in normal with Ang II (Figure 9C, D) with predicted diuresis response [185] (Figure 9E). The very early albuminuria after Ang II administration might responsible from the rapid hemodynamic change or the direct effect of Ang II to kidney [185]. The removal of Ang II after 10 days of administration did not decrease albuminuria or reduced kidney histology severity at later time point so the pathological change might occur within 10 days of Ang II administration (data not shown). The rapid progression of albuminuria after Ang II administration also reciprocal with progressive loss of kidney function (Figure 9F, G), kidney/ cardiac pathology (Figure 10) and weight loss (data not shown) which mimic rapid natural history in CD-1 with 5/6 Nx (Figure 2-5). However, many characters of C57BL/6 5/6 Nx with Ang II seems more severe than CD-1 5/6Nx (BUN, Scr, kidney and cardiac histology) which might be the direct effect of Ang II in different organs (which demonstrated in normal with Ang II; microalbuminuria, diuresis, cardiac injury, high MAP) or the longer exposure to higher MAP (high MAP start from wk1 in C57BL/6 5/6 Nx with Ang II (Figure 9A) but from wk2 in CD-1 5/6 Nx (Figure 6B). It is important to note that Ang II administration in normal did not decrease glomerular filtration rate and kidney histology which correspond to previous study [185] but did increase cardiac fibrosis area (data not shown), urine volume and urine albuminuria (Figure 9C-E). The Ang II induced cardiac fibrosis in normal group might be the result of higher blood pressure compare with 5/6 Nx group (Figure 9A, B), however, there were other non BP factors in 5/6 Nx [178] which

responsible for more severe cardiac fibrosis in 5/6 Nx. Further studies on uremic cardiomyopathy in this model will be very interesting. It is interesting that deoxycorticosterone (DOCA) with salt water caused hypertension in 5/6 Nx C57BL/6 mice (Figure 8) but did not increase urine ACR profoundly and no CKD characters. Ang II seems to be more important than BP in CKD progression. However, BP from DOCA-salt was a little lower than from Ang II which is non- statistically value. But these differences might be clinically important as report in patient studies. In any case, the C57BL/6 5/6 Nx with Ang II will be the interesting model to explore the importance of different gene in CKD in several available C57BL/6 knock out/ transgenic back ground.

The kidney fibrosis in different models and microCT approach

Fibrosis is the accumulation of collagenous extracellular matrix results from inflammation from several initial injury [190-193]. The rapid glomerulosclerosis and tubulointerstitial fibrosis lesions are inhomogeneous so the method that can explore kidney as a whole might be useful for studying this topic. We used microCT based Virtual Histology™ (microCT), submicron resolution imaging which can be differentially stained using heavy metal elements and explore several aspect of tissue without actually destroy tissue specimens to achieve physiological distinction in a 3D data of structures in different directions [177], in kidney fibrosis models. Different from other conventional histological method which tissue has to be cut, stain in only partial part of organs, microCT explore the whole kidney at the same time so there will be more benefit in inhomogenous pathology comparison. The different aspects in detail of the structure can be seen by the 3D reconstruction picture with different technique base on density difference which can be digitally cut to scoring the interesting parameters from whole kidney. In this study, we showed, for the first time, microCT pictures of 5/6 Nx at wk4, FA at wk2, Chr I/R at wk12, control normal and 2/6 Nx kidney (Figure 11). We interpreted these pictures by matching with clinical characteristics (table 1) and conventional histopathology in each models. In the VR and DS picture, the clearly smooth kidney surface and possible vasculature of kidney (VR picture: red) and possible urinary network (DS picture: blue) shown in normal kidney but the prominent irregular surface

and obscure structure found in fibrosis kidney (Figure 11). The patching or clump of the red color in VR picture and the patchy yellow/orange lesion in DS picture were found tremendously in 5/6 Nx, moderately in Chr I/R and none in FA/ 2/6 Nx (Fig 11) correlated with the severity of albuminuria (table 1). However, there was prominent fibrosis in FA model histology but no abnormal patchy yellow/ orange colors in FA microCT DS picture so these yellow/orange lesion in microCT DS picture were not fibrosis scar. We postulated that the clumping red lesion (VR picture) might be the nephron hyperfiltration and patchy yellow/orange lesion (DS picture) might be the streak of protein or the secondary change of high albuminuria. Further studies need to be performed to validate the interpretation, quantification and application of this interesting technology. In any case, the difference in 5/6 Nx and 2/6 Nx (Lt. kidney) can easily found in microCT picture (Figure 11) which demonstrated the possibility to use this tool to compare the whole kidney difference in future study.

At this point, we initiated new rapid CKD models; 5/6 Nx in CD-1 outbred genetic background and 5/6 Nx with Ang II in C57BL/6 inbred genetic background. Consequently, we use those models for sepsis study in pre-existing CKD. We selected cecal ligation and puncture (CLP) as sepsis model because of the clinically relevant in this model from literatures. Then we performed CLP on 5/6 Nx in all 3 mouse strains when they showed progressive proteinuria and kidney injury. The main interested groups will be CLP in CD-1 5/6 Nx and 129 S3 5/6 Nx. The C57BL/6 5/6 Nx CLP used as control kidney injury. We will keep the 5/6 Nx with Ang II in case we interested in genetic deficiency mouse later.

Pre-existing chronic kidney disease predisposes mice to more severe sepsis.

We found that the severity of sepsis in C57BL/6 mice, which showed a mild degree of chronic kidney injury after 5/6 nephrectomy (Scr 0.3-0.4 mg/dl; Fig 11), was similar to that observed when the composite first stage sham surgery group without CKD was subjected to CLP-induced sepsis (Figure 12). In contrast, mice with a higher degree of pre-existing chronic kidney injury (CD-1 and 129S3) developed more severe sepsis (kidney, liver, and spleen injury; inflammatory cytokines) (Figure 12-14). Thus,

underlying chronic kidney injury predisposed mice to more severe sepsis (either with folic acid as previously reported [15] , or 5/6 Nx in this study), consistent with previous studies of host defense defects in CKD, where a variety of immune cell functions are impaired, by yet undefined factors that presumably include circulating uremic toxins [20]. Because serum inflammatory cytokines, VEGF [15, 62, 163], and HMGB1 [114, 162] are all increased following sepsis in healthy mice, we first explored the importance of these factors in CKD alone, sepsis alone, and the amplification caused by the combination of pre-existing CKD and sepsis.

Inflammatory cytokines. Human and animal studies have indicated that CKD includes an inflammatory state, with corresponding increases in inflammatory cytokines (TNF- α , IL-6, IL-10) that may enhance protein catabolism, malnutrition and atherosclerosis [28-30, 194]. We found relatively mild accumulation of these cytokines in serum (approximately 2-fold above baseline), even at late stages of CKD in 5/6 Nx (Figure 15D-F). After 5/6 Nx and sepsis, all three strains had relatively similar accumulations of TNF- α , IL-6 and IL-10 (Figure 15D-F), despite a dramatic enhancement of sepsis severity in CD-1 and 129S3 vs. C57BL/6 (Figure 12). Accumulation of these cytokines seems to be enhanced, in part, because of reduced renal excretion (Fig 17); 70 -80% of the cytokine elimination was via a renal route. Thus, neither prototypical pro- (TNF- α , IL-6) nor anti-inflammatory (IL-10) cytokines could account for strain-dependent differences in susceptibility to CKD, before or after sepsis. However, sub-clinical infections could help explain the higher inflammatory cytokine levels that have been reported in CKD patients [195, 196].

VEGF. VEGF is increased in CKD both in animals and humans [15, 160]. High levels of VEGF can cause vascular endothelial leakage and have been associated with a higher severity of human sepsis [197, 198]. VEGF increased very early after 5/6 Nx surgery and continued to increase in parallel to the rate of CKD progression (Figure 15C). This early increase might promote healing of the surgical wound [199, 200]. Most exogenously administered VEGF was cleared via the kidney (Figure 17B), suggesting that the VEGF increase after CKD was primarily derived by decreased renal elimination

rather than increased production. In contrast to prototypical pro- and anti-inflammatory cytokines, both VEGF and HMGB1 did differ among strains during the progression of CKD, and the circulating levels of both mediators corresponded to the severity of CKD. VEGF increased to very high levels after sepsis, with or without CKD, as previously described [15, 62, 160, 163, 197, 198]. We found that exogenously administered sFLT-1, an endogenous neutralizing, soluble VEGF receptor, did not attenuate sepsis severity after CKD by 5/6 Nx (Figure 18) nor after folate-induced fibrotic injury [15], despite effectiveness of this treatment in mouse CLP sepsis without pre-existing kidney injury [62, 163]. Hence, the participation of VEGF in CKD progression and sepsis appears to act independently, rather than synergistically interacting to amplify the severity of sepsis after CKD.

HMGB1. The pro-inflammatory cytokine HMGB1 is passively released from dying cells that are either undergoing apoptosis or necrosis [201], and it induces the release of other cytokines from macrophages and other cell types [43, 202-204]. HMGB1 can induce additional release of HMGB1 in macrophage-like RAW 264.7 cells [162], thus HMGB1 can exhibit positive-feedback amplification. In sepsis, HMGB1 has been proposed as a late-appearing pro-inflammatory cytokine, and HMGB1 neutralizing therapy improved mortality [43, 143, 162, 204, 205], even when it was started 24 hrs after surgery [143]. We found that serum HMGB1 increased in the late phase of CKD (4 weeks after 5/6 Nx in CD-1 and after 12 weeks in 129S3) and was especially elevated at the peak of the kidney injury and albuminuria (Figure 15B, 12), similar to what has been described in a few patients with CKD [44]. This time course suggests that HMGB1 alone does not drive CKD progression, as HMGB1 levels have probably not reached a critical mass for positive feedback, but rather accumulates as renal function deteriorates. Indeed, 50% of HMGB1 clearance was via renal route (Figure 17A). HMGB1 was elevated following sepsis, but the timing depended on how much renal function remained prior to sepsis. In normal and BiNx animals, HMGB1 was a late-appearing cytokine (increased at 12 h) as previously demonstrated [143, 205]; whereas, in sepsis following CKD, HMGB1 was an early responding cytokine (6 h) (Figure 16A). From our data we propose the following framework: because HMGB1 levels are higher during the

progression of CKD, and the capacity for renal clearance of HMGB1 is reduced, the small increases in HMGB1 during the early phase of sepsis can now trigger an autocrine or positive feedback loop where HMGB1 is high enough to induce more HMGB1 release [143, 205]. This view is supported by a temporal shift in the HMGB1 appearance from late in sepsis alone to early after CKD-sepsis. On the other hand, an earlier increase in HMGB1 could be an indicator of more severe injury as recently mentioned in moribund trauma patients [206]. We found that a single dose of anti-HMGB1 neutralizing antibody started at 6 h after CLP—when HMGB1 increased—attenuated sepsis severity and improved survival in 5/6 Nx-CLP but not in normal-CLP mice (Figure 19, 20). Because neutralizing HMGB1, but not VEGF (by sFLT-1), was effective, the attenuation of pro-inflammatory response might be more beneficial than decreasing vascular leakage in CKD-sepsis. Alternatively, HMGB1 might drive VEGF, high levels of VEGF could induce a beneficial adaptation in endothelial cells, and/or sFLT-1 could have additional toxic effects; whereas high levels of HMGB1 may have induced only harmful effects, including positive feedback. Since the same dose of anti-HMGB1 showed effectiveness only in CLP with CKD but not CLP alone (Figure 19), HMGB1 might only induce tissue damage above a critical threshold. However, co-induced factors often complicate any simple interpretation. It is interesting that the higher mean arterial pressure (MAP) in CKD from 5/6 Nx did not help maintain blood pressure after sepsis. The MAP started to drop as early as 3 hr in both normal and 5/6 Nx mice (Figure 20A). Anti-HMGB1 treatment appeared to maintain cardiovascular function in the 'late' sepsis phase (after 18 hr) (Figure 20A) as previously mentioned [207-209]. However, some of the mice with improved MAP died after 40-48 hr (Figure 20C), and additional anti-HMGB1 might be needed to maximize efficacy [143]. Thus, HMGB1 seems to be more central to the amplification seen in CKD-sepsis. Anti-HMGB1 treatment, which showed therapeutic benefit in previous studies on sepsis from healthy mice [114, 143, 162], might have a greater impact on sepsis with underlying CKD. Considering the increasing prevalence of CKD patients with a higher rate of sepsis [20] and longer lengths of hospital stay [21], anti-HMGB1 is a promising candidate for combination pre-emption and treatment strategies.

Role of spleen apoptosis in HMGB1 accumulation in both CKD and sepsis

We then turned to cellular immune defects, since both CKD and sepsis are associated with immunomodulatory and immune depression defects [210], including uremia-induced immune cell apoptosis in CKD [22, 211-215]. Because HMGB1 is released from apoptotic cells [143], we explored the role of the spleen, the largest lymphoid organ [216-218] and a major site of apoptosis following sepsis [114]. We surprisingly found spleen apoptosis in CKD (before CLP surgery) that started as early as 4 and 8 weeks after 5/6 Nx in CD-1 and 129S3 mice, respectively (Figure 14 left panels, Figure 15A). Although CKD and uremia have been shown to induce immune cell apoptosis, we could not find any previous animal or human studies of spontaneous cell apoptosis in lymphoid organs. Interestingly, the susceptibility of mice to 5/6 Nx-induced CKD was strain-dependent; Ang II could overcome the resistance to CKD in C57BL/6 mice whereas olmesartan could diminish the susceptibility to CKD in CD-1 mice (Figure 22). We found that these maneuvers induced parallel changes in splenic apoptosis and serum HMGB1 levels; both were increased following chronic Ang II infusion and reduced by chronic olmesartan treatment (Figure 23A). These data indicate that there may be a causal relationship between splenic apoptosis and HMGB1 during the progression of CKD. Whether Ang II acts on the kidney, extrarenal sites, or directly on the spleen [219] is unknown. The slower rate of CKD progression in the 129S3 mouse strain allowed us to observe a significant increase in splenic apoptosis before HMGB1 increased (Figure 15). Intravenous injection of recombinant HMGB1 (6 mg/kg) did not cause splenic apoptosis (data not shown). To further test this association, we performed splenectomy at the same time as CLP surgery. Splenectomy reduced serum HMGB1 after CLP in both normal and 5/6 Nx mice (Figure 23B). Furthermore, HMGB1 neutralizing antibody did not decrease splenic apoptosis (Figure 19H). Collectively, our results support a pathway where splenic apoptosis is temporally and mechanistically upstream of HMGB1 during CKD progression, sepsis, and CKD-sepsis.

In conclusion

Successfully translating treatments from pre-clinical animal models to human patients

has been exceedingly difficult in sepsis. Some of this difficulty may arise because the animal models do not faithfully reproduce enough features of human sepsis; alternatively, candidate drugs are typically tested in young healthy animals, whereas a majority of sepsis occurs in the setting of a pre-existing medical condition. We modified the standard CLP model to incorporate a common pre-existing condition – progressive chronic kidney disease, thereby creating a more clinically relevant model that more closely resembles the complexity of human sepsis. We found that pre-existing CKD amplified sepsis, and that a major amplification factor was HMGB1 that was released primarily by apoptotic cells in spleen and could not be cleared by the injured kidney. In addition, we found that spontaneous spleen apoptosis in 5/6 Nx CKD was largely responsible for increasing serum HMGB1 level in CKD. A high baseline of HMGB1 levels in CKD can trigger additional HMGB1 release after sepsis, resulting in a positive feedback loop. Interception with anti-HMGB1 reduced sepsis after CKD but not in normal animals. Thus, the two-stage CKD sepsis model has dramatically increased mortality, differing mechanisms, and therapeutic targets than a sepsis model in young mice. Models that more closely replicate the underlying co-morbidity might be more suitable for testing biomarkers and therapeutic agents for use in human sepsis. The interplay between CKD and sepsis is inherently complex, and this initial study will require extensive follow-up studies to gain further mechanistic insight that can guide more comprehensive treatment strategies for CKD-sepsis. By comparing both CKD and sepsis components vs. CKD-sepsis, we can begin to isolate which progression factors for CKD and sepsis act in concert, which factors act independently, and which factors may even counteract. For example, routine examination of baseline values of typical sepsis outcomes post-CKD/pre-sepsis led to our discovery of splenic apoptosis as a potentially important mediator of CKD progression. This unconventional line of thinking was made possible by dissecting the complex clinical problem of CKD-sepsis into two distinct and disparate components, then systematically examining the models for each component alone or in combination.

REFERENCES

- [1]. Angus DC, Linde-Zwirble WT, Lidicker J, *et al.*: Epidemiology of severe sepsis in the United States: analysis of incidence, outcome, and associated costs of care. *Crit Care Med* 29 (2001): 1303-1310.
- [2]. Martin GS, Mannino DM, Eaton S, *et al.*: The epidemiology of sepsis in the United States from 1979 through 2000. *N Engl J Med* 348 (2003): 1546-1554.
- [3]. Dombrovskiy VY, Martin AA, Sunderram J, *et al.*: Rapid increase in hospitalization and mortality rates for severe sepsis in the United States: a trend analysis from 1993 to 2003. *Crit Care Med* 35 (2007): 1244-1250.
- [4]. Vincent JL, Martinez EO, Silva E: Evolving concepts in sepsis definitions. *Crit Care Clin* 25 (2009): 665-675.
- [5]. Levy MM, Fink MP, Marshall JC, *et al.*: 2001 SCCM/ESICM/ACCP/ATS/SIS International Sepsis Definitions Conference. *Crit Care Med* 31(2003): 1250-1256.
- [6]. Russell JA, Singer J, Bernard GR, *et al.*: Changing pattern of organ dysfunction in early human sepsis is related to mortality. *Crit Care Med* 28 (2000): 3405-3411.
- [7]. Uchino S, Kellum JA, Bellomo R, *et al.*: Acute renal failure in critically ill patients: a multinational, multicenter study. *Jama* 294 (2005): 813-818.
- [8]. Bagshaw SM, Laupland KB, Doig CJ, *et al.*: Prognosis for long-term survival and renal recovery in critically ill patients with severe acute renal failure: a population-based study. *Crit Care* 9 (2005): R700-709.
- [9]. Neveu H, Kleinknecht D, Brivet F, *et al.*: Prognostic factors in acute renal failure due to sepsis. Results of a prospective multicentre study. The French Study Group on Acute Renal Failure. *Nephrol Dial Transplant* 11 (1996): 293-299.
- [10]. Silvester W, Bellomo R, Cole L: Epidemiology, management, and outcome of severe acute renal failure of critical illness in Australia. *Crit Care Med* 29 (2001): 1910-1915.

- [11]. Riedemann NC, Guo RF, Ward PA: The enigma of sepsis. *J Clin Invest* 112 (2003): 460-467.
- [12]. Rittirsch D, Hoesel LM, Ward PA: The disconnect between animal models of sepsis and human sepsis. *J Leukoc Biol* 81 (2007): 137-143.
- [13]. Dyson A, Singer M: Animal models of sepsis: why does preclinical efficacy fail to translate to the clinical setting? *Crit Care Med* 37 (2009): S30-37.
- [14]. Esmon CT: Why do animal models (sometimes) fail to mimic human sepsis? *Crit Care Med* 32 (2004): S219-222.
- [15]. Doi K, Leelahavanichkul A, Hu X, *et al.*: Pre-existing renal disease promotes sepsis-induced acute kidney injury and worsens outcome. *Kidney Int* 74 (2008): 1017-1025.
- [16]. K/DOQI clinical practice guidelines for chronic kidney disease: evaluation, classification, and stratification. *Am J Kidney Dis* 39 (2002): S1-266.
- [17]. Patel SS, Kimmel PL, Singh A: New clinical practice guidelines for chronic kidney disease: a framework for K/DOQI. *Semin Nephrol* 22 (2002) : 449-458.
- [18]. Coresh J, Astor BC, Greene T, *et al.*: Prevalence of chronic kidney disease and decreased kidney function in the adult US population: Third National Health Nutrition Examination Survey. *Am J Kidney Dis* 41(2003):1-12.
- [19]. Mitka M: Report notes increase in kidney disease. *Jama* 300(2008):2473-2474.
- [20]. Dalrymple LS, Go AS: Epidemiology of acute infections among patients with chronic kidney disease. *Clin J Am Soc Nephrol* 3 (2008):1487-1493.
- [21]. Naqvi SB, Collins AJ: Infectious complications in chronic kidney disease. *Adv Chronic Kidney Dis* 13(2006): 199-204.
- [22]. Cohen G, Haag-Weber M, Horl WH: Immune dysfunction in uremia. *Kidney Int Suppl* 62 (1997): S79-82.
- [23]. Eleftheriadis T, Antoniadi G, Liakopoulos V, *et al.*: Disturbances of acquired immunity in hemodialysis patients. *Semin Dial* 20 (2007): 440-451.
- [24]. Minnaganti VR, Cunha BA: Infections associated with uremia and dialysis. *Infect Dis Clin North Am* 15 (2001):385-406.

- [25]. Pesanti EL: Immunologic defects and vaccination in patients with chronic renal failure. *Infect Dis Clin North Am* 15 (2001): 813-832.
- [26]. Vanholder R, Ringoir S: Infectious morbidity and defects of phagocytic function in end-stage renal disease: a review. *J Am Soc Nephrol* 3 (1993): 1541-1554
- [27]. Carrero JJ, Yilmaz MI, Lindholm B, *et al.*: Cytokine dysregulation in chronic kidney disease: how can we treat it? *Blood Purif* 26 (2008):291-299.
- [28]. Stenvinkel P, Heimbürger O, Paulre F, *et al.*: Strong association between malnutrition, inflammation, and atherosclerosis in chronic renal failure. *Kidney Int* 55 (1999): 1899-1911.
- [29]. Stenvinkel P, Ketteler M, Johnson RJ, *et al.*: IL-10, IL-6, and TNF-alpha: central factors in the altered cytokine network of uremia--the good, the bad, and the ugly. *Kidney Int* 67 (2005): 1216-1233.
- [30]. Zoccali C, Mallamaci F, Tripepi G: Inflammation and atherosclerosis in end-stage renal disease. *Blood Purif* 21 (2003): 29-36.
- [31]. Alberti C, Brun-Buisson C, Goodman SV, *et al.*: Influence of systemic inflammatory response syndrome and sepsis on outcome of critically ill infected patients. *Am J Respir Crit Care Med* 168 (2003): 77-84.
- [32]. Hutchinson TA, Thomas DC, MacGibbon B: Predicting survival in adults with end-stage renal disease: an age equivalence index. *Ann Intern Med* 96 (1982): 417-423.
- [33]. Bemelmans MH, Gouma DJ, Buurman WA: Influence of nephrectomy on tumor necrosis factor clearance in a murine model. *J Immunol* 150 (1993) : 2007-2017.
- [34]. Poole S, Bird TA, Selkirk S, *et al.*: Fate of injected interleukin 1 in rats: sequestration and degradation in the kidney. *Cytokine* 2 (1990): 416-422.
- [35]. Casey LC, Balk RA, Bone RC: Plasma cytokine and endotoxin levels correlate with survival in patients with the sepsis syndrome. *Ann Intern Med* 119 (1993): 771-778.
- [36]. Honore PM, Joannes-Boyou O, Gressens B: Blood and plasma treatments: the

- rationale of high-volume hemofiltration. *Contrib Nephrol* 156 (2007): 387-395.
- [37]. Li L, Pan J, Yu Y: Development of sorbent therapy for multiple organ dysfunction syndrome (MODS). *Biomed Mater* 2 (2007): R12-16.
- [38]. Descamps-Latscha B, Herbelin A, Nguyen AT, *et al.*: Immune system dysregulation in uremia. *Semin Nephrol* 14 (1994): 253-260.
- [39]. Descamps-Latscha B, Jungers P, Witko-Sarsat V: Immune system dysregulation in uremia: role of oxidative stress. *Blood Purif* 20 (2002): 481-484.
- [40]. Bustin M, Reeves R: High-mobility-group chromosomal proteins: architectural components that facilitate chromatin function. *Prog Nucleic Acid Res Mol Biol* 54 (1996): 35-100.
- [41]. Bennekou P, Barksman TL, Jensen LR, *et al.*: Voltage activation and hysteresis of the non-selective voltage-dependent channel in the intact human red cell. *Bioelectrochemistry* 62 (2004): 181-185
- [42]. Czura CJ, Yang H, Tracey KJ: High mobility group box-1 as a therapeutic target downstream of tumor necrosis factor. *J Infect Dis* 187 Suppl 2 (2003): S391-396.
- [43]. Yang H, Wang H, Czura CJ, *et al.*: The cytokine activity of HMGB1. *J Leukoc Biol* 78 (2005): 1-8.
- [44]. Bruchfeld A, Qureshi AR, Lindholm B, *et al.*: High Mobility Group Box Protein-1 correlates with renal function in chronic kidney disease (CKD). *Mol Med* 14 (2008): 109-115.
- [45]. Dellinger RP, Levy MM, Carlet JM, *et al.*: Surviving Sepsis Campaign: international guidelines for management of severe sepsis and septic shock: 2008. *Crit Care Med* 36 (2008): 296-327.
- [46]. Doi K, Leelahavanichkul A, Yuen PS, *et al.*: Animal models of sepsis and sepsis-induced kidney injury. *J Clin Invest* 119 (2009): 2868-2878.
- [47]. Tracey KJ, Fong Y, Hesse DG, *et al.*: Anti-cachectin/TNF monoclonal antibodies prevent septic shock during lethal bacteraemia. *Nature* 330 (1987): 662-664.
- [48]. McNamara MJ, Norton JA, Nauta RJ, *et al.*: Interleukin-1 receptor antibody (IL-

- 1rab) protection and treatment against lethal endotoxemia in mice. *J Surg Res* 54 (1993): 316-321.
- [49]. Taveira da Silva AM, Kaulbach HC, Chuidian FS, *et al.*: Brief report: shock and multiple-organ dysfunction after self-administration of Salmonella endotoxin. *N Engl J Med* 328 (1993): 1457-1460.
- [50]. Cunningham PN, Wang Y, Guo R, *et al.*: Role of Toll-like receptor 4 in endotoxin-induced acute renal failure. *J Immunol* 172 (2004): 2629-2635.
- [51]. Tiwari MM, Brock RW, Megyesi JK, *et al.*: Disruption of renal peritubular blood flow in lipopolysaccharide-induced renal failure: role of nitric oxide and caspases. *Am J Physiol Renal Physiol* 289 (2005): F1324-1332.
- [52]. Knotek M, Rogachev B, Wang W, *et al.*: Endotoxemic renal failure in mice: Role of tumor necrosis factor independent of inducible nitric oxide synthase. *Kidney Int* 59 (2001): 2243-2249.
- [53]. Fisher CJ, Jr., Agosti JM, Opal SM, *et al.*: Treatment of septic shock with the tumor necrosis factor receptor:Fc fusion protein. The Soluble TNF Receptor Sepsis Study Group. *N Engl J Med* 334 (1996): 1697-1702.
- [54]. Fisher CJ, Jr., Dhainaut JF, Opal SM, *et al.*: Recombinant human interleukin 1 receptor antagonist in the treatment of patients with sepsis syndrome. Results from a randomized, double-blind, placebo-controlled trial. Phase III rhIL-1ra Sepsis Syndrome Study Group. *Jama* 271 (1994): 1836-1843.
- [55]. Remick DG, Newcomb DE, Bolgos GL, *et al.*: Comparison of the mortality and inflammatory response of two models of sepsis: lipopolysaccharide vs. cecal ligation and puncture. *Shock* 13 (2000): 110-116.
- [56]. Eskandari MK, Bolgos G, Miller C, *et al.*: Anti-tumor necrosis factor antibody therapy fails to prevent lethality after cecal ligation and puncture or endotoxemia. *J Immunol* 148 (1992): 2724-2730.
- [57]. Brandtzaeg P, Kierulf P, Gaustad P, *et al.*: Systemic meningococcal disease: a model infection to study acute endotoxemia in man. *Prog Clin Biol Res* 272 (1988): 263-271.
- [58]. Johannes T, Mik EG, Ince C: Nonresuscitated endotoxemia induces

- microcirculatory hypoxic areas in the renal cortex in the rat. *Shock* 31 (2009): 97-103.
- [59]. Yuen PS, Dunn SR, Miyaji T, *et al.*: A simplified method for HPLC determination of creatinine in mouse serum. *Am J Physiol Renal Physiol* 286 (2004): F1116-1119.
- [60]. Wang W, Falk SA, Jittikanont S, *et al.*: Protective effect of renal denervation on normotensive endotoxemia-induced acute renal failure in mice. *Am J Physiol Renal Physiol* 283 (2002): F583-587.
- [61]. Wang W, Jittikanont S, Falk SA, *et al.*: Interaction among nitric oxide, reactive oxygen species, and antioxidants during endotoxemia-related acute renal failure. *Am J Physiol Renal Physiol* 284 (2003): F532-537.
- [62]. Yano K, Liaw PC, Mullington JM, *et al.*: Vascular endothelial growth factor is an important determinant of sepsis morbidity and mortality. *J Exp Med* 203 (2006): 1447-1458.
- [63]. Deitch EA: Rodent models of intra-abdominal infection. *Shock* 24 Suppl 1 (2005): 19-23.
- [64]. Rittirsch D, Huber-Lang MS, Flierl MA, *et al.*: Immunodesign of experimental sepsis by cecal ligation and puncture. *Nat Protoc* 4 (2009): 31-36.
- [65]. Freise H, Bruckner UB, Spiegel HU: Animal models of sepsis. *J Invest Surg* 14 (2001): 195-212.
- [66]. Hollenberg SM, Dumasius A, Easington C, *et al.*: Characterization of a hyperdynamic murine model of resuscitated sepsis using echocardiography. *Am J Respir Crit Care Med* 164 (2001): 891-895.
- [67]. Echtenacher B, Falk W, Mannel DN, *et al.*: Requirement of endogenous tumor necrosis factor/cachectin for recovery from experimental peritonitis. *J Immunol* 145 (1990): 3762-3766.
- [68]. Swan R, Chung CS, Albina J, *et al.*: Polymicrobial sepsis enhances clearance of apoptotic immune cells by splenic macrophages. *Surgery* 142 (2007): 253-261.

- [69]. Dear JW, Yasuda H, Hu X, *et al.*: Sepsis-induced organ failure is mediated by different pathways in the kidney and liver: acute renal failure is dependent on MyD88 but not renal cell apoptosis. *Kidney Int* 69 (2006): 832-836.
- [70]. Muenzer JT, Davis CG, Dunne BS, *et al.*: Pneumonia after cecal ligation and puncture: a clinically relevant "two-hit" model of sepsis. *Shock* 26 (2006): 565-570.
- [71]. Fink MP, MacVittie TJ, Casey LC: Inhibition of prostaglandin synthesis restores normal hemodynamics in canine hyperdynamic sepsis. *Ann Surg* 200 (1984): 619-626.
- [72]. Minneci PC, Deans KJ, Hansen B, *et al.*: A canine model of septic shock: balancing animal welfare and scientific relevance. *Am J Physiol Heart Circ Physiol* 293 (2007): H2487-2500.
- [73]. Carraway MS, Welty-Wolf KE, Miller DL, *et al.*: Blockade of tissue factor: treatment for organ injury in established sepsis. *Am J Respir Crit Care Med* 167 (2003): 1200-1209.
- [74]. Welty-Wolf KE, Carraway MS, Miller DL, *et al.*: Coagulation blockade prevents sepsis-induced respiratory and renal failure in baboons. *Am J Respir Crit Care Med* 164 (2001): 1988-1996.
- [75]. Welty-Wolf KE, Carraway MS, Ortel TL, *et al.*: Blockade of tissue factor-factor X binding attenuates sepsis-induced respiratory and renal failure. *Am J Physiol Lung Cell Mol Physiol* 290 (2006): L21-31.
- [76]. Langenberg C, Wan L, Egi M, *et al.*: Renal blood flow in experimental septic acute renal failure. *Kidney Int* 69 (2006): 1996-2002.
- [77]. Di Giandomasso D, May CN, Bellomo R: Vital organ blood flow during hyperdynamic sepsis. *Chest* 124 (2003): 1053-1059.
- [78]. Wu L, Gokden N, Mayeux PR: Evidence for the role of reactive nitrogen species in polymicrobial sepsis-induced renal peritubular capillary dysfunction and tubular injury. *J Am Soc Nephrol* 18 (2007): 1807-1815.
- [79]. Wu L, Tiwari MM, Messer KJ, *et al.*: Peritubular capillary dysfunction and renal

- tubular epithelial cell stress following lipopolysaccharide administration in mice. *Am J Physiol Renal Physiol* 292 (2007): F261-268.
- [80]. Zhou H, Pisitkun T, Aponte A, *et al.*: Exosomal Fetuin-A identified by proteomics: a novel urinary biomarker for detecting acute kidney injury. *Kidney Int* 70 (2006): 1847-1857.
- [81]. Gupta A, Berg DT, Gerlitz B, *et al.*: Role of protein C in renal dysfunction after polymicrobial sepsis. *J Am Soc Nephrol* 18 (2007): 860-867.
- [82]. De Backer D, Creteur J, Preiser JC, *et al.*: Microvascular blood flow is altered in patients with sepsis. *Am J Respir Crit Care Med* 166 (2002): 98-104.
- [83]. De Backer D, Creteur J, Dubois MJ, *et al.*: The effects of dobutamine on microcirculatory alterations in patients with septic shock are independent of its systemic effects. *Crit Care Med* 34 (2006): 403-408.
- [84]. Sakr Y, Dubois MJ, De Backer D, *et al.*: Persistent microcirculatory alterations are associated with organ failure and death in patients with septic shock. *Crit Care Med* 32 (2004): 1825-1831.
- [85]. Bhatia M, He M, Zhang H, *et al.*: Sepsis as a model of SIRS. *Front Biosci* 14 (2009): 4703-4711.
- [86]. Parker SJ, Watkins PE: Experimental models of gram-negative sepsis. *Br J Surg* 88 (2001): 22-30.
- [87]. Poyart C, Pellegrini E, Marceau M, *et al.*: Attenuated virulence of *Streptococcus agalactiae* deficient in D-alanyl-lipoteichoic acid is due to an increased susceptibility to defensins and phagocytic cells. *Mol Microbiol* 49 (2003): 1615-1625.
- [88]. Coalson JJ, Archer LT, Benjamin BA, *et al.*: A morphologic study of live *Escherichia coli* organism shock in baboons. *Exp Mol Pathol* 31 (1979): 10-22.
- [89]. Philips JB, 3rd, Lyrene RK, Godoy G, *et al.*: Hemodynamic responses of chronically instrumented piglets to bolus injections of group B streptococci. *Pediatr Res* 23 (1988): 81-85.
- [90]. Sato T, Tanaka J, Cottrell JR, *et al.*: The pathophysiology of septic shock:

- comparison of systemic hemodynamical responses in the rat following a sonicated, heat-killed, and live E coli injection. *Adv Shock Res* 9 (1983): 115-123.
- [91]. Schutze E, Hildebrandt J, Liehl E, *et al.*: Protection of mice from mortality caused by living and heat-killed bacteria by SDZ MRL 953. *Circ Shock* 42 (1994): 121-127.
- [92]. Hinshaw LB, Taylor FB, Jr., Chang AC, *et al.*: Staphylococcus aureus-induced shock: a pathophysiologic study. *Circ Shock* 26 (1988): 257-265.
- [93]. Good DW, George T, Watts BA, 3rd: Lipopolysaccharide directly alters renal tubule transport through distinct TLR4-dependent pathways in basolateral and apical membranes. *Am J Physiol Renal Physiol* 297 (2009): F866-874.
- [94]. Wichterman KA, Baue AE, Chaudry IH: Sepsis and septic shock--a review of laboratory models and a proposal. *J Surg Res* 29 (1980): 189-201.
- [95]. Dahiya P: Burns as a model of SIRS. *Front Biosci* 14 (2009): 4962-4967.
- [96]. Lange M, Hamahata A, Traber DL, *et al.*: A murine model of sepsis following smoke inhalation injury. *Biochem Biophys Res Commun* 391(2001): 1555-1560.
- [97]. Murakami K, Bjertnaes LJ, Schmalstieg FC, *et al.*: A novel animal model of sepsis after acute lung injury in sheep. *Crit Care Med* 30 (2002) : 2083-2090.
- [98]. Timlin M, Condrón C, Toomey D, *et al.*: N-acetylcysteine attenuates lung injury in a rodent model of fracture. *Acta Orthop Scand* 75 (2004): 61-65.
- [99]. Hermreck AS, Thal AP: Mechanisms for the high circulatory requirements in sepsis and septic shock. *Ann Surg* 170 (1969): 677-695.
- [100]. Cronenwett JL, Lindenauer SM: Hemodynamic effects of cecal ligation sepsis in dogs. *J Surg Res* 33 (1982): 324-331.
- [101]. Rector F, Goyal S, Rosenberg IK, *et al.*: Sepsis: a mechanism for vasodilatation in the kidney. *Ann Surg* 178 (1973): 222-226.
- [102]. Macias WL, Nelson DR, Williams M, *et al.*: Lack of evidence for qualitative

- treatment by disease severity interactions in clinical studies of severe sepsis. *Crit Care* 9 (2005): R607-622.
- [103]. Chvojka J, Sykora R, Krouzecky A, *et al.*: Renal haemodynamic, microcirculatory, metabolic and histopathological responses to peritonitis-induced septic shock in pigs. *Crit Care* 12 (2008): R164.
- [104]. Bauhofer A, Lorenz W, Kohlert F, *et al.*: Granulocyte colony-stimulating factor prophylaxis improves survival and inflammation in a two-hit model of hemorrhage and sepsis. *Crit Care Med* 34 (2006): 778-784.
- [105]. Horton JW: A model of myocardial inflammation and dysfunction in burn complicated by sepsis. *Shock* 28 (2007): 326-333.
- [106]. Vincent JL: Dear SIRS, I'm sorry to say that I don't like you. *Crit Care Med* 25 (1997): 372-374.
- [107]. Neild GH: Multi-organ renal failure in the elderly. *Int Urol Nephrol* 32 (2001): 559-565.
- [108]. Saito H, Sherwood ER, Varma TK, *et al.*: Effects of aging on mortality, hypothermia, and cytokine induction in mice with endotoxemia or sepsis. *Mech Ageing Dev* 124 (2003): 1047-1058.
- [109]. Turnbull IR, Wlzonek JJ, Osborne D, *et al.*: Effects of age on mortality and antibiotic efficacy in cecal ligation and puncture. *Shock* 19 (2003) : 310-313.
- [110]. Dear JW, Kobayashi H, Jo SK, *et al.*: Dendrimer-enhanced MRI as a diagnostic and prognostic biomarker of sepsis-induced acute renal failure in aged mice. *Kidney Int* 67 (2005): 2159-2167.
- [111]. Leelahavanichkul A, Yasuda H, Doi K, *et al.*: Methyl-2-acetamidoacrylate, an ethyl pyruvate analog, decreases sepsis-induced acute kidney injury in mice. *Am J Physiol Renal Physiol* 295 (2008): F1825-1835.
- [112]. Doi K, Hu X, Yuen PS, *et al.*: AP214, an analogue of alpha-melanocyte-stimulating hormone, ameliorates sepsis-induced acute kidney injury and mortality. *Kidney Int* 73 (2008): 1266-1274.

- [113]. Akira S, Takeda K, Kaisho T: Toll-like receptors: critical proteins linking innate and acquired immunity. *Nat Immunol* 2 (2001): 675-680.
- [114]. Huston JM, Wang H, Ochani M, *et al.*: Splenectomy protects against sepsis lethality and reduces serum HMGB1 levels. *J Immunol* 181 (2008): 3535-3539.
- [115]. Holly MK, Dear JW, Hu X, *et al.*: Biomarker and drug-target discovery using proteomics in a new rat model of sepsis-induced acute renal failure. *Kidney Int* 70 (2006): 496-506.
- [116]. Chawla LS, Seneff MG, Nelson DR, *et al.*: Elevated plasma concentrations of IL-6 and elevated APACHE II score predict acute kidney injury in patients with severe sepsis. *Clin J Am Soc Nephrol* 2 (2007): 22-30.
- [117]. Doetschman T: Interpretation of phenotype in genetically engineered mice. *Lab Anim Sci* 49 (1999): 137-143.
- [118]. Pugin J: Immunostimulation is a rational therapeutic strategy in sepsis. *Novartis Found Symp* 280 (2007): 21-27; discussion 27-36, 160-164.
- [119]. Steinhäuser ML, Hogaboam CM, Kunkel SL, *et al.*: IL-10 is a major mediator of sepsis-induced impairment in lung antibacterial host defense. *J Immunol* 162 (1999): 392-399.
- [120]. Xiao H, Siddiqui J, Remick DG: Mechanisms of mortality in early and late sepsis. *Infect Immun* 74 (2006): 5227-5235.
- [121]. Manley MO, O'Riordan MA, Levine AD, *et al.*: Interleukin 10 extends the effectiveness of standard therapy during late sepsis with serum interleukin 6 levels predicting outcome. *Shock* 23 (2005): 521-526.
- [122]. Laughlin RS, Musch MW, Hollbrook CJ, *et al.*: The key role of *Pseudomonas aeruginosa* PA-I lectin on experimental gut-derived sepsis. *Ann Surg* 232 (2000): 133-142.
- [123]. Guidet B, Aegerter P, Gauzit R, *et al.*: Incidence and impact of organ dysfunctions associated with sepsis. *Chest* 127(2005): 942-951.
- [124]. Mehta RL, Pascual MT, Soroko S, *et al.*: Spectrum of acute renal failure in the

- intensive care unit: the PICARD experience. *Kidney Int* 66 (2004): 1613-1621.
- [125]. Sarnak MJ, Jaber BL: Mortality caused by sepsis in patients with end-stage renal disease compared with the general population. *Kidney Int* 58 (2000): 1758-1764.
- [126]. Thamer M, Ray NF, Fehrenbach SN, *et al.*: Relative risk and economic consequences of inpatient care among patients with renal failure. *J Am Soc Nephrol* 7 (1996): 751-762.
- [127]. James MT, Laupland KB, Tonelli M, *et al.*: Risk of bloodstream infection in patients with chronic kidney disease not treated with dialysis. *Arch Intern Med* 168 (2008): 2333-2339.
- [128]. Fogelgren B, Yang S, Sharp IC, *et al.*: Deficiency in Six2 during prenatal development is associated with reduced nephron number, chronic renal failure, and hypertension in Br/+ adult mice. *Am J Physiol Renal Physiol* 296 (2009): F1166-1178.
- [129]. Miner JH, Sanes JR: Molecular and functional defects in kidneys of mice lacking collagen alpha 3(IV): implications for Alport syndrome. *J Cell Biol* 135 (1996): 1403-1413.
- [130]. Fogo AB: Animal models of FSGS: lessons for pathogenesis and treatment. *Semin Nephrol* 23 (2003): 161-171.
- [131]. Ma LJ, Fogo AB: Model of robust induction of glomerulosclerosis in mice: importance of genetic background. *Kidney Int* 64 (2003): 350-355.
- [132]. Gagnon RF, Ansari M: Development and progression of uremic changes in the mouse with surgically induced renal failure. *Nephron* 54 (1990): 70-76.
- [133]. Gagnon RF, Duguid WP: A reproducible model for chronic renal failure in the mouse. *Urol Res* 11 (1983): 11-14.
- [134]. Gagnon RF, Gallimore B: Characterization of a mouse model of chronic uremia. *Urol Res* 16 (1988): 119-126.
- [135]. Hostetter TH, Olson JL, Rennke HG, *et al.*: Hyperfiltration in remnant nephrons: a

- potentially adverse response to renal ablation. *Am J Physiol* 241 (1981): F85-93.
- [136]. Zeisberg M, Soubasakos MA, Kalluri R: Animal models of renal fibrosis. *Methods Mol Med* 117 (2005): 261-272.
- [137]. Pippin JW, Brinkkoetter PT, Cormack-Aboud FC, *et al.*: Inducible rodent models of acquired podocyte diseases. *Am J Physiol Renal Physiol* 296 (2009): F213-229.
- [138]. Basile DP, Donohoe D, Roethe K, *et al.*: Renal ischemic injury results in permanent damage to peritubular capillaries and influences long-term function. *Am J Physiol Renal Physiol* 281 (2001): F887-899.
- [139]. Basile DP, Fredrich K, Alausa M, *et al.*: Identification of persistently altered gene expression in the kidney after functional recovery from ischemic acute renal failure. *Am J Physiol Renal Physiol* 288 (2005): F953-963.
- [140]. Seok YM, Kim J, Park MJ, *et al.*: Wen-pi-tang-Hab-Wu-ling-san attenuates kidney fibrosis induced by ischemia/reperfusion in mice. *Phytother Res* 22 (2008): 1057-1063.
- [141]. Whitesall SE, Hoff JB, Vollmer AP, *et al.*: Comparison of simultaneous measurement of mouse systolic arterial blood pressure by radiotelemetry and tail-cuff methods. *Am J Physiol Heart Circ Physiol* 286 (2004) : H2408-2415.
- [142]. Karatas A, Hegner B, de Windt LJ, *et al.*: Deoxycorticosterone acetate-salt mice exhibit blood pressure-independent sexual dimorphism. *Hypertension* 51 (2008): 1177-1183.
- [143]. Yang H, Ochani M, Li J, *et al.*: Reversing established sepsis with antagonists of endogenous high-mobility group box 1. *Proc Natl Acad Sci U S A* 101 (2004): 296-301.
- [144]. Leelahavanichkul A, Yan Q, Hu X, *et al.*: Angiotensin II overcomes strain-dependent resistance of rapid CKD progression in a new remnant kidney mouse model. *Kidney Int* 78 (2010): 1136-53.
- [145]. Yamada S, Maruyama I: HMGB1, a novel inflammatory cytokine. *Clin Chim Acta*

- 375 (2007): 36-42.
- [146]. Doi K, Yuen PS, Eisner C, *et al.*: Reduced Production of Creatinine Limits Its Use as Marker of Kidney Injury in Sepsis. *J Am Soc Nephrol*, 20 (2009): 1217-21
- [147]. Tse FL, Nedelman JR: Serial versus sparse sampling in toxicokinetic studies. *Pharm Res* 13 (1996): 1105-1108.
- [148]. Farris FF, Dedrick RL, King FG: Cisplatin pharmacokinetics: applications of a physiological model. *Toxicol Lett* 43 (1988): 117-137.
- [149]. Leelahavanichkul A, Areepium N, Vadcharavivad S, *et al.*: Pharmacokinetics of sirolimus in Thai healthy volunteers. *J Med Assoc Thai* 88 Suppl 4 (2005): S157-162.
- [150]. MacKay K, Striker LJ, Pinkert CA, *et al.*: Glomerulosclerosis and renal cysts in mice transgenic for the early region of SV40. *Kidney Int* 32 (1987): 827-837.
- [151]. Srisawat N, Manotham K, Eiam-Ong S, *et al.*: Erythropoietin and its non-erythropoietic derivative: do they ameliorate renal tubulointerstitial injury in ureteral obstruction? *Int J Urol* 15 (2008):1011-1017.
- [152]. Johnson JT, Hansen MS, Wu I, *et al.*: Virtual histology of transgenic mouse embryos for high-throughput phenotyping. *PLoS Genet* 2 (2006): e61.
- [153]. Kren S, Hostetter TH: The course of the remnant kidney model in mice. *Kidney Int* 56 (1999): 333-337.
- [154]. Bellizzi V, Sabbatini M, Fuiano G, *et al.*: The impact of early normalization of haematocrit by erythropoietin on renal damage in the remnant kidney model. *Nephrol Dial Transplant* 13 (1998): 2210-2215.
- [155]. Priyadarshi A, Periyasamy S, Burke TJ, *et al.*: Effects of reduction of renal mass on renal oxygen tension and erythropoietin production in the rat. *Kidney Int* 61 (2002): 542-546.
- [156]. Crowley SD, Gurley SB, Herrera MJ, *et al.*: Angiotensin II causes hypertension and cardiac hypertrophy through its receptors in the kidney. *Proc Natl Acad Sci U S A* 103 (2006): 17985-17990.

- [157]. Francois H, Athirakul K, Mao L, *et al.*: Role for thromboxane receptors in angiotensin-II-induced hypertension. *Hypertension* 43 (2004): 364-369.
- [158]. Diz DI, Baer PG, Nasjletti A: Angiotensin II-induced hypertension in the rat. Effects on the plasma concentration, renal excretion, and tissue release of prostaglandins. *J Clin Invest* 72 (1983): 466-477.
- [159]. Hotchkiss RS, Nicholson DW: Apoptosis and caspases regulate death and inflammation in sepsis. *Nat Rev Immunol* 6 (2006): 813-822.
- [160]. Harper SJ, Downs L, Tomson CR, *et al.*: Elevated plasma vascular endothelial growth factor levels in non-diabetic predialysis uraemia. *Nephron* 90 (2002): 341-343.
- [161]. Pawlak K, Pawlak D, Mysliwiec M: Possible association between circulating vascular endothelial growth factor and oxidative stress markers in hemodialysis patients. *Med Sci Monit* 12 (2006): CR181-185.
- [162]. Qin S, Wang H, Yuan R, *et al.*: Role of HMGB1 in apoptosis-mediated sepsis lethality. *J Exp Med* 203 (2006): 1637-1642.
- [163]. Tsao PN, Chan FT, Wei SC, *et al.*: Soluble vascular endothelial growth factor receptor-1 protects mice in sepsis. *Crit Care Med* 35 (2007): 1955-1960.
- [164]. Ulloa L, Tracey KJ: The "cytokine profile": a code for sepsis. *Trends Mol Med* 11 (2005): 56-63.
- [165]. Kim do J, Park SH, Sheen MR, *et al.*: Comparison of experimental lung injury from acute renal failure with injury due to sepsis. *Respiration* 73 (2006) : 815-824.
- [166]. Zurovsky Y, Eligal Z, Grossman S: Increased sensitivity to bilateral nephrectomy in rat caused by endotoxemia. *Exp Toxicol Pathol* 47 (1995): 353-358.
- [167]. Wu FT, Stefanini MO, Mac Gabhann F, *et al.*: A systems biology perspective on sVEGFR1: its biological function, pathogenic role and therapeutic use. *J Cell Mol Med* 14 (2010) :528-552
- [168]. Schnaper HW, Kopp JB: Renal fibrosis. *Front Biosci* 8:e68-86, 2003
- [169]. Megyesi J, Price PM, Tamayo E, *et al.*: The lack of a functional p21(WAF1/CIP1) gene ameliorates progression to chronic renal failure. *Proc Natl Acad*

- Sci U S A* 96 (1999): 10830-10835.
- [170]. Risdon RA, Sloper JC, De Wardener HE: Relationship between renal function and histological changes found in renal-biopsy specimens from patients with persistent glomerular nephritis. *Lancet* 2 (1968): 363-366.
- [171]. Doi K, Yuen PS, Eisner C, *et al.*: Reduced production of creatinine limits its use as marker of kidney injury in sepsis. *J Am Soc Nephrol* 20 (2009) : 1217-1221.
- [172]. Schreiner GF: Renal toxicity of albumin and other lipoproteins. *Curr Opin Nephrol Hypertens* 4 (1995): 369-373.
- [173]. Kopple JD, Greene T, Chumlea WC, *et al.*: Relationship between nutritional status and the glomerular filtration rate: results from the MDRD study. *Kidney Int* 57 (2000): 1688-1703.
- [174]. Jelkmann W, Hellwig-Burgel T: Biology of erythropoietin. *Adv Exp Med Biol* 502 (2001): 169-187.
- [175]. Marsden JT: Erythropoietin-- measurement and clinical applications. *Ann Clin Biochem* 43 (2006): 97-104
- [176]. Freedman BI, Sedor JR: Hypertension-associated kidney disease: perhaps no more. *J Am Soc Nephrol* 19 (2008): 2047-2051.
- [177]. Kramer K, Kinter L, Brockway BP, *et al.*: The use of radiotelemetry in small laboratory animals: recent advances. *Contemp Top Lab Anim Sci* 40 (2001): 8-16.
- [178]. Kennedy DJ, Elkareh J, Shidyak A, *et al.*: Partial nephrectomy as a model for uremic cardiomyopathy in the mouse. *Am J Physiol Renal Physiol* 294 (2008): F450-454.
- [179]. Pickering TG, Kario K: Nocturnal non-dipping: what does it augur? *Curr Opin Nephrol Hypertens* 10 (2001): 611-616.
- [180]. Aoki J, Ikari Y, Nakajima H, *et al.*: Clinical and pathologic characteristics of dilated cardiomyopathy in hemodialysis patients. *Kidney Int* 67 (2005): 333-340.

- [181]. Mall G, Huther W, Schneider J, *et al.*: Diffuse intermyocardiocytic fibrosis in uraemic patients. *Nephrol Dial Transplant* 5 (1990): 39-44.
- [182]. Kennedy DJ, Vetteth S, Periyasamy SM, *et al.*: Central role for the cardiotoxic steroid marinobufagenin in the pathogenesis of experimental uremic cardiomyopathy. *Hypertension* 47 (2006): 488-495.
- [183]. Mall G, Rambašek M, Neumeister A, *et al.*: Myocardial interstitial fibrosis in experimental uremia--implications for cardiac compliance. *Kidney Int* 33 (1988): 804-811.
- [184]. Gross ML, Ritz E: Hypertrophy and fibrosis in the cardiomyopathy of uremia--beyond coronary heart disease. *Semin Dial* 21 (2008): 308-318.
- [185]. Granger JP, Schnackenberg CG: Renal mechanisms of angiotensin II-induced hypertension. *Semin Nephrol* 20 (2000): 417-425.
- [186]. Hall JE: Control of sodium excretion by angiotensin II: intrarenal mechanisms and blood pressure regulation. *Am J Physiol* 250 (1986): R960-972.
- [187]. Blaquier P, Hoobler SW, Schroeder J, *et al.*: Effect of bilateral nephrectomy on pressor response to renin. *Am J Physiol* 203 (1962): 339-343.
- [188]. Gabelman EH, Rondell PA: Protracted pressor response to angiotensin after bilateral nephrectomy in rats. *Circ Res* 18 (1966): 705-713.
- [189]. Valles P, Wysocki J, Battle D: Angiotensin II and renal tubular ion transport. *ScientificWorldJournal* 5 (2005): 680-690.
- [190]. Chatziantoniou C, Dussaule JC: Insights into the mechanisms of renal fibrosis: is it possible to achieve regression? *Am J Physiol Renal Physiol* 289 (2005): F227-234.
- [191]. Khwaja A, El Kossi M, Floege J, *et al.*: The management of CKD: a look into the future. *Kidney Int* 72 (2007): 1316-1323.
- [192]. Wynn TA: Cellular and molecular mechanisms of fibrosis. *J Pathol* 214 (2008): 199-210.
- [193]. Yu HT: Progression of chronic renal failure. *Arch Intern Med* 163 (2003): 1417-1429.

- [194]. Fleet M, Osman F, Komaragiri R, *et al.*: Protein catabolism in advanced renal disease: role of cytokines. *Clin Nephrol* 70 (2008): 91-100.
- [195]. Kimmel PL, Phillips TM, Simmens SJ, *et al.*: Immunologic function and survival in hemodialysis patients. *Kidney Int* 54 (1998): 236-244.
- [196]. Pertosa G, Grandaliano G, Gesualdo L, *et al.*: Clinical relevance of cytokine production in hemodialysis. *Kidney Int Suppl* 76 (2000): S104-111.
- [197]. Pickkers P, Sprong T, Eijk L, *et al.*: Vascular endothelial growth factor is increased during the first 48 hours of human septic shock and correlates with vascular permeability. *Shock* 24 (2005): 508-512.
- [198]. van der Flier M, van Leeuwen HJ, van Kessel KP, *et al.*: Plasma vascular endothelial growth factor in severe sepsis. *Shock* 23 (2005): 35-38.
- [199]. Szabo S, Vincze A: Growth factors in ulcer healing: lessons from recent studies. *J Physiol Paris* 94 (2000): 77-81.
- [200]. Barrientos S, Stojadinovic O, Golinko MS, *et al.*: Growth factors and cytokines in wound healing. *Wound Repair Regen* 16 (2008): 585-601.
- [201]. Scaffidi P, Misteli T, Bianchi ME: Release of chromatin protein HMGB1 by necrotic cells triggers inflammation. *Nature* 418 (2002): 191-195.
- [202]. Andersson U, Wang H, Palmblad K, *et al.*: High mobility group 1 protein (HMG-1) stimulates proinflammatory cytokine synthesis in human monocytes. *J Exp Med* 192 (2000): 565-570.
- [203]. Bonaldi T, Talamo F, Scaffidi P, *et al.*: Monocytic cells hyperacetylate chromatin protein HMGB1 to redirect it towards secretion. *Embo J* 22 (2003): 5551-5560.
- [204]. Li J, Kokkola R, Tabibzadeh S, *et al.*: Structural basis for the proinflammatory cytokine activity of high mobility group box 1. *Mol Med* 9 (2003): 37-45.
- [205]. Wang H, Bloom O, Zhang M, *et al.*: HMG-1 as a late mediator of endotoxin lethality in mice. *Science* 285 (1999): 248-251.
- [206]. Peltz ED, Moore EE, Eckels PC, *et al.*: HMGB1 is markedly elevated within 6 hours of mechanical trauma in humans. *Shock* 32 (2009): 17-22.
- [207]. Li W, Li J, Ashok M, *et al.*: A cardiovascular drug rescues mice from lethal

- sepsis by selectively attenuating a late-acting proinflammatory mediator, high mobility group box 1. *J Immunol* 178 (2007): 3856-3864.
- [208]. Tzeng HP, Fan J, Vallejo JG, *et al.*: Negative inotropic effects of high-mobility group box 1 protein in isolated contracting cardiac myocytes. *Am J Physiol Heart Circ Physiol* 294 (2008): H1490-1496.
- [209]. Yoshida K, Xu HL, Kawamura T, *et al.*: Chronic angiotensin-converting enzyme inhibition and angiotensin II antagonism in rats with chronic renal failure. *J Cardiovasc Pharmacol* 40 (2002): 533-542.
- [210]. Dinarello CA: Interleukin-1 and interleukin-1 receptor antagonist production during haemodialysis: which cytokine is a surrogate marker for dialysis-related complications? *Nephrol Dial Transplant* 10 Suppl 3 (1995): 25-28
- [211]. Cendoroglo M, Jaber BL, Balakrishnan VS, *et al.*: Neutrophil apoptosis and dysfunction in uremia. *J Am Soc Nephrol* 10 (1999): 93-100.
- [212]. Heidenreich S, Schmidt M, Bachmann J, *et al.*: Apoptosis of monocytes cultured from long-term hemodialysis patients. *Kidney Int* 49 (1996): 792-799.
- [213]. Jaber BL, Cendoroglo M, Balakrishnan VS, *et al.*: Apoptosis of leukocytes: basic concepts and implications in uremia. *Kidney Int Suppl* 78 (2001) : S197-205.
- [214]. Matsumoto Y, Shinzato T, Amano I, *et al.*: Relationship between susceptibility to apoptosis and Fas expression in peripheral blood T cells from uremic patients: a possible mechanism for lymphopenia in chronic renal failure. *Biochem Biophys Res Commun* 215 (1995): 98-105.
- [215]. Perianayagam MC, Murray SL, Balakrishnan VS, *et al.*: Serum soluble Fas (CD95) and Fas ligand profiles in chronic kidney failure. *J Lab Clin Med* 136 (2000): 320-327.
- [216]. Beilhack A, Rockson SG: Immune traffic: a functional overview. *Lymphat Res Biol* 1 (2003): 219-234.
- [217]. Jirillo E, Mastronardi ML, Altamura M, *et al.*: The immunocompromised host: immune alterations in splenectomized patients and clinical implications. *Curr Pharm Des* 9 (2003): 1918-1923.

- [218]. Timens W: The human spleen and the immune system: not just another lymphoid organ. *Res Immunol* 142 (1991): 316-320.
- [219]. Swirski FK, Nahrendorf M, Etzrodt M, *et al.*: Identification of splenic reservoir monocytes and their deployment to inflammatory sites. *Science* 325 (2009): 612-616.

APPENDIX

DETAIL PROTOCOL

1. The fluorescein isothiocyanate (FITC)-labeled inulin clearance for GFR measurement

Reagent Preparation:

1. 5% FITC-inulin: dissolved 100mg of FITC-inulin in 2 ml of 0.9% NaCl by heating the solution in boiling water.
2. 500 mM HEPES buffer: dissolved 59.6g of HEPES in 500 ml of deionized water and adjust pH to 7.4 using 10N NaOH.

Preparation of 5% FITC-inulin solution:

1. 5% FITC-inulin (Sigma-Aldrich) is dissolved in two ml of 0.9% NaCl -- facilitated by heating the solution in boiling water.
2. To remove residual FITC not bound to inulin, the solution is filled into a 1000 Daltons cut-off dialysis membrane (Spectra/Pro 6, Spectrum Laboratories Inc., Rancho Dominguez, CA).
3. Put the dialysis membrane filled with FITC-inulin into 1000 ml 0.9% NaCl for 24 hours at room temperature.
4. Prior to use, this dialyzed solution is sterilized by filtration through a 0.22 μm filter (e.g, Costar).

Intravenous injection and blood collection:

1. Mice are anesthetized using Isoflurane, which for approximately 20 seconds.
2. 5% FITC-inulin (3.74 μl /g body weight) is injected retroorbitally under anesthesia within 10 seconds.
3. After fully regaining consciousness the mouse is restrained inside a 50 mL centrifuge tube with large air-holes drilled in the tip.
4. The inner thigh was closely shaven and wiped with 75% ethanol, revealing the saphenous vein. Approximately 20 μl blood is collected in a heparinized capillary tube (Fisher Scientific) by venepuncture using a sterile 23 gauges syringe needle. On average, this yields 10 μl of plasma following centrifugation (4,000 RPM, 10 min).
5. Blood was sampled via the saphenous vein at 3, 7, 10, 15, 35, 55, 75 minutes post injection of FITC-inulin.

Calculation of GFR:

A two – compartment clearance model was used for the calculation of GFR. The initial, rapid decay phase represents redistribution of the tracer from the intravascular compartment to the extracellular fluid. Systemic elimination also occurs, but the distribution process is relatively dominant during this initial phase. During the later, slower decay in concentration of the tracer systemic clearance of the tracer from the plasma predominates. At any given time (tX), the plasma concentration of the tracer (Y) equals to $Ae^{-\alpha t_x} + Be^{-\beta t_x} + \text{Plateau}$. The parameters of above equation could be calculated using a non-linear regression curve-fitting program (GraphPad Prism, GraphPad Software, Inc., San Diego, CA.). GFR was calculated using the equation: $GFR = I / (A/\alpha + B/\beta)$, where I is the amount of FITC-inulin delivered by the bolus injection; A (Span1) and B (Span2) are the y -intercept values of the two decay rates, and α and β are the decay constants for the distribution and elimination phases, respectively.

2. Periodic acid-Schiff (PAS) staining

Solutions and Reagents:

0.5% Periodic Acid Solution: Periodic acid 0.5 g with distilled water 100 ml

Test for Schiff reagent: Pour 10 ml of 37% formalin into a watch glass then drop the reagent. A good Schiff reagent will rapidly turn a red-purple color.

Procedure:

1. Deparaffinize and hydrate to water.
2. Oxidize in 0.5% periodic acid solution for 5 minutes.
3. Rinse in distilled water.
4. Place in Schiff reagent for 15 minutes (Sections become light pink color).
5. Wash in lukewarm tap water for 5 minutes (Immediately sections turn dark pink color).
6. Counterstain in Mayer's hematoxylin for 1 minute.
7. Wash in tap water for 5 minutes.
8. Dehydrate and coverslip using a synthetic mounting medium.

3. Masson's trichrome staining

Solutions and Reagents:

Bouin's Solution: Picric acid (saturated) 75 ml with Formaldehyde (37-40%) 25 ml And Glacial acetic acid 5 ml

Weigert's Iron Hematoxylin Solution: Mixed stock Solution A (Hematoxylin 1 g with 95% Alcohol 100 ml) with stock Solution B (29% Ferric chloride in water 4 ml with distilled water 95 ml and concentrated hydrochloric acid 1ml) in equal volume.

Biebrich Scarlet-Acid Fuchsin Solution: 1% aqueous Biebrich scarlet 90 ml with 1% aqueous acid fuchsin 10 ml and glacial acetic acid 1 ml

Phosphomolybdic-Phosphotungstic Acid Solution: 5% Phosphomolybdic acid 25 ml with 5% Phosphotungstic acid 25 ml

Aniline Blue Solution: Aniline blue 2.5 g with glacial acetic acid 2 ml and distilled water 100 ml

1% Acetic Acid Solution: Glacial acetic acid 1 ml in distilled water 99 ml

Procedure:

1. Deparaffinize and hydrate
2. Bouin's Solution: immerse slides for- 1 hour in oven or overnight at 60 degrees
3. Running Water- let slides sit until yellow clears
4. Weigert's Iron Hematoxylin- 10 minutes
5. Running Water- 5 minutes
6. Biebrich Scarlet-Acid Fuchsin- 5 minutes
7. Wash with distilled water
8. Phosphotungstic-Phosphomolybdic Acid:5 minutes
9. Aniline Blue- 5 minutes
10. 1% Acetic Acid- 2 minutes
11. Rinse with distilled water
12. Dehydrate, Clear and coverslip in fume hood

BIOGRAPHY

Mr. Asada Leelahavanichkul was born on December 27th, 1972 in Bangkok. He received his bachelor degree with honors in medicine from Faculty of Medicine, Chulalongkorn University in 1996 then worked for his internship and general practice in Thailand rural area for 3 years. He received board for internal medicine, family medicine and nephrology in 2002, 2003 and 2004 respectively. Then he worked as an instructor in division of nephrology Chulalongkorn University for 1 year and received the fellowship award in National Institute of Diabetes and Digestive and Kidney Disease, National Institute of Health, USA since 2005. He participated in Medical Microbiology program, Graduate School, Chulalongkorn University in 2008.

Selected publications and presentations:

Published articles,

1. Leelahavanichkul A, Yasuda H, Doi K, et al. Methyl-2-acetamidoacrylate decrease sepsis induced acute kidney injury in CD-1 mice. *Am J Physiol Renal Physiol*. 2008 Dec; **295**(6):F1825-35.
2. Nemeth K*, Leelahavanichkul A *, Yuen PS, Mayer B, et al. Bone marrow stromal cells significantly attenuate mouse poly-microbial sepsis via monocyte/macrophage derived IL-10. *Nature Medicine*. 2009 Jan; **15**(1):42-9. (* distribution equally)
3. Leelahavanichkul A, Yan Q, Hu X, et al. Angiotensin II overcomes strain-dependent resistance of rapid CKD progression in a new remnant kidney mouse model. *Kidney Int* 2010 Dec; **78**(11): 1136-53.

International oral presentation, Annual meeting of the American Society of Nephrology

2007 “Bone marrow stromal cell attenuate sepsis”, San Francisco, CA

2009 “Rapid CKD progression in a new mouse kidney remnant model: dominant role of blood pressure on strain- dependent susceptibility”, San Diego, CA

2010 “Absence or Blockade of SR-BI/II and CD36 Receptors Improves Sepsis Survival and Acute Outcomes in Mice”, Denver, CO

Text books, several topics in “Nephrology” edited by Eiam-Ong S. Bangkok: Text and journal publication Co., 2004 and 2011.